USGS Award Number 08HQGR0085

CHARACTERIZING LIQUEFACTION POTENTIAL OF PLEISTOCENE SOIL DEPOSITS IN THE CHARLESTON AREA, SOUTH CAROLINA

Doctor of Philosophy Dissertation by Tahereh Heidari
with Ronald D. Andrus Dissertation Advisor

Department of Civil Engineering
Clemson University
Lowry Hall, Box 340911
Clemson, South Carolina 29634-0911 USA
Telephone: (864) 656-0488
Fax: (864) 656-2670
E-mail: randrus@clemson.edu

May 2008 to October 2010

ABSTRACT

Liquefaction potential of major Pleistocene deposits in the Greater Charleston area, South Carolina is investigated in this dissertation. The data considered to characterize liquefaction potential include field performance information from the 1886 Charleston earthquake and the results of many seismic cone penetration tests with pore water measurements (SCPTu). The investigation begins with the Mount Pleasant area, and then expands to the entire Greater Charleston area.

A liquefaction potential map of Mount Pleasant is created through reviewing available first-hand accounts of ground behavior during the 1886 earthquake, analyzing cone penetration test and shear wave velocity data, and correlating the results with geology. Careful review of the first-hand accounts reveals that nearly all cases of surface effects of liquefaction can be associated with the younger sand deposits that lie adjacent to the harbor, rivers, and creeks. Only one documented case of minimal surface effect of liquefaction can be definitely associated with the older sand deposits of the 100,000-year-old Wando Formation. Ratios of measured to estimated shear wave velocity (MEVR) indicate that the younger sand deposits and the older sand deposits have measured velocities that are 9% and 38%, respectively, greater than 6-year-old sand deposits with the same cone tip resistances. Liquefaction potential is expressed in terms of the liquefaction potential index (LPI) proposed by Iwasaki and others. LPI values for the older sands computed from the SCPTu profiles are incorrectly high, if no age corrections are applied. If age corrections are applied, computed LPI values match well the observed field behavior in both the younger sands and the older sands. The results are combined with a 1:24,000 scale geologic map to produce a liquefaction potential map of Mount Pleasant. The findings of the Mount Pleasant study agree remarkably well with a previous liquefaction potential study of aged soil deposits on Charleston peninsula.

Liquefaction potential of Pleistocene sand deposits in the Greater Charleston area is characterized by reviewing cases of conspicuous craterlets and horizontal ground displacement that occurred during the 1886 earthquake, and analyzing eighty-two seismic cone soundings. Nearly half of the cases of ground failure in sand deposits are associated with the 200,000-year-old Ten Mile Hill beds located within 13 km of the Woodstock fault, the likely source of the earthquake. One quarter of the cases of ground failure are associated with the 100,000-year-old Wando Formation located within 17 km of the fault; and another quarter are associated with the younger deposits that lie adjacent to the harbor, rivers, and creeks located within 31 km of the fault. The influence of distance to the fault on LPI and MEVR is investigated. Computed LPIs are corrected for the influence of diagenetic processes using MEVR. The liquefaction probability curves developed for four major sand groups agree well with the 1886 field observations.

The influence of depth to top of the Cooper Marl and depth to the groundwater table on LPI values of the younger sand facies of Wando Formation (Qws) is also investigated. Liquefaction probability curves are developed considering the influence of depth to the groundwater table and depth to the non-liquefiable Cooper Marl.

Liquefaction potential of areas now covered by artificial fill (af) in the Charleston area are characterized through reviewing cases of conspicuous craterlets and horizontal ground displacement that occurred during the 1886 earthquake, and analyzing twenty-three seismic cone soundings. All cases of 1886 ground failure that plot in af areas on Charleston Peninsula and around Mount Pleasant are located where Qhes or younger sand deposits are believed to be in the subsurface. SCPTu sites mapped in af are grouped into three categories based on dominant geology in the top 10 m. Liquefaction probability curves are developed for the three categories considering the influence of depth to the groundwater table and depth to the non-liquefiable Cooper Marl.

The liquefaction potential of areas covered by surficial clayey deposits in the Greater Charleston area are characterized through reviewing liquefaction and ground failure cases that plot in these areas and analyzing thirty-two seismic cone soundings. Liquefaction probability curves developed for four major clay groups are compared with the liquefaction cases that plot in the surficial clayey deposits. The liquefaction probability curves developed for the surficial clayey deposits do not agree well with the high number of ground failures that occurred in these deposits during the 1886 earthquake. Conservative liquefaction probability curves are suggested for the surficial clayey deposits.

Laboratory tests conducted on samples collected from various Pleistocene deposits indicate little or no carbonate in the beach sand deposits in the Greater Charleston area. Thus, the higher shear wave velocity and MEVR values associated with Qws are not the result of carbonate cementation.

The probability curves can be used to develop geology-based liquefaction hazard maps of the Charleston area. Liquefaction hazard maps are useful tools for identifying areas with high likelihood of liquefaction-induced ground deformation, a major cause of damage in many earthquakes. Information about areas with high likelihood of ground deformation can be used for effective regional earthquake hazard planning and mitigation. Liquefaction hazard maps are also useful for identifying areas where specific investigations for liquefaction hazard are needed or should be required prior to project development, but in general these maps should not be used for site-specific engineering design.

CHARACTERIZING LIQUEFACTION POTENTIAL OF PLEISTOCENE SOIL DEPOSITS IN THE CHARLESTON AREA, SOUTH CAROLINA

A Dissertation
Presented to
the Graduate School of
Clemson University

In Partial Fulfillment
of the Requirements for the Degree
Doctor of Philosophy
Civil Engineering

---

by
Tahereh Heidari
May 2011

Accepted by:
Dr. Ronald D. Andrus, Committee Chair
Dr. C. Hsein Juang
Dr. Stephen Moysey
Dr. Nadarajah Ravichandran

Much of this research was supported by the United States Geological Survey (USGS), Department of the Interior, under Grant No. 08HQGR0085. The views and conclusions contained in this document are those of the author and should not be interpreted as necessarily representing the official policies, either expressed or implied, of the United States Government.

ABSTRACT

Liquefaction potential of major Pleistocene deposits in the Greater Charleston area, South Carolina is investigated in this dissertation. The data considered to characterize liquefaction potential include field performance information the 1886 Charleston earthquake and the results of many seismic cone penetration tests with pore water measurements (SCPTu). The investigation begins with the Mount Pleasant area, and then expands to the entire Greater Charleston area.

A liquefaction potential map of Mount Pleasant is created through reviewing available first-hand accounts of ground behavior during the 1886 earthquake, analyzing cone penetration test and shear wave velocity data, and correlating the results with geology. Careful review of the first-hand accounts reveals that nearly all cases of surface effects of liquefaction can be associated with the younger sand deposits that lie adjacent to the harbor, rivers, and creeks. Only one documented case of minimal surface effect of liquefaction can be definitely associated with the older sand deposits of the 100,000-year-old Wando Formation. Ratios of measured to estimated shear wave velocity (MEVR) indicate that the younger sand deposits and the older sand deposits have measured velocities that are 9% and 38%, respectively, greater than 6-year-old sand deposits with the same cone tip resistances. Liquefaction potential is expressed in terms of the liquefaction potential index (LPI) proposed by Iwasaki and others. LPI values for the older sands computed from the SCPTu profiles are incorrectly high, if no age corrections

are applied. If age corrections are applied, computed LPI values match well the observed field behavior in both the younger sands and the older sands. The results are combined with a 1:24,000 scale geologic map to produce a liquefaction potential map of Mount Pleasant. The findings of the Mount Pleasant study agree remarkably well with a previous liquefaction potential study of aged soil deposits on Charleston peninsula.

Liquefaction potential of Pleistocene sand deposits in the Greater Charleston area is characterized by reviewing cases of conspicuous craterlets and horizontal ground displacement that occurred during the 1886 earthquake, and analyzing eighty-two seismic cone soundings. Nearly half of the cases of ground failure in sand deposits are associated with the 200,000-year-old Ten Mile Hill beds located within 13 km of the Woodstock fault, the likely source of the earthquake. One quarter of the cases of ground failure are associated with the 100,000-year-old Wando Formation located within 17 km of the fault; and another quarter are associated with the younger deposits that lie adjacent to the harbor, rivers, and creeks located within 31 km of the fault. The influence of distance to the fault on LPI and MEVR is investigated. Computed LPIs are corrected for the influence of diagenetic processes using MEVR. The liquefaction probability curves developed for four major sand groups agree well with the 1886 field observations.

The influence of depth to top of the Cooper Marl and depth to the groundwater table on LPI values of the younger sand facies of Wando Formation (Qws) is also

investigated. Liquefaction probability curves are developed considering the influence of depth to the groundwater table and depth to the non-liquefiable Cooper Marl.

Liquefaction potential of areas now covered by artificial fill (af) in the Charleston area are characterized through reviewing cases of conspicuous craterlets and horizontal ground displacement that occurred during the 1886 earthquake, and analyzing twenty-three seismic cone soundings. All cases of 1886 ground failure that plot in af areas on Charleston Peninsula and around Mount Pleasant are located where Qhes or younger sand deposits are believed to be in the subsurface. SCPTu sites mapped in af are grouped into three categories based on dominant geology in the top 10 m. Liquefaction probability curves are developed for the three categories considering the influence of depth to the groundwater table and depth to the non-liquefiable Cooper Marl.

The liquefaction potential of areas covered by surficial clayey deposits in the Greater Charleston area are characterized through reviewing liquefaction and ground failure cases that plot in these areas and analyzing thirty-two seismic cone soundings. Liquefaction probability curves developed for four major clay groups are compared with the liquefaction cases that plot in the surficial clayey deposits. The liquefaction probability curves developed for the surficial clayey deposits do not agree well with the high number of ground failures that occurred in these deposits during the 1886 earthquake. Conservative liquefaction probability curves are suggested for the surficial clayey deposits.

Laboratory tests conducted on samples collected from various Pleistocene deposits indicate little or no carbonate in the beach sand deposits in the Greater Charleston area. Thus, the higher shear wave velocity and MEVR values associated with Qws are not the result of carbonate cementation.

The probability curves can be used to develop geology-based liquefaction hazard maps of the Charleston area. Liquefaction hazard maps are useful tools for identifying areas with high likelihood of liquefaction-induced ground deformation, a major cause of damage in many earthquakes. Information about areas with high likelihood of ground deformation can be used for effective regional earthquake hazard planning and mitigation. Liquefaction hazard maps are also useful for identifying areas where specific investigations for liquefaction hazard are needed or should be required prior to project development, but in general these maps should not be used for site-specific engineering design.

DEDICATION

This dissertation is dedicated to my parents in recognition of their support and love.

ACKNOWLEDGMENTS

I would like to express my sincere gratitude to my advisor, Dr. Ronald Andrus for his guidance, support and patience throughout the years of my study at Clemson University. I am honored to have had the opportunity to be a student in his classes and be a member of his research team. I would also like to thank my other committee members, Dr. C. Hsein Juang, Dr. Nadarajah Ravichandran, and Dr. Stephen Moysey, for their support and for their timely review of my dissertation.

I would like to thank the many individuals who assisted with the data collection process during the past several years and before I began my research, in particular, William M. Camp of S&ME; William B. Wright and Thomas J. Casey of WPC; and Cedric D. Fairbanks, Nisha P. Mohanan, Aniket Shrikhande, Daniel R. Balon, Ronald C. Boller, Hossein Hayati, Aaron J. Geiger, and Akhtar Hossein, former and current graduate students at Clemson University. I am also indebted to Peter G. Chirico of USGS for providing the digital geologic map of the Greater Charleston area, and Mary Julia Royall, lifelong resident and historian of Mount Pleasant, for making available copies of *The Berkeley Gazette* as well as other historic information. I express my thanks to Shimelies Aboye, a graduate student at Clemson University, who helped me collect auger samples in the Greater Charleston area. I also express thanks to Elena A. Mikhailova and Taghi Darroudi of Clemson University who assisted with understanding of various methods carbonate testing.

I would like to thank my family for their love and support throughout the various stages of my life. This dissertation would have not been possible without their encouragement during my time at Clemson University. I am also grateful to all my friends who made my time at Clemson University a pleasant and memorable experience.

Finally, much of this research was supported by the United States Geological Survey (USGS) under grant number 08HQGR0085. Additional support for collecting boreholes samples at three sites in the South Carolina Coastal Plain was provided by the National Science Foundation (NSF), under grant CMS-0556006. The financial assistance from the USGS and NSF is greatly appreciated.

TABLE OF CONTENTS

Page

TITLE PAGE i

ABSTRACT iii

DEDICATION vii

ACKNOWLEDGMENTS viii

TABLE OF CONTENTS x

LIST OF TABLES xiii

LIST OF FIGURES xvi

CHAPTER

1. INTRODUCTION 1

    1.1 Background and Purpose of Research 1
    1.2 Scope and Objectives 4
    1.3 Organization 5

2. MAPPING LIQUEFACTION POTENTIAL OF AGED SOIL DEPOSITS IN MOUNT PLEASANT, SOUTH CAROLINA 6

    2.1 Introduction 6
    2.2 Geology and Seismology 10
    2.3 Historic Liquefaction Map 16
    2.4 CPTu Database 23
    2.5 Deposits Susceptible to Liquefaction 29
    2.6 Liquefaction Potential Calculation and Analysis 32
    2.7 1886 Liquefaction Potential Map 40

Table of Contents (Continued) Page

2.8 Conclusion 45

3. LIQUEFACTION POTENTIAL OF PLEISTOCENE SANDS IN THE CHARLESTON AREA, SOUTH CAROLINA 47

3.1 Introduction 47
3.2 Geology and Seismology 48
3.3 1886 Liquefaction and Ground Failure 52
3.4 SCPTu Database 57
3.5 Measured to Estimated Velocity Ratio 65
3.6 Liquefaction Potential Calculation 72
3.7 Liquefaction Potential Based on a Scenario Shaking 76
3.8 Liquefaction Probability Curves 82
3.9 Conclusion 87

4. CHARACTERIZING THE LIQUEFACTION POTENTIAL OF THE PLEISTOCENE-AGE WANDO FORMATION IN THE CHARLESTON AREA, SOUTH CAROLINA 89

4.1 Introduction 89
4.2 Liqefaction Potential 90
4.3 Liquefaction Potential Based on a Scenario Earthquake 95
4.4 Liquefaction Probability Curves 98
4.5 Conclusion 102

5. LIQUEFACTION POTENTIAL OF ARTIFICIAL FILL AREAS IN THE CHARLESTON AREA, SOUTH CAROLINA 103

5.1 Introduction 103
5.2 1886 Liquefaction and Ground Failure 104
5.3 SCPTu Database 106
5.4 Liquefaction Potential based on a Scenario Earthquake 109
5.5 Liquefaction Probability Curves 115
5.6 Conclusion 122

6. LIQUEFACTION POTENTIAL OF SURFICIAL CLAYEY DEPOSITS IN THE CHARLESTON AREA, SOUTH CAROLINA 123

Table of Contents (Continued) Page

6.1 Introduction 123
6.2 Geology 123
6.3 1886 Liquefaction and Ground Failure 126
6.4 SCPTu Database 131
6.5 Liquefaction Potential based on a Scenario Earthquake 131
6.6 Liquefaction Probability Curves 136
6.7 Conclusion 146

7. CARBONATE CONTENT OF SOIL DEPOSITS IN THE GREATER CHARLESTON AREA, SOUTH CAROLINA 148

7.1 Introduction 148
7.2 Review of Possible Soil Aging Mechanisms 148
7.3 Database 154
7.4 Methodology 160
7.5 Calibration of the Carbonate Analyzer 164
7.6 Results 168
7.7 Conclusion 177

8. SUMMARY, CONCLUSIONS, AND RECOMMENDATIONS 178

8.1 Summary and Conclusions 178
8.1.1 Mount Pleasant 179
8.1.2 Pleistocene Sand Deposits 181
8.1.3 Artificial Fill Areas 183
8.1.4 Surficial Clayey Deposits 184
8.1.5 Carbonate Content of Surface Sand Deposits 185
8.2 Recommendations for Future Work 186

APPENDIX A

Locations of 1886 Horizontal Ground Displacement and Conspicuous Craterlets Mapped by Earle Sloan 187

REFERENCE 191

LIST OF TABLES

Table Page

2.1 Description of geologic units (adapted from Weems and Lemons 1993; Hayati and Andrus 2008a). 12

2.2 Cases of surface effects of liquefaction in Mount Pleasant. 20

2.3 Cases of no surface effects of liquefaction in Mount Pleasant. 22

2.4 Cone soundings from Mount Pleasant. 24

2.5 Measured to estimated V_{s1} ratios for two sands in Mount Pleasant. 31

2.6 Statistic of LPI assuming M_w = 6.9 and a_{max} = 0.25g. 39

3.1 Summary of 1886 ground displacement mapped by Earle Sloan (Dutton 1889, PL. XXVII) for seven Quaternary seven sands. 54

3.2 Summary of 1886 conspicuous craterlet areas mapped by Earle Sloan (Dutton 1889, PL. XXVIII) for seven Quaternary sands. 55

3.3 SCPTu soundings from the Greater Charleston area that plot in surficial sand deposits. 59

3.4 Measured to estimated V_{s1} ratios for four Quaternary sand groups. 67

3.5 Statistic of LPI assuming M_w = 6.9 and a_{max}= 0.25g for four Quaternary sand groups. 81

4.1 Coefficients of the fitted liquefaction probability curves based on values for Qws surficial deposits.. 101

5.1 SCPTu soundings from the Greater Charleston area that plot in areas of af. 108

5.2 Statistic of LPI assuming M_w = 6.9 and a_{max}= 0.25g for the af sites grouped by surficial geology. 111

Table Page

5.3 Coefficients of the fitted liquefaction probability curves based on values for af and af III categories... 121

6.1 Summary of 1886 ground displacement areas mapped by Earle Sloan (Dutton 1889, PL. XXVII) for eight surficial clayey deposits. 128

6.2 Summary of 1886 conspicuous craterlet areas mapped by Earle Sloan (Dutton 1889, PL. XXVIII) for eight surficial clayey deposits. 129

6.3 SCPTu soundings from the Greater Charleston area that plot in surficial clayey deposits..... 134

6.4 Statistic of LPI assuming M_w = 6.9 and a_{max}= 0.25g for four surficial clayey deposits..... 135

6.5 Coefficients of the fitted liquefaction probability curves based on values for the combined Qlc and Qpc surficial deposits. 144

6.6 Coefficients of the fitted liquefaction probability curves based on values for Qhs/Qhes and Qts surficial deposits. 145

7.1 Soil index properties and calcite equivalent for the samples collected from near-surface layers below the groundwater table using a hand auger..... 158

7.2 Soil index properties and calcite equivalent for the samples collected from boring B-3 at CREC (modified from Boller 2008). 170

7.3 Soil index properties and calcite equivalent for the samples collected from boring B-1at the Hobcaw Borrow Pit site (modified from Geiger 2010). 171

7.4 Soil index properties and calcite equivalent for the samples collected from boring B-1 at the Rest Area Ponds site (modified from Geiger 2010)..... 172

Table Page

A.1 Location of 1886 conspicuous craterlet areas mapped by Earle Sloan (Dutton 1889, PL. XXVIII). 188

A.2 Location of 1886 ground displacement mapped by Earle Sloan (Dutton 1889, PL. XXVII). 189

LIST OF FIGURES

Figure Page

2.1 Geologic map of Mount Pleasant (adapted from Weems and Lemon, 1993) showing locations of CPTu sites. 11

2.2 Geologic map of Mount Pleasant (adapted from Weems and Lemon 1993) showing locations of 1886 surface effects of liquefaction. 19

2.3 Representative profiles of cone, V_s, and geology from CPTu site Number 19. 27

2.4 Calculation of LPI for CPTu site Number 19 based on M_w = 6.9 and a_{max} = 0.25g. 37

2.5 Complementary cumulative distribution functions of LPI for various site categories assuming M_w = 6.9, a_{max} = 0.25g, K_{DR} = 1.45 for the Wando Formation, and K_{DR} = 1.15 for Qhes and younger sands. 41

2.6 Liquefaction potential map of Mount Pleasant based on 1886 field performance data and deposit resistance-corrected LPI assuming M_w = 6.9, a_{max} = 0.25g, and $K_{DR} \neq 1$. 44

3.1 Map of the Greater Charleston area showing the inferred Woodstock fault presented in Durá-Gómez and Talwani (2009) and locations of 1886 liquefaction and ground failure from Dutton (1889). 50

3.2 Frequency of mapped 1886 craterlet and ground displacement areas (Dutton 1889) grouped by surficial sand deposits. 56

3.3 Map showing the inferred Woodstock fault presented in Durá-Gómez and Talwani (2009) and location of SCPTu sites plotted in surficial sand deposits. 58

3.4 Representative profiles of cone, V_S, and geology from SCPTu site No. 74. 64

3.5 Variation of MEVR with depth for four sand groups. 69

Figure Page

3.6 Variation of site mean MEVR with distance to inferred Woodstock fault for four Quaternary sand groups. 71

3.7 Calculation of LPI for SCPTu site No. 74 based on M_w = 6.9, a_{max} = 0.25g, and I_c > 2.6 as the criterion for non-susceptible clay-rich soils. 77

3.8 Variation of K_{DR}-corrected LPI with distance to inferred Woodstock fault for four Quaternary sand groups assuming M_w=6.9, a_{max}=0.25g, and I_c > 2.6 as the criterion for non-susceptible clay-rich soils. 80

3.9 Liquefaction probability curves for four Quaternary sand groups, assuming I_c > 2.6 as the criterion for non-susceptible clay-rich soils. Note that the circles in the figure represent probability based on lognormal distribution, and the triangles represent probability based on experimental cumulative distribution. 83

3.10 Comparison of liquefaction probability curves for four Quaternary sand groups, assuming I_c > 2.6 as the criterion for non-susceptible clay-rich soils. 86

4.1 Map of the Greater Charleston area showing the Woodstock fault zone (Durá-Gómez and Talwani 2009) and the locations of SCPTu sites plotted in Qws. 92

4.2 Variation of K_{DR}-corrected LPI with (a) distance to the Woodstock fault, (b) depth to top of the Cooper Marl, and (c) depth to the groundwater table for 42 SCPTu sites plotted in Qws assuming M_w=6.9, a_{max}=0.25g. 97

Figure Page

4.3 Liquefaction probability curves assuming various depths to the groundwater table (a) 1 m and (b) 3 m, and depth to top of Cooper Marl of 5, 10, 15 m for Qws surficial deposits in the Charleston area. Note that the circles in the figure represent probability based on lognormal distribution, and the triangles represent probability based on experimental cumulative distribution. 99

5.1 Map of the Greater Charleston area showing the Woodstock fault presented in Durá-Gómez and Talwani (2009) and the locations of 1886 liquefaction and ground failure in af areas from Dutton (1889).. 105

5.2 Map of the Greater Charleston area showing the Woodstock fault presented in Durá-Gómez and Talwani (2009) and the locations of SCPTu sites in areas of af.. 107

5.3 Variation of K_{DR}-corrected LPI with (a) distance to the Woodstock fault, (b) depth to top of the Cooper Marl, and (c) depth to the groundwater table for all 23 SCPTu sites in af assuming M_w = 6.9, a_{max} = 0.25g. 112

5.4 Variation of K_{DR}-corrected LPI with (a) distance to the Woodstock fault, (b) depth to top of the Cooper Marl, and (c) depth to the groundwater table for the 10 SCPTu sites of group af I assuming M_w = 6.9, a_{max} = 0.25g. 113

5.5 Variation of K_{DR}-corrected LPI with (a) distance to the Woodstock fault, (b) depth to top of the Cooper Marl, and (c) depth to the groundwater table for the 10 SCPTu sites of group af III assuming M_w = 6.9, a_{max} = 0.25g. 114

5.6 Liquefaction probability curves for (a) all af sites, (b) af I sites, and (c) af III sites. Note that the circles in the figure represent probability based on lognormal distribution, and the triangles represent probability based on experimental cumulative distribution. 116

Figure Page

5.7 Comparison of liquefaction probability curves for three af categories. 117

5.8 Liquefaction probability curves assuming depths to the groundwater table of (a) 1 m and (b) 3 m, and depths to top of the Cooper Marl of 5, 10, 15 m for **af** surficial deposits in the Charleston area. Note that the circles in the plots represent probability based on lognormal distribution, and the triangles represent probability based on experimental cumulative distribution. 119

5.9 Liquefaction probability curves assuming depths to the groundwater table of (a) 1 m and (b) 3 m, and depths to top of the Cooper Marl of 5, 10, 15 m for **af III** surficial deposits in the Charleston area. Note that the circles in the plots represent probability based on lognormal distribution, and the triangles represent probability based on experimental cumulative distribution. 120

6.1 Map of the Greater Charleston area showing the Woodstock fault as presented in Durá-Gómez and Talwani (2009) and the locations of 1886 liquefaction and ground failure from Dutton (1889) that plot in surficial clayey deposits. 125

6.2 Frequency of 1886 ground displacement and craterlet areas (Dutton 1889, PLs. XXVII & XXVIII) grouped by surficial clayey deposits. 130

6.3 Map of the Greater Charleston area showing the Woodstock fault as presented in Durá-Gómez and Talwani (2009) and the locations of SCPTu sites that plot in surficial clayey deposits. 133

6.4 Liquefaction probability curves for four surficial clayey deposits. Note that the circles in the plots represent probability based on lognormal distribution, and the triangles represent probability based on experimental cumulative distribution. 138

Figure Page

6.5 Comparison of liquefaction probability curves for four surficial clayey deposits. 139

6.6 Liquefaction probability curves for the combined Qlc and Qpc surficial deposits assuming depths to the groundwater table of (a) 1 m and (b) 3 m, and depths to top of the Cooper Marl of 5 and 10 m. Note that the circles in the plots represent probability based on lognormal distribution, and the triangles represent probability based on experimental cumulative distribution. 140

6.7 Liquefaction probability curves for Qhs/Qhes, recommended for Qht/Qhec surficial deposits, assuming depths to the groundwater table of (a) 1 m and (b) 3 m, and depths to top of the Cooper Marl of 5, 10, 15 m. Note that the circles in the plots represent probability based on lognormal distribution, and the triangles represent probability based on experimental cumulative distribution. 141

6.8 Liquefaction probability curves for Qts, recommended for Qtc surficial deposits, assuming depths to the groundwater table of (a) 1 m and (b) 3 m, and depths to top of the Cooper Marl of 5 and 10 m. Note that the circles in the plots represent probability based on lognormal distribution, and the triangles represent probability based on experimental cumulative distribution. 142

7.1 Map of the Greater Charleston area showing the Woodstock fault as presented in Durá-Gómez and Talwani (2009) and the locations of auger samples for carbonate testing. 156

7.2 Collection of near-surface samples using a hand auger. 157

7.3 Rapid carbonate analyzer manufactured by Humboldt. 163

7.4 Results of calibration tests showing (a) variations of the cylinder gas pressure with time for various amounts of calcium carbonate (b) after correcting for the blank test. 166

Figure Page

7.5 Calibration curve for the carbonate analyzer at 2 hours. 167

7.6 Profiles of cone, geology and calcite equivalent for the boring B-3 at CREC (modified from Boller et al. 2008). 173

CHAPTER ONE

INTRODUCTION

1.1 Background and Purpose of Research

On August 31, 1886 Charleston, South Carolina was severely shaken by an earthquake with magnitude of about 7.0. This earthquake was the largest historic seismic event to have occurred in the eastern United States (Bollinger 1977). Côté (2006) estimated that the 1886 Charleston earthquake caused 124 deaths and more than $460 million (2006 dollars) in damage. A major cause of damage was liquefaction-induced ground failure (Dutton 1889). The primary objective of this dissertation is to characterize the liquefaction potential of major Pleistocene (10,000 to 1.8 million years) deposits present in the Greater Charleston area.

Liquefaction potential is commonly computed using the simplified procedure originally proposed by Seed and Idriss (1971) based on standard penetration test blow count. Since 1971, the Seed-Idriss simplified procedure has experienced several updates and modifications to include methods based on cone tip resistance, shear wave velocity, and dilatometer horizontal stress index (Seed et al. 1985; Shibata and Teparaksa 1988; Tokimatsu and Uchida 1990; Robertson et al. 1992; Youd et al. 2001; Juang et al. 2002; Andrus et al. 2004b; Cetin et al. 2004; Monaco et al. 2005; Moss et al. 2006; Idriss and Boulanger 2008). Liquefaction potential can be expressed in terms of factor of safety,

probability, or other index that depends on the seismic loading and the soil's ability to resist micro-structural collapse and pore-water pressure buildup leading to liquefaction. The soil's ability to resist liquefaction is represented by a variable called the cyclic resistance ratio (CRR).

Most methods for computing CRR are based on semi-empirical procedures derived from case history data associated with soil deposits less than a few thousand years old (Youd et al. 2001). This can be a limitation of computed CRR in Pleistocene deposits, because diagenetic processes (e.g., compaction, addition of material, removal of material, cementation, change of mineral phase) affect small- to medium-strain dynamic soil properties, where as in situ tests involve small-, medium- or high-strain measurements, and rearrangement of soil particles and pore-water pressure buildup are medium- to high-strain events (Drnevich and Richart 1970; Youd 1972; Park and Silver 1975; Dobry et al. 1982; Seed et al. 1983; Chang et al. 2007).

Pleistocene deposits often exhibit more resistance to liquefaction than younger deposits (Youd and Perkins 1978). One notable exception is the Pleistocene sand deposits in the South Carolina Coastal Plain that liquefied during the 1886 Charleston earthquake (Martin and Clough 1990; Lewis et al. 1999). Attempts to quantify the influence of age on liquefaction resistance have been made by several investigators (Seed 1979; Troncoso et al. 1988; Arango et al. 2000; Leon et al. 2006; Moss et al. 2008; Hayati and Andrus 2008a, 2009). Complicating efforts to quantify the influence of age

on liquefaction resistance is the great spatial variability that can result from diagenetic processes, including disturbances during previous liquefaction events.

A promising approach to quantifying the influence of age (or diagenetic processes) on liquefaction resistance is to use two in situ tests that involve different levels of strain. For example, cone tip resistance (q_c) is a high strain (> 1%) measurement whereas shear wave velocity (V_S) is typically a small strain (< 0.001%) measurement. Shear wave velocity is directly related to small-strain shear modulus ($G_{max} = V_s^2$ multiplied by the mass density of the soil). Significant age effect in penetration resistance-V_S relationships has been observed by various investigations (e.g., Ohta and Goto 1978; Rollins et al. 1998; Andrus et al. 2009). Roy (2008) used ratios of measured q_c to measured G_{max} to draw two different CRR curves for Holocene and Pleistocene deposits. Andrus et al. (2009) believed that more than two CRR curves are needed and proposed correcting commonly used CRR curves using ratios of measured V_S to estimated V_S based on a relationship for young sands.

The measured-to-estimated shear wave velocity ratio (MEVR) was used in liquefaction studies of Charleston Peninsula by Hayati and Andrus (2008a), Mount Pleasant by Heidari and Andrus (2010), and this dissertation study to justify corrections to computed CRR for the older sand. Charleston Peninsula and Mount Pleasant are located about 23 and 26 km, respectively, from the fault associated with the 1886 earthquake. Severe liquefaction occurred in the younger sand, while little to no liquefaction occurred in the older sand. Without any correction to CRR, both sands

exhibited similar liquefaction potentials based on cone tip resistance. On Charleston Peninsula, average computed MEVRs were 0.93 for the younger sand, and 1.37 for the older sand. In Mount Pleasant, average computed MEVRs were 1.09 for the younger sand, and 1.38 for the older sand. It should be noted that these results may not be valid for Pleistocene deposits closer to the fault which experienced liquefaction in 1886 (Martin and Clough 1990; Lewis et al. 1999).

1.2 Scope and Objectives

The scope of the research presented in this dissertation is to better determine liquefaction potential of aged soil deposits in the Greater Charleston area. To do so, the specific objectives of this dissertation are to:

1. Present the development of the liquefaction potential map of Mount Pleasant published in Heidari and Andrus (2010).
2. Review cases of conspicuous craterlets and horizontal ground displacement that occurred in the Greater Charleston area during the 1886 Charleston earthquake.
3. Develop liquefaction potential curves for the areas covered by different geologic deposits, including artificial fill, clayey deposits and sand deposits.

4. Examine the influence of distance to the Woodstock fault, depth to the groundwater table, and depth to the Cooper Marl on liquefaction potential.

5. Examine the possibility of carbonate cementation as a mechanism responsible for the aging effects in sandy deposits of the Greater Charleston area.

1.3 Organization

This dissertation is organized into eight chapters. The introduction is presented in the current chapter, Chapter 1. Presented in Chapter 2 is the liquefaction potential mapping study of Mount Pleasant. Chapter 3 involves characterization of the liquefaction potential of major Pleistocene sand deposits present in the Greater Charleston area. Chapter 4 extends the characterization of barrier island sand facies of the 100,000-year-old Wando Formation (Qws) to include an analysis of the influence of depth to the groundwater table and depth to the Cooper Marl on liquefaction potential. Chapter 5 presents the characterization of liquefaction potential of areas covered by artificial fill (af) in the Charleston area. Chapter 6 presents the characterization of liquefaction potential of areas covered by clayey deposits in the Greater Charleston area. Chapter 7 presents the results of carbonate content tests on soil samples from the Greater Charleston area. Finally, the major conclusions of this dissertation are summarized in Chapter 8.

CHAPTER TWO

MAPPING LIQUEFACTION POTENTIAL OF AGED SOIL DEPOSITS IN MOUNT PLEASANT, SOUTH CAROLINA*

2.1 Introduction

Liquefaction hazard maps are useful tools for identifying areas with high likelihood of liquefaction-induced ground deformation, a major cause of damage in many earthquakes. Information about areas with high likelihood of ground deformation can be used for effective regional earthquake hazard planning and mitigation. Liquefaction hazard maps are also useful for identifying areas where specific investigations for liquefaction hazard are needed or should be required prior to project development, but in general these maps should not be used for site-specific engineering design.

Youd and Perkins (1978) introduced the basic procedures used in liquefaction hazard mapping. Many investigators since then have applied and further developed the procedures, including Youd et al. (1978), Dupré and Tinsley (1980), Anderson et al. (1982), Tinsley et al. (1985), Youd and Perkins (1987), Elton and Hadj-Hamou (1990), Mabey et al. (1993), Sowers et al. (1994), CDMG (1996), Knudsen et al. (1996), Holzer

* A similar form of this chapter was published in Engineering Geology; Heidari, T., and Andrus, R. D. (2010). "Mapping Liquefaction Potential of Aged Soil Deposits in Mount Pleasant, South Carolina."

et al. (2006), and Hayati and Andrus (2008a). Summaries of these and other mapping efforts are presented in Power and Holzer (1996) and Holzer (2008).

Liquefaction hazard maps can be grouped into four general categories (Power and Holzer 1996)—historic maps, susceptibility maps, potential maps, and ground failure maps. Historic maps identify areas where liquefaction has occurred in the historic past and will likely occur again. Susceptibility maps identify areas with materials that can liquefy based on historic information, geology (e.g., environment of deposition, age of deposit, groundwater table depth), composition, and initial density (Youd and Hoose 1977; Youd and Perkins 1978). Potential maps consider both the susceptibility of the deposit and the earthquake ground shaking, either for a certain exposure time period or a scenario earthquake. Ground failure maps attempt to predict the amounts of liquefaction-induced permanent ground displacements associated with an exposure time period or a scenario earthquake.

Aged soil is an expression that is often used in geotechnical engineering to refer to the results of various diagenetic processes that occur naturally in soil (or sediment) over time. As explained by Friedman and Sanders (1978, p. 145), ”diagenesis involves, among other things: (1) compaction, (2) addition of new material, (3) removal of material, and transformation of material by (4) change of mineral phase or (5) replacement of one mineral phase by another.” The removal of material creates new pore spaces and may be the source of cements. Weak cementing bonds due to dissolution/precipitation of cements, such as silica or carbonate, may start forming soon

after deposition (Mitchell and Solymar 1984). During compaction (or secondary compression), soil particles rearrange and interlock in response to the weight of overlying materials (Schmertmann 1987). Youd and Hoose (1977) noted that cementing and compaction are important factors that reduce liquefaction susceptibility with time.

Although age of deposit was explicitly considered in characterizing liquefaction susceptibility by Youd and Perkins (1978), their criteria only provide qualitative estimates of susceptibility (e.g., <500 years beach deposit = moderate to high susceptibility, Holocene beach deposit = low to moderate susceptibility, Pleistocene beach deposit = low to very low susceptibility). In addition, their criteria incorrectly estimate low susceptibility for several Pleistocene deposits in the South Carolina Coastal Plain which liquefied during the 1886 Charleston earthquake (Martin and Clough 1990; Lewis et al. 1999). The main purposes of this study are to characterize the liquefaction potential of aged soil deposits in Mount Pleasant, South Carolina, and to develop a liquefaction potential map for the area based on 1886 ground motion parameters.

This study expands the work of Hayati and Andrus (2008a) who characterized the liquefaction potential of soil deposits on Charleston peninsula through study of cases of liquefaction and ground deformation, and analysis of 44 cone penetration test (CPTu) profiles. Hayati and Andrus (2008a) found that nearly all of the cases of liquefaction and ground deformation during the 1886 earthquake occurred in the Holocene to late Pleistocene beach deposits and man-made fills that flank the higher-ground sediments of the 100,000-year-old Wando Formation. Only one case of documented liquefaction

could be associated with the Wando Formation. They also found that an age correction factor was needed to correctly predict lower liquefaction potential of the Wando Formation on Charleston peninsula.

Previous liquefaction mapping efforts of Mount Pleasant have predicted medium to high hazard levels across much of the area in a future 1886-like earthquake (Balon and Andrus 2006; Juang and Li 2007). Balon and Andrus (2006) analyzed 87 CPTu profiles from the Greater Charleston region and predicted that over 97% of the Mount Pleasant area would experience moderate to severe surface manifestations of liquefaction. Juang and Li (2007) used many of the same CPTu data and came up with a similar prediction. As discussed by Hayati and Andrus (2008a), both of these studies suffer from a lack of adequate attention to geology, a poor understanding of the relationship between 1886 ground behavior and geology, a limited CPTu data set, and a lack of adequate knowledge concerning the influence of soil age on liquefaction resistance.

This study presents for the first time a detailed summary of documented liquefaction and no liquefaction cases that occurred in and around the old town Mount Pleasant in 1886, and plots the cases on the geology map by Weems and Lemon (1993). The cases of liquefaction and no liquefaction are compared with computed liquefaction potentials from 31 CPTu profiles. Based on the computed liquefaction potentials and the geologic map, a new liquefaction potential map of Mount Pleasant is developed and compared with similar sediments on Charleston peninsula.

2.2 Geology and Seismology

The town of Mount Pleasant is located on the east side of Charleston harbor approximately 7 km from Charleston peninsula and the city of Charleston. Separating Mount Pleasant and Charleston peninsula are the Cooper and Wando rivers which flow together into the harbor. Presented in Figure 2.1 is the geologic map of much of present-day Mount Pleasant by Weems and Lemon (1993). At the time of the 1886 earthquake, Mount Pleasant was a small town of about 740 people located south of Shem Creek (McIver 1994, p. 93). The town was severely shaken by the earthquake at 9:54 pm on August 31, 1886. Although there was much damage in the town, no houses were thrown down and there was no loss of life (Berkeley Gazette 1886a).

Weems and Lemon (1993) mapped six surficial geologic units in the Mount Pleasant area (see Figure 2.1). Brief descriptions of these six units, as well as four other units present in the subsurface, are given in Table 2.1. Major Holocene deposits (af, Qal, Qht, parts of Qhec) are confined to the low lying areas adjacent to the harbor, rivers, and creeks. Much of the af deposits were placed after the 1886 earthquake. Also abundant in the low laying areas are younger Pleistocene deposits (parts of Qhec, Qhes). The higher natural ground is formed by older Pleistocene sand deposits (Qws) that are part of the Wando Formation. The average ground surface elevation of Qws is about 4 m above mean sea level.

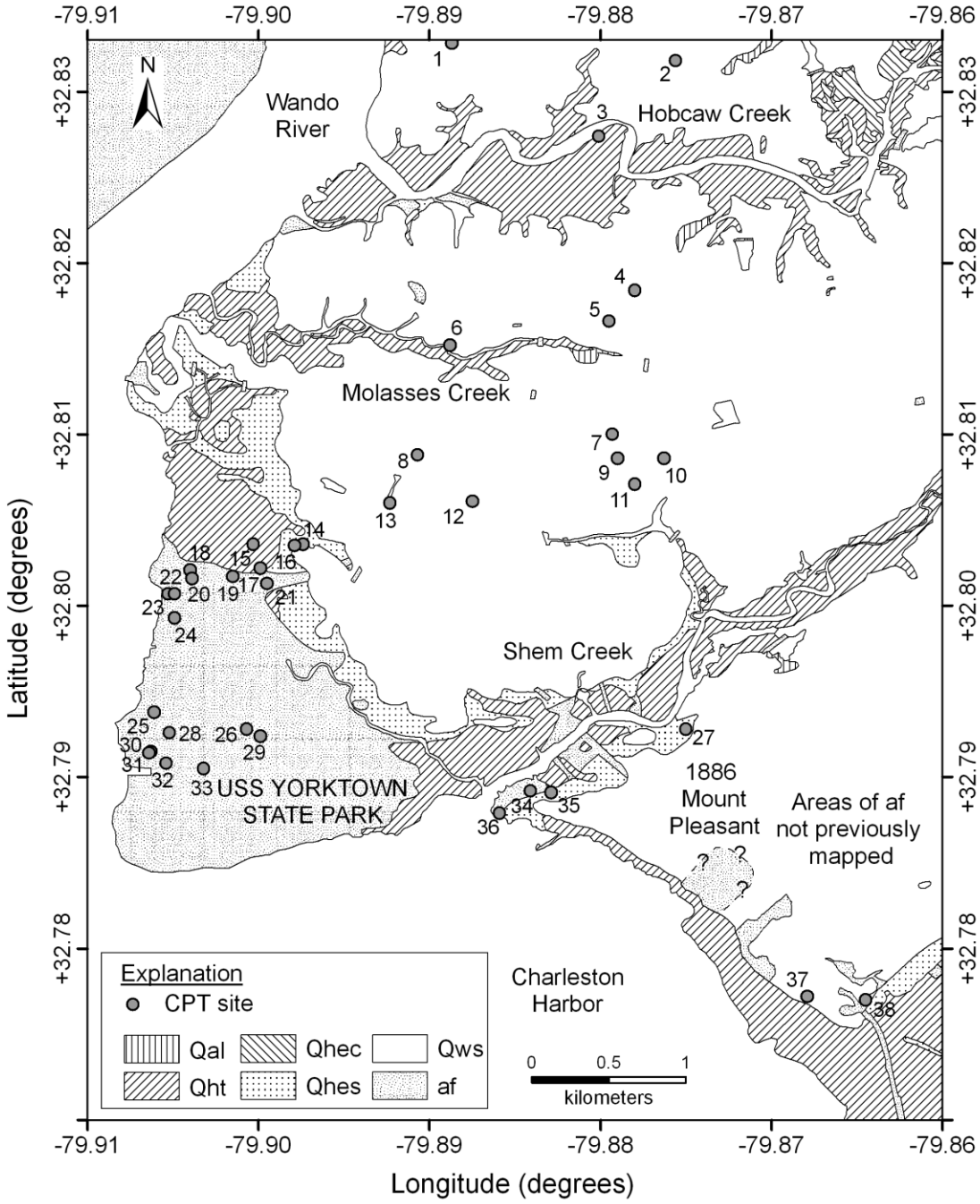

Figure 2.1 Geologic map of Mount Pleasant (adapted from Weems and Lemon, 1993) showing locations of CPTu sites.

Table 2.1 Description of geologic units (adapted from Weems and Lemons 1993; Hayati and Andrus 2008a).

Symbol	Name	Age (years)	Predominant Soil Type	Typical cone tip resistance, q_t (MPa)	Typical shear wave velocity, V_s (m/s)
af	Artificial fill	< 300	Sand, clayey sand	3.1	160
Qal	Holocene alluvium	< 10 k	Sand	-	-
Qht	Holocene tidal-marsh deposit	< 5 k	Organic rich clayey sand, clay	0.5	100
Qhec	Holocene to Pleistocene estuarine deposit	6-85 k	Silty to sandy clay	1.1	140
Qhes	Young Pleistocene beach deposit	33-85 k	Fine grained, well sorted sand	2.6	140
Qws	Wando Formation barrier island sand facies	70-130 k	Fine grained sand	6.2	210
Qwc	Wando Formation estuarine to fluvial facies	70-130 k	Clayey sand, clay	1.6	180
Qds	Daniel Island beds	730-1600 k	Clayey sand, silty to sandy clay, clay	-	-
Tmh	Marks Head Formation	~ 18 M	Fine grained quartz-phosphate sand	-	-
Ta	Ashley Formation of the Cooper Group (Marl)	~ 30 M	Calcarenite, silty clay to clayey silt	3.6 top 25 m	400 Top 25 m

Plotted in the southeast corner of the geologic map shown in Figure 2.1 are four areas of artificial fill (af) not previously mapped by Weems and Lemon (1993). These areas of af, which were placed before the 1886 earthquake, have been added to the map based on a review of early Mount Pleasant history. The old town of Mount Pleasant was established in the mid 1800s by incorporating several small villages and settlements (Greenwich, Mount Pleasant, Hilliardsville, and Lucasville). An early plan drawing of part of the village of Hilliardsville is presented in McIver (1994, p. 30). Shown on that drawing are the locations of three swamp areas. These swamps correspond to the three new areas of af that are surrounded by solid curves in Figure 2.1. The forth new area of af is surrounded by a dash boundary, and includes Ferry Street in the old town. Concerning this area, McIver (1994, p. 29-31) writes:

> The low swampy area was considered unhealthy but Jugnot and Hilliard "By a system of thorough expensive drainage", made the region as healthy as any. Their Ferry Company built a wharf on property known as Shell Hall, which had been the summer home of Charles Pinckney of Snee Farm. Ferry Street was then laid out and led to their long wharf and Ferry House.

Although an early detailed plan drawing of Ferry Street was not available for this study, the above citation provides strong evidence for a swamp and a fill at the Ferry Street location.

It is important to also note that the water front south of Shem Creek was not all Holocene tidal marsh (Qht) deposits in the 1880s, as illustrated in Figure 2.1. McIver (1994, p. 26) writes: "Beach Street was at the time a good sandy stretch with no marsh, it is said to have changed its character when the jetties at the harbor entrance were built." Specific areas of sandy beach are identified on a map presented in City of Charleston (1885). Thus, much of Qht along Mount Pleasant's water front south of Shem Creek (see Figure 2.1) is a thin marsh deposit underlain by beach sand (most likely Qhes).

Other geologic units present in the subsurface include a clayey member of the Wando Formation (Qwc), sandy sediments of the Daniel Island beds (Qds), quartz-phosphate sand of the Marks Head Formation (Tmh), and the calcareous silts and clays of the Ashley Formation (Ta) of the Cooper Group. According to information presented by Weems and Lemon (1993), Tmh is common in the south-eastern half of the mapped area in Figure 2.1 and Ta underlies the entire area. The Cooper Group is locally known as the Cooper Marl and is generally considered as nonliquefiable material (Li et al. 2007; Hayati and Andrus 2008b).

Regarding source and size of the 1886 Charleston earthquake, there is considerable uncertainty. Based on a study of displaced river channels and their relationship with the 1886 epicentral area, Marple and Talwani (2000) concluded that the southern end of the "East Coast fault system", called the Woodstock fault, is the likely source of the Charleston earthquake. The Woodstock fault is approximately 35 km from old town Mount Pleasant. From dating of buried sand blows features in the South

Carolina Coastal Plain, Talwani and Schaeffer (2001) and Talwani and Gassman (2008) estimated a recurrence time of about 500 years for 1886-like earthquakes near Charleston.

Bollinger (1977) developed an isoseismal map for the 1886 earthquake based on a review of damage reported by Dutton (1889). Using this isoseismal map, Bollinger (1986) inferred a seismic moment for the 1886 earthquake which corresponds to a moment magnitude (M_w) of 7.0. Johnston (1996) and Bakun and Hopper (2004) also considered available ground shaking intensity information, but assumed different attenuation models and site corrections, to obtain M_w estimates of about 7.3±0.3 and 6.9±0.3, respectively. Frankel et al. (2002) assumed 7.3 as the largest possible magnitude for the Charleston area in the development of the 2002 update of the National Seismic Hazard Maps.

Values of M_w for the 1886 earthquake have also been estimated using liquefaction and no liquefaction case history data. Martin and Clough (1994) estimated M_w = 7.0-7.5 based on liquefaction evidence in the South Carolina Coastal Plain and liquefaction prediction methods. Hayati and Andrus (2008a) estimated M_w = 6.8-7.3 based on case history data from Charleston peninsula and assuming liquefaction resistance correction factors for aged sands (K_{DR}) proposed by Arango et al. (2000) for Qws (K_{DR} = 1.3 to 2.3). If updated liquefaction resistance correction factors proposed by Hayati and Andrus (2009) are assumed for Qws (K_{DR} = 1.25 to 1.65), the back-calculated range for M_w is 6.8-7.0 based on the Charleston peninsula case history data. This M_w range agrees

remarkably well the range of 6.7-7.0 estimated by Talwani and Gassman (2008) based on liquefaction case history data from the South Carolina Coastal Plain.

Considering both the ground shaking intensity studies and the liquefaction studies, M_w = 6.9 for the 1886 earthquake is assumed in this study of Mount Pleasant.

2.3 Historic Liquefaction Map

Much of the known first-hand observations of liquefaction in Mount Pleasant during the 1886 earthquake are contained in the old town newspaper called *The Berkeley Gazette* and the Charleston newspaper called *The News & Courier*. Summarized in Table 2.2 are ten documented cases of surface effects of liquefaction (e.g., sand boils, fissures, settlement). The locations of these ten cases are plotted on the geologic map shown in Figure 2.2, and were determined using information given in the newspapers or other reports, the June 1893 Digital Sanborn Maps (http://sanborn.umi.com), and the 2009 Google Earth free software. Numerous sand boils occurred along the beach in front of the old town (Case 1). Ejected water and sand also occurred at several locations in the town (Cases 3, 5, 6, 7) and along Shem Creek (Case 9). According to the Berkeley Gazette (1886a) water in nearly every well in the town "was turned a milky white and made unfit for use". Fissures without ejected sand or water were also noted at a few locations (Cases 2, 4, 8).

It should be mentioned that several reported cases of liquefaction and ground deformation that occurred around Mount Pleasant could not be adequately located and are

not listed in Table 2.2. The Berkeley Gazette (1886a) reported flooding in Sam Robinson's and Mr. Lewis' yards, cracks large enough to contain a grown person on Boyd Bro's plantation north of Shem Creek, numerous upheavals on Mr. Edmondston's farm, and large fissures in Hilliardsville including the largest one on Capt. W. M. Hales farm. From the fissures on Capt. Hales farm flowed "thousands of gallons of water and a dozen cartloads of mud and sand". The News & Courier (1886b) also reported that parts of the Georgetown Road leading out of Mount Pleasant for 15 km were perforated with fissures, spouts and upheavals.

Five cases of no surface effects of liquefaction are summarized in Table 2.3. Much of the middle part of the old town was free of fissures and water spouts (Cases A, B, C). In addition, at two locations outside the old town (Cases D, E) very minimal or no evidence of liquefaction was observed by Stephen F. Obermeier during a careful examination of the sides of excavations (Martin and Clough, 1990).

Comparing the locations of liquefaction and no-liquefaction cases with the mapped geology of Mount Pleasant (see Figure 2.2), it is concluded that much of Qhes and younger sandy soil deposits along the beach and creeks liquefied in 1886. On the other hand, little to no liquefaction occurred throughout much of Qws. This conclusion is supported by the fact that only one documented case of minimal liquefaction (Case 10) definitely plots within mapped Qws. Although Case 8 also plots within Qws, it occurs on sloping ground where it is possible an unmapped contact between Qws and Qhes exists. The observation that little or no liquefaction occurred in Qws is similar to the observation

of Hayati and Andrus (2008a) who found only one documented case of liquefaction in Qws in the city of Charleston.

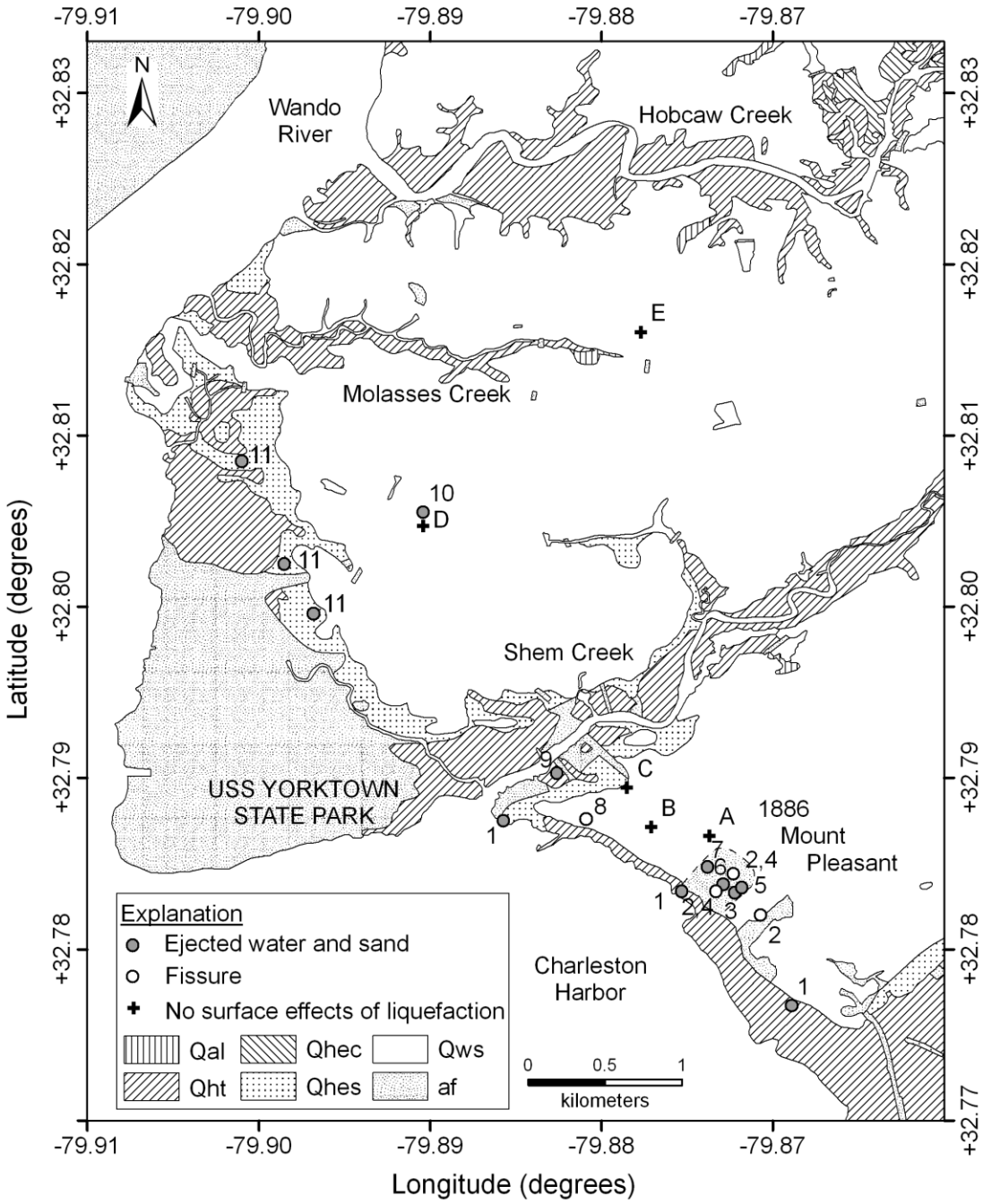

Figure 2.2 Geologic map of Mount Pleasant (adapted from Weems and Lemon 1993) showing locations of 1886 surface effects of liquefaction.

Table 2.2 Cases of surface effects of liquefaction in Mount Pleasant.

Site number and description		Location	Latitude (deg)	Longitude (deg)	Source
1	Hundreds of mounds, with centers filled with "quicksand and fresh water"; brick breakwaters considerably damaged	On beach in front of Mount Pleasant old town	32.7875 32.7834 32.7767	-79.8857 -79.8753 -79.8689	Berkeley Gazette (1886a; 1886b); News & Courier (1886b); City of Charleston (1886, p. 365); Dutton(1889, p. 224)
2	"Upheavals were thickly scattered, nearly always in groups extending in a line more or less serpentine"; fissures up to 150-200 mm wide and as much as 3-5 m long	Ferry street to Hilliardsville	32.7820 32.7834 32.7844	-79.8707 -79.8733 -79.8723	Berkeley Gazette (1886a)
3	"Immense quantities of water and mud were thrown out" of town well and filled the street	Front of Lutheran church, 604 Pitt street	32.7833	-79.8722	Berkeley Gazette (1886a); News & Courier (1886b); City of Charleston (1886, p. 365); Dutton (1889, p. 224)
4	"The brick drain leading through Ferry street was shaken through in several places"	Ferry street	32.7834 32.7844	-79.8733 -79.8723	Berkeley Gazette (1886a)
5	Flooded with the discharge from cracks on the hill side	Back of Lutheran church, 604 Pitt street	32.7836	-79.7818	Berkeley Gazette (1886a); News & Courier (1886a); City of Charleston (1886, p. 365); Dutton (1889, p. 224)
6	"An immense mud spout"	Ferry and Pitt streets	32.7838	-79.8729	News & Courier (1886b)
7	"Fissures and mounds in the rear; in the front, water and mud rushed out of a fissure with such force as to wash away the thickly grown turf for fully [3 m] from the opening"	Gazette office, Bank and Pitt streets	32.7848	-79.8738	Berkeley Gazette (1886a)
8	"Fissures in the street, some running east and west, and some north and south"	George's Hall, 107 Hibben street	32.7876	-79.8809	News & Courier (1886b)
9	Fissures over 3 m long surrounded by sinks of fresh water and mud	A cabin near Shem Creek	32.7903	-79.8826	News & Courier (1886a)

Table 2.2 Cases of surface effects of liquefaction in Mount Pleasant (Continued).

Site number and description	Location	Latitude (deg)	Longitude (deg)	Source
10 Small liquefaction vent	Strip Mall, about 2 km southwest of Mount Pleasant pits site	32.8056	-79.8904	Martin and Clough (1990, p. 258)
11 "Area conspicuous for craterlets"	North of Shem Creek	32.8085 32.8025 32.7996	-79.9010 -79.8985 -79.8968	Dutton (1889, Plate XXVIII)

Table 2.3 Cases of no surface effects of liquefaction in Mount Pleasant.

Site letter and description	Location	Latitude (deg)	Longitude (deg)	Source
A. "No damage was done to the jail"	Jail, Commons street (changed in 1950 to Royall Ave.)	32.7866	-79.8737	Berkeley Gazette (1886a)
B. Area without cavities and water spouts	Middle part of Mount Pleasant village	32.7871	-79.8771	News & Courier (1886b)
C. "Only slight damage to plastering"	Presbyterian church, 302 Hibben street	32.7894	-79.8785	Berkeley Gazette (1886a; 1886b)
D. "Very minimal liquefaction occurred at the site in the form of a small liquefaction vent"	Strip Mall, about 2 km southwest of Mount Pleasant pits site	32.8056	-79.8904	Martin and Clough (1990, p. 258)
E. No signs of liquefaction were observed on sides of pit excavations	Mount Pleasant Pits site, north of Mathis Ferry Road and Ponsbury Road	32.8160	-79.8777	Martin and Clough (1990, p. 258)

2.4 CPTu Database

Locations of 38 CPTu sites compiled for this study are shown in Figure 2.1. Summary information for these CPTu sites is provided in Table 2.4. Site codes begin with a letter representing the organization performing the test. The two digits following the initial letter indicate the year the test was conducted follow by the project number and the test site designation. For example, the site code S00164-B2 refers to a CPTu performed by S&ME in 2000 as part of project number 164 at test location B2.

Electronic files are available for 33 of the 38 CPTu sites plotted in Figure 2.1 (Fairbanks et al. 2004; Mohanan et al. 2006). The other 5 CPTu sites without electronic file are useful for interpreting geology at the specific location, but are not used in the LPI calculations. Twelve of the 38 CPTu sites also have available small-strain shear wave velocity (V_s) measurements.

Table 2.4 Cone soundings from Mount Pleasant.

Site No.	Site Code[a]	Latitude (deg)	Longitude (deg)	Electronic file available?	Maximum test depth (m)	Water table depth (m)	Top of Cooper Marl depth (m)	Top of Wando Formation depth (m)	Near-surface geology category[b]
1	S00164-B2	32.8328	-79.8887	Yes	17.6	2.6	17.3	0.0	E
2	W01135-C1	32.8318	-79.8756	No	7.9	1.8	17[c]	0.0	E
3	S00746-B1	32.8274	-79.8801	Yes	15.2	1.2	15.2[c]	8.0	D_2
4	W03372	32.8184	-79.8780	No	8.3	2.0	20.0[c]	0.0	E
5	S01104-B2	32.8166	-79.8795	No	9.1	2.1	20.0[c]	0.0	E
6	S01112-C1	32.8152	-79.8888	Yes	15.2	1.5	20.0[c]	0.0	E
7	S00340-B2	32.8100	-79.8793	Yes	16.5	1.7	20.0[c]	0.0	E
8	W02103-SC3	32.8088	-79.8907	Yes	16.9	3.0	16.4	0.0	E
9	S01780-B10	32.8086	-79.8790	Yes	24.6	1.8	19.2	0.0	E
10	S01018-B1	32.8086	-79.8763	Yes	24.3	0.5	14.7	0.0	E
11	S01513-B1	32.8071	-79.8780	Yes	18.3	0.9	14.6	0.0	E
12	W02182-SC1	32.8061	-79.8875	Yes	15.9	1.3	16.2?[d]	0.0	E
13	S05196-C1	32.8060	-79.8923	Yes	15.3	2.3	14.9	0.0	E
14	S1772-CPT4	32.8036	-79.8974	Yes	18.0	1.7	15.6	3.0	D_1
15	S04709-C4	32.8036	-79.9003	Yes	24.4	0.6	13.4	5.3	D_1
16	S1772-CPT3	32.8035	-79.8979	Yes	25.8	1.7	12.6	7.5	D_1
17	C98706-C31	32.8022	-79.8999	No	53.6	1.1	15.5	8.5	D_1
18	C98706-C27	32.8021	-79.9040	No	53.6	2.3	19.5	11.0	D_1
19	S99634-DS1	32.8017	-79.9015	Yes	36.6	0.3	12.6	8.0	D_1
20	S99634-C27	32.8016	-79.9039	Yes	27.5	1.2	20.5	12.5	D_1
21	S99634-MPE5	32.8013	-79.8995	Yes	18.3	0.5	14.9	7.8	D_1
22	S99897-B2	32.8007	-79.9053	Yes	25.9	2.4	21.5	12.6	D_1
23	S99897-B5	32.8007	-79.9049	Yes	25.9	2.4	23.0	12.9	D_1
24	S04832-C1	32.7993	-79.9049	Yes	26.8	0.3	22.5	14.0	D_1
25	S01083-B6	32.7938	-79.9061	Yes	23.5	4.3	21.7	8.8	D_3
26	S01735-CPT2	32.7928	-79.9007	Yes	22.7	2.0	22.0	12.6	D_3
27	S02120-B1	32.7928	-79.8750	Yes	22.7	2.0	?	2.6	D_2
28	S01083-B8	32.7926	-79.9052	Yes	23.1	4.3	21.1	12.7	D_3
29	S01735-CPT1	32.7924	-79.8999	Yes	25.3	1.8	22.9	15.2	D_3
30	S00777-B18	32.7915	-79.9063	Yes	24.1	3.4	23.8	9.7	D_3
31	S00777-B16	32.7914	-79.9064	Yes	23.5	3.4	22.6	9.1	D_3
32	S02058-B1	32.7908	-79.9054	Yes	24.3	2.0	22.1	12.2	D_3
33	S00777-SC3	32.7905	-79.9032	Yes	22.2	3.1	20.7	9.4	D_3
34	W01182-C1	32.7892	-79.8841	Yes	15.2	1.8	13.1	6.0	D_2
35	W01268-CPT1	32.7891	-79.8829	Yes[e]	9.1	1.8	7.6	4.5	D_2
36	S02371-C1	32.7879	-79.8859	Yes	15.2	2.1	13.5	7.9	D_2

Table 2.5 Cone soundings from Mount Pleasant (Continued).

Site No.	Site Code[a]	Latitude (deg)	Longitude (deg)	Electronic file available?	Maximum test depth (m)	Water table depth (m)	Top of Cooper Marl depth (m)	Top of Wando Formation depth (m)	Near-surface geology category[b]
37	W03042-C2	32.7772	-79.8679	Yes	15.5	1.6	14.0	0.0	E
38	W01333-C1	32.7770	-79.8645	Yes	15.2	1.5	14.3	2.9	D_2

[a]*First letter in site code: C = ConeTec; S = S&ME; W = WPC.*

[b]*D_1 = Qhes or younger sands present below the groundwater table on the north side of Yorktown State Park; D_2 = Qhes or younger sands present below the groundwater table along Hobcow and Shem Creeks; D_3 = Qhes or younger sands present below the groundwater table in the central part of Yorktown State Park; E = Qws present at the ground surface or the groundwater table.*

[c]*Estimated from Weems and Lemon (1993).*

[d]*? = some uncertainty; value listed is conservative estimate.*

[e]*Not considered in LPI analysis because sleeve friction measurements are not reasonable.*

Representative CPTu, V_s and geologic profiles are presented in Figure 2.3. These profiles are from CPTu site Number 19 (see Figure 2.1). CPTu tip resistances shown in Figure 2.3(a) are corrected to account for the effect of water pressure acting behind the cone tip (q_t). The friction ratio (*FR*) profile shown in Figure 2.3(b) is defined as the cone sleeve resistance measurement (f_s) divided by q_t. Values of *FR* are usually much greater (over 1%) in clayey soils than sandy soils. In Figure 2.3(c), cone pore water pressures (u_2) are measured by a transducer located behind the cone tip, and hydrostatic pore pressures (u_0) are assumed equal to the depth below the groundwater table multiplied by the unit weight of water. Values of u_2 close to u_0 indicate freely draining soil (e.g., sand); and higher u_2 values indicate lower permeable soil (e.g., clay). Thus, in Figure 2.3 the materials at depths of 1.4-3.6 m, 9.2-10.7 m and 12.6-20.0 m are clayey soils. Ranging from about 100 to 400 m/s, values of V_s shown in Figure 2.3(d) are directly related to soil stiffness (i.e., small-strain shear modulus = V_s^2 multiplied by the mass density of the soil).

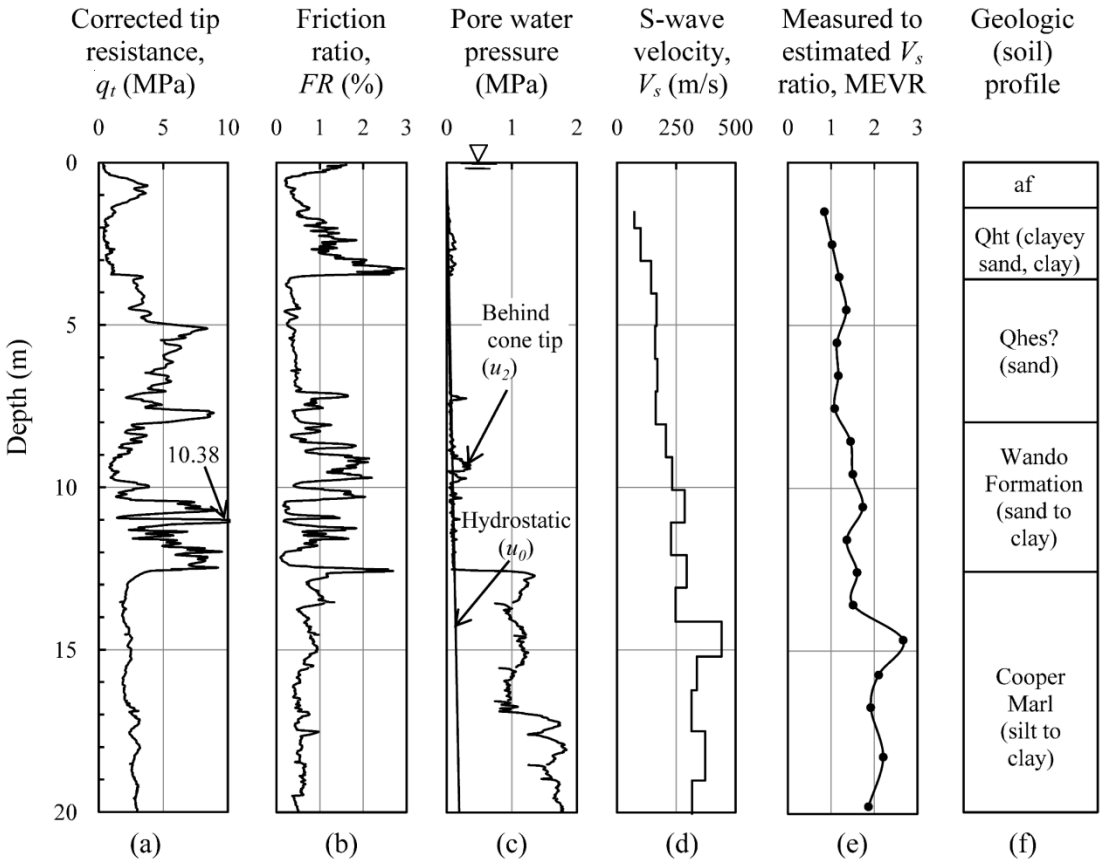

Figure 2.3 Representative profiles of cone, V_s, and geology from CPTu site Number 19.

The ratio of measured-to-estimated shear wave velocity (MEVR) shown in Figure 2.3(e) is an index property that depends on various factors such as time since deposition, degree of cementation, and soil compressibility of the deposit (Andrus et al. 2009). The estimated V_s corrected for overburden stress and fines content is calculated from the following relationship determined for uncemented Holocene-age sands (Andrus et al. 2004a):

$$(V_{s1})_{cs} = 62.6\left[(q_{t1N})_{cs}\right]^{0.231} \tag{2.1}$$

where $(V_{s1})_{cs}$ = equivalent clean sand value of stress-corrected shear wave velocity in m/s, and $(q_{t1N})_{cs}$ = equivalent clean-sand cone tip resistance normalized to atmospheric pressure. To normalize tip resistance and correct to an equivalent clean-sand value, the equations recommended by Youd et al. (2001) have been used. The profile of MEVR in Figure 2.3(e) was determined from dividing the corrected V_s values shown in Figure 2.3(d) by the estimated V_s values using Equation 2.1 and normalized q_t values shown in Figure 2.3(a). MEVR close to 1.0 indicates uncemented 6-year-old soil, while greater MEVRs suggest older and/or cemented soils.

The geologic profile shown in Figure 2.3(f) indicates that materials beneath site Number 19 consist of 1.4 m of af underlain by 2.2 m of Qht. Between 3.6 and 8.0 m, values of MEVR near 1.0 provide evidence that this layer is a younger sand deposit (perhaps Qhes) that may have liquefied in 1886. Between 8.0 and 12.6 m, values of MEVR average around 1.5 suggest materials that are part of the Wando Formation. At

depths greater than 12.6 m, a fairly uniform q_t profile, values of u_2 > 1 MPa and V_s > 300 m/s, and MEVR around 2 are typical of the Cooper Marl.

2.5 Deposits Susceptible to Liquefaction

In general, plastic clayey soils are considered not susceptible to liquefaction (e.g., Seed and Idriss 1982; Robertson and Wride 1998; Youd et al. 2001; Bray and Sancio 2006; Boulanger and Idriss 2006). According to the CPT-based liquefaction susceptibility criteria by Robertson and Wride (1998), soils with soil behavior type index (I_c) more than 2.6 are too plastic to be susceptible to liquefaction. I_c is defined as (Lunne et al. 1997):

$$I_c = [(3.47 - log_{10}Q)^2 + (log_{10}F + 1.22)^2]^{0.5} \tag{2.2}$$

where Q = normalized cone tip resistance, and F = normalized friction ratio.

Considering CPTu data from Charleston, Hayati and Andrus (2008b) concluded that the cutoff I_c value of 2.6 is adequate for identifying the three clayey estuarine deposits (Qht, Qhec, and Qwc) as non-susceptible to liquefaction. Although the deep marine sediments of the Cooper Marl have typical I_c values around 2.4, Hayati and Andrus (2008b) found that much of the Marl exhibits normalized cone pore pressure ratios greater than 0.5 and recommended that the CPT-based criteria be modified to also include this limit. Thus, in Mount Pleasant, only Qws, Qhes and younger sands are considered susceptible to liquefaction.

Summarized in Table 2.5 are average values of V_s, stress- and fines-corrected shear wave velocity [$(V_{s1})_{,cs}$], and MEVR for Qhes and younger sands, and Qws. The criteria for selecting these values were as follows: measurements were below the groundwater table, measurements included at least two V_s test intervals, corresponding test intervals were within a uniform layer, and geology of the layer could be reasonably inferred. The average MEVRs of 1.09 and 1.38 indicate that Qhes has velocities about 9% greater than uncemented 6-year old sand, while Qws has velocities about 38% greater than uncemented 6-year-old sand with the same cone tip resistance. These MEVR values are similar to MEVR values of 0.93 and 1.37 determined by Hayati and Andrus (2008a) for Qhes and Qws on Charleston peninsula.

Andrus et al. (2009) developed the following relationship between MEVR and time since initial deposition or last critical disturbance (e.g., liquefaction) for sands and silty sands ($I_c < 2.25$):

$$\text{MEVR} = 0.0820 \log_{10}(t) + 0.935 \tag{2.3}$$

where t = time in years. Based on Equation 2.3, MEVR should be around 1.11 for sands that liquefied in 1886. As noted in Table 2.5, the computed probabilities that MEVR will be < 1.11 are 56% in Qhes and younger sands and 17% in Qws. These results agree well with the moderate to severe liquefaction observations in Qhes and younger sands, and the little or no liquefaction observations in Qws.

Table 2.6 Measured to estimated V_{s1} ratios for two sands in Mount Pleasant.

Site No.	Depth of susceptible layer[a] (m)	Number of V_s test intervals	Measured: Average V_s (m/s)	Measured: Average $(V_{s1})_{cs}$[b] (m/s)	Estimated: Average $(V_{s1})_{cs}$[c] (m/s)	MEVR[c] average	MEVR[c] range	Probability MEVR < 1.11[e] (%)
(a) Qhes and younger sands								
15	5.6-9.9	4	175	198	190	1.05	0.93-1.33	63
16	1.7-7.5	6	143	177	174	1.02	0.88-1.22	78
19	4.0-8.0	4	165	204	169	1.21	1.12-1.38	20
20	1.2-4.4; 10.5-12.5	2; 2	168	200	181	1.11	1.05-1.17	49
21	1.4-7.4	6	133	176	170	1.04	0.81-1.14	71
Average			157	191	177	1.09		56
(b) Qws								
8	3.0-6.7; 7.7-8.7	3; 1	212	248	185	1.35	0.99-1.76	24
10	1.3-5.1	4	157	220	186	1.18	1.10-1.30	20
12	1.5-6.5	5	214	275	190	1.45	1.07-1.75	13
19	8.1-9.1; 10.1-12.1	1; 2	240	270	168	1.60	1.53-1.74	0
21	7.8-9.4	2	228	252	189	1.33	1.09-1.57	26
Average			210	253	184	1.38		17

[a] *Susceptible if $I_c < 2.6$ and below the groundwater table.*

[b] $(V_{s1})_{CS} = K_{CS} V_s (\frac{P_a}{\sigma'_{V0}})^{0.25}$ *(Robertson et al., 1992; Juang et al., 2002) where $(V_{S1})_{CS}$ = equivalent clean sand overburden-corrected shear wave velocity, K_{CS} =correction factor for fines content, P_a = 100 KPa and σ'_{v0} = initial effective vertical stress.*

[c] *Estimated* $(V_{s1})_{CS} = 62.6\left[(q_{c1N})_{CS}\right]^{0.231}$ *in m/s for uncemented, Holocene clean sand (Andrus et al., 2004a).*

[e] *Assuming normal distribution.*

2.6 Liquefaction Potential Calculation and Analysis

To provide results comparable with the U. S. Geological Survey liquefaction hazard mapping efforts (Holzer et al. 2006, 2009) and the liquefaction potential map of Charleston peninsula by Hayati and Andrus (2008a), similar procedures for calculating liquefaction potential are followed in this study. These previous studies used the liquefaction potential index (LPI) to quantify liquefaction potential. LPI is defined as (Iwasaki et al. 1978, 1982):

$$\mathrm{LPI} = \int_0^{20} F w(z) dz \tag{2.4}$$

where F = a function of factor of safety against liquefaction (FS) defined as $F = 1 - FS$ for $FS \leq 1$ and $F = 0$ for $FS > 1$; z = depth in meters; and $w(z)$ = a depth-weighting factor equal to $10 - 0.5z$. Equation 2.4 considers just the profile in the top 20 m, and weighs factor of safety and thickness of potentially liquefiable layers according to the proximity of layers to the ground surface. LPI values calculated using Equation 2.4 theoretically could range from 0 to 100. The minimum value of 0 is obtained where $FS > 1$ over the entire 20 m depth. The maximum value of 100 is obtained where $FS = 0$ over the entire 20 m depth.

Toprak and Holzer (2003) used CPTu data from sites shaken by the 1989 Loma Prieta California earthquake to calibrate LPI with the severity of surface manifestations of liquefaction. For computing *FS*, they applied the Robertson and Wride (1998) procedure recommended by Youd et al. (2001). Toprak and Holzer (2003) found that

sites in the Monterey Bay region with LPI values of 5 and 15 correspond to probabilities of showing surface manifestations of liquefaction of 58% and 93%, respectively. They concluded that LPI = 5 generally represents the threshold for sand boil generation. These findings are consistent with the severity scale proposed by Iwasaki et al. (1982) based on standard penetration blow counts at Japanese sites.

Factor of safety is defined as the cyclic resistance ratio (CRR) divided by the cyclic stress ratio (CSR). Cyclic stress ratio represents the seismic loading on the soil and can be expressed as (Seed and Idriss 1971; Youd et al. 2001):

$$\mathrm{CSR} = 0.65\left(\frac{a_{\max}}{g}\right)\left(\frac{\sigma_v}{\sigma_v'}\right)(r_d)/(MSF) \tag{2.5}$$

where a_{max} = peak horizontal acceleration at the ground surface; g = acceleration of gravity; σ_v and σ_v' = total and effective vertical overburden stresses, respectively; r_d = stress reduction coefficient; and MSF = magnitude scaling factor that accounts for effects of shaking duration. The procedures to calculate each variable in Equation 2.5 recommended by Youd et al. (2001) are followed in this study.

Cyclic resistance ratio represents the resistance of the soil to liquefaction. For computing CRR from CPTu measurements, the following relationship developed by Robertson and Wride (1998) and recommended by Youd et al. (2001) is used:

$$\text{If } (q_{t1N})_{CS} < 50, \qquad \text{CRR} = 0.833\left(\frac{(q_{t1N})_{CS}}{1000}\right) + 0.05 \tag{2.6a}$$

$$\text{If } 50 \le (q_{t1N})_{CS} < 160, \quad \text{CRR} = 93\left(\frac{(q_{t1N})_{CS}}{1000}\right)^3 + 0.08 \tag{2.6b}$$

It should be noted that Equation 2.6 is primarily based on fairly young soil deposits (Youd et al. 2001).

To account for the effect of aging on CRR, a correction factor is applied according to the following equation (Seed 1979; Arango et al. 2000; Andrus et al. 2004b):

$$\text{CRR}_k = \text{CRR} \times K_{DR} \tag{2.7}$$

where CRR_k = deposit resistance-corrected cyclic resistance ratio. Based on cases of laboratory and/or field tests, Hayati and Andrus (2009) suggested the following relationships to estimate K_{DR} based on time or MEVR:

$$K_{DR} = 0.13\log(t) + 0.83 \tag{2.8}$$

$$K_{DR} = 1.08\text{MEVR} - 0.08 \tag{2.9}$$

where t = time since initial soil deposition or last critical disturbance in years. It should be noted that Equations 2.8 and 2.9 are derived using data from sand and silty sand deposits ($I_c < 2.25$). Because diagenesis may be different in fine-grained soils, Equations 2.8 and 2.9 should be used cautiously in susceptible fine-grained soils ($2.25 < I_c < 2.6$).

In this study, LPI values are obtained from CPTu profiles with acceptable electronic files after first screening out all measurements in the Cooper Marl and any measurement interval above the Cooper Marl with $I_c > 2.6$. Of the 33 CPTu sites with electronic file, 18 extend to depths ≥ 20 m, which is the minimum depth required for LPI calculations. Twelve of the 15 CPTu sites with maximum depths less than 20 m extend into the Cooper Marl. Maximum depths of the other 3 CPTu soundings (Numbers 6, 7, 12) are less than 20 m and do not extend into the Marl. Site Number 6, which extends 4.8 m above the Marl, is not considered in the LPI analysis. For site Number 7, the missing portion between 16.5 and 20 m is assumed to be the same as the 3.5 m above the bottom of the CPTu profile (from 13 to 16.5 m). For site Number 12, the missing 0.3 m portion is assumed to be the same as the last 0.3 m of the CPTu profile. The CPTu from site Number 35 is not considered in the LPI analysis because sleeve friction measurements are not reasonable. Thus, LPI values are calculated for 31 of the 33 CPTu sites.

To simplify the analysis, CPTu sites are grouped into categories and subcategories based on dominant geology in the top 10 m (see last column of Table 2.4). Category D includes sites where Qhes or younger sands are present below the groundwater table. Category D is divided into three subcategories based on location─1) D_1 includes sites located on the north side of USS Yorktown State Park; 2) D_2 includes sites located along the creeks; and 3) D_3 includes sites located in the middle of USS Yorktown State Park. Category E includes sites where the Wando Formation is present at the ground surface or the groundwater table.

For the LPI calculations the middle range M_w of 6.9 and an a_{max} value of 0.25g based on the ground motion study by Chapman et al. (2006) are used. Presented in Figure 2.4 is an example of the LPI calculations applied to site Number 19. Profiles of q_t and I_c versus depth are plotted in Figure 2.4(a) and (b), respectively. Figure 2.4(c) depicts the calculated CSR and CRR values versus depth. Values of *FS* versus depth are presented in Figure 2.4(d). The shaded sections in Figure 2.4(d) are the portions of profile considered non-susceptible to liquefaction and screened out before LPI calculation. Presented in Figure 2.4(e) is the accumulation of LPI with depth. The LPI value obtained for site Number 19 is 34, assuming $K_{DR} = 1.0$ for all layers.

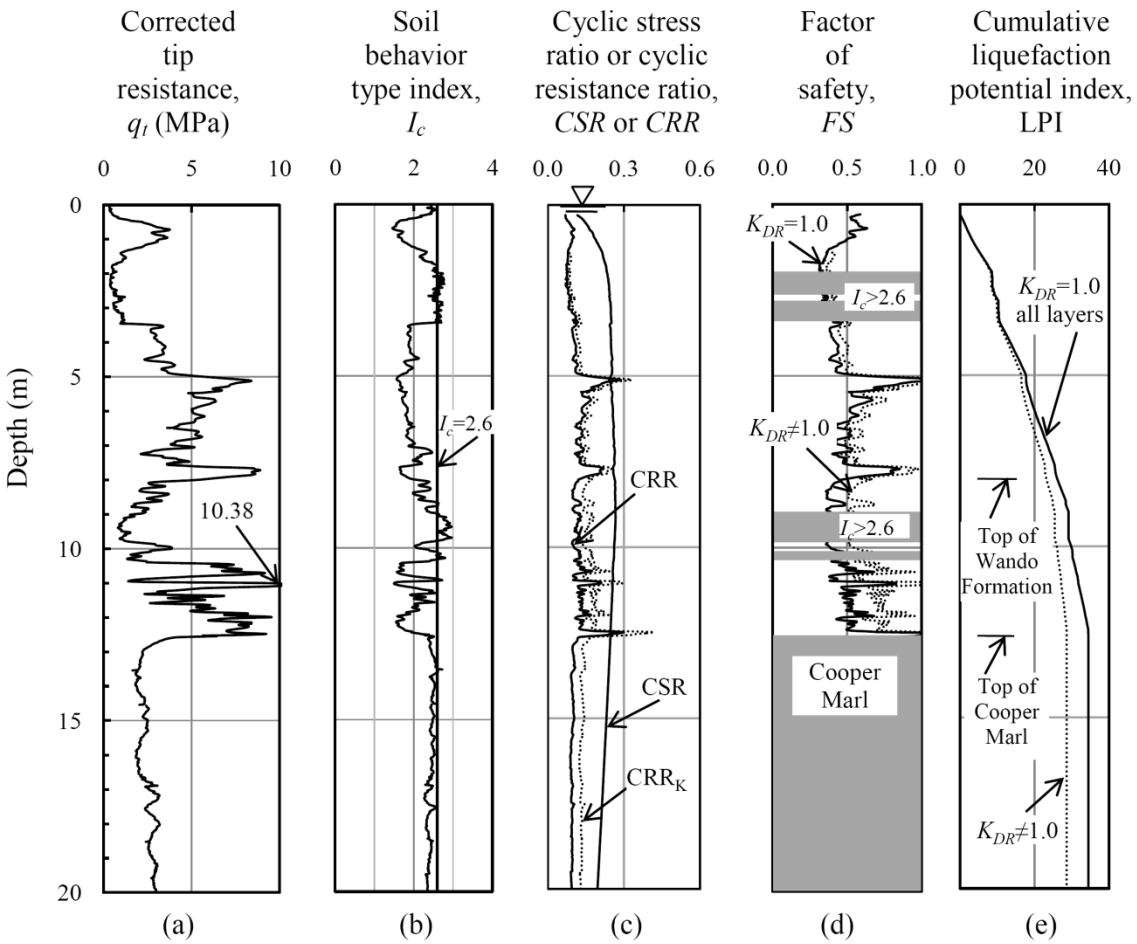

Figure 2.4 Calculation of LPI for CPTu site Number 19 based on M_w = 6.9 and a_{max} = 0.25g.

Summarized in Table 2.6 are median, mean, and ±1 standard deviation values of LPI for the five categories and subcategories. The mean and ±1 standard deviation values are determined assuming a log-normal distribution, as suggested by Balon and Andrus (2006). Assuming K_{DR} = 1.0 for all layers, median LPI values range from 7 to 15 for all categories, suggesting moderate liquefaction potential. A median LPI of 11 for Category E sites is too high because little or no liquefaction was observed in the Wando Formation in 1886. This finding provides additional strong evidence for the need of a deposit resistance correction to CRR.

Assuming the ages of 100,000 years for the Wando Formation and 500 years for the previous time Qhes and younger sand deposits liquefied, K_{DR} values of 1.5 and 1.2 are obtained, respectively, from Equation 2.8. From Equation 2.9, K_{DR} values of 1.4 and 1.1 are obtained assuming average MEVRs of 1.38 for the Wando Formation and 1.11 for Qhes and younger sands. A MEVR of 1.11 is assumed for Qhes and younger sands as an estimate for deposits that are 120 years old (Andrus et al. 2009), the time since 1886. Based on these estimates, average K_{DR} values of 1.45 and 1.15 are assumed for the Wando Formation and Qhes and younger sand deposits, respectively, for an improved LPI analysis of Mount Pleasant.

Table 2.7 Statistic of LPI assuming $M_w = 6.9$ and $a_{max} = 0.25$g.

Near-surface geology category	Number of CPTus	$K_{DR} = 1.0$ for all layers		$K_{DR} = 1.15$ for Qhes and younger $K_{DR} = 1.45$ for Qws	
		Median (Mean) LPI*	±1 Standard deviation*	Median (Mean) LPI*	±1 Standard deviation*
D_1	9	15 (17)	9-24	9 (13)	4-21
D_2	5	10 (11)	6-16	5 (6)	2-10
$D_{1\&2}$	14	13 (14)	8-21	7 (10)	3-17
D_3	8	7 (8)	4-12	3 (3)	1-5
E	9	11 (12)	8-16	4 (5)	3-7

**Assuming log-normal distribution*

Presented in the last two columns of Table 2.6 are median, mean, and ±1 standard deviation values of LPI assuming $K_{DR} \neq 1$. Median LPI values are 9, 5, 3 and 4 for categories D_1, D_2, D_3 and E, respectively. A median LPI value of 4 for E sites agrees well with the observations of little or no liquefaction in 1886. A median LPI value of 5 for D_2 sites seems low for younger deposits adjacent to the creeks, and may be due to the limited test data available. For this reason, D_1 and D_2 sites have been combined to provide a more reasonable median LPI of 7 for deposits adjacent to creeks. Based on a careful review of the CPTu profiles of D_3 sites, much of the near surface sediments are clayey (Qht or Qhec) above Qws. Thus, a median LPI of 3 seems appropriate for the D_3 sites.

2.7 1886 Liquefaction Potential Map

The corrected LPI values based on K_{DR} = 1.45 for the Wando Formation, K_{DR} = 1.15 for Qhes and younger sands, M_w = 6.9 and a_{max} = 0.25 g are used to create the 1886 liquefaction potential map. Following the mapping approach of Holzer et al. (2006), probability of exceeding LPI = 5 is used to characterized the zones of different liquefaction potential. Presented in Figure 2.5 are five LPI versus complementary cumulative distribution curves fitting lognormal distributions for each category. As can be seen in Figure 2.5, the probabilities of exceeding LPI of 5 are 65%, 15% and 30% for Categories $D_{1\&2}$, D_3 and E, respectively.

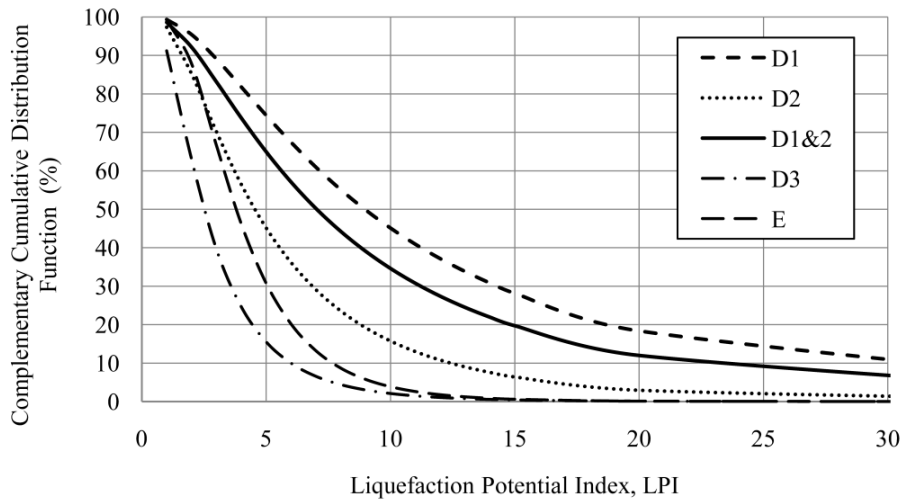

Figure 2.5 Complementary cumulative distribution functions of LPI for various site categories assuming M_w = 6.9, a_{max} = 0.25g, K_{DR} = 1.45 for the Wando Formation, and K_{DR} = 1.15 for Qhes and younger sands.

Shown in Figure 2.6 is the Mount Pleasant area divided into three liquefaction potential zones. Also plotted on the map are LPI values for the CPTu sites with available electronic files. The zone of 65% probability of exceeding LPI of 5 includes all areas covered by af, Qhes, Qhec, Qht and Qal on the geology map by Weems and Lemon (1993); except the south-western part of USS Yorktown State Park. Because no test data are available for the portion of Daniel Island located in north-western corner of the study area, that area is included in the 65% zone. The prediction of 65% probability is supported by the many cases of 1886 liquefaction and ground deformation that occurred along the creeks and rivers. The three cases of LPI $\geq$ 15 indicate severe liquefaction potential at some locations in the 65% zone.

The zone of 30% probability of exceeding LPI of 5 corresponds to areas where Qws is exposed at the ground surface. The two sites with 5 < LPI < 15 indicate moderate liquefaction potential is possible at some locations, which agrees with the small liquefaction vent reported by S. F. Obermeier at the mall construction site (Case D). The 30% probability of exceeding LPI of 5 is also supported by the cases of no surface effects of liquefaction (Cases A, B, C, E).

The zone of 15% probability of exceeding LPI of 5 includes an area covered by af in the south-western part of USS Yorktown State Park where 8 CPTu profiles are available. It is possible that there are other areas along the harbor, rivers and creeks with similar low probability of exceeding LPI of 5, due to thick clayey sediment deposits.

Further testing is needed to confidentially identify other areas with 15% probability of exceeding LPI of 5.

The computed liquefaction potentials of soil deposits in Mount Pleasant are similar to deposits on Charleston peninsula. Hayati and Andrus (2008a) calculated 95% and 45% probabilities of exceeding LPI of 5 for the Qhes and younger sand sites and the Wando Formation sites, respectively, assuming M_w = 7.1, a_{max} = 0.3 g, K_{DR} = 1.8 for the Wando Formation, and K_{DR} = 1.0 for all younger materials. When these assumptions are applied to the Mount Pleasant CPTu profiles, 85% and 40% probabilities of exceeding LPI of 5 are obtained. Thus, in both areas, the liquefaction potentials are similar and about two times greater in Qhes and younger sands, than in Qws.

The liquefaction potential map shown in Figure 2.6 serves as a useful tool for planners and engineers working to mitigate liquefaction hazards in Mount Pleasant in future earthquakes. Areas mapped as 65% probability of LPI ≥ 5 should be expected to experience moderate to severe liquefaction and ground deformation in a future 1886-like earthquake. Buildings and utilities that straddle the zones of 65% and 30% probability of LPI ≥ 5 are particularly vulnerable to failure caused by lateral ground displacement. Although areas of lower probability of liquefaction suggest less potential for ground deformation, site specific evaluations should be done for final project design.

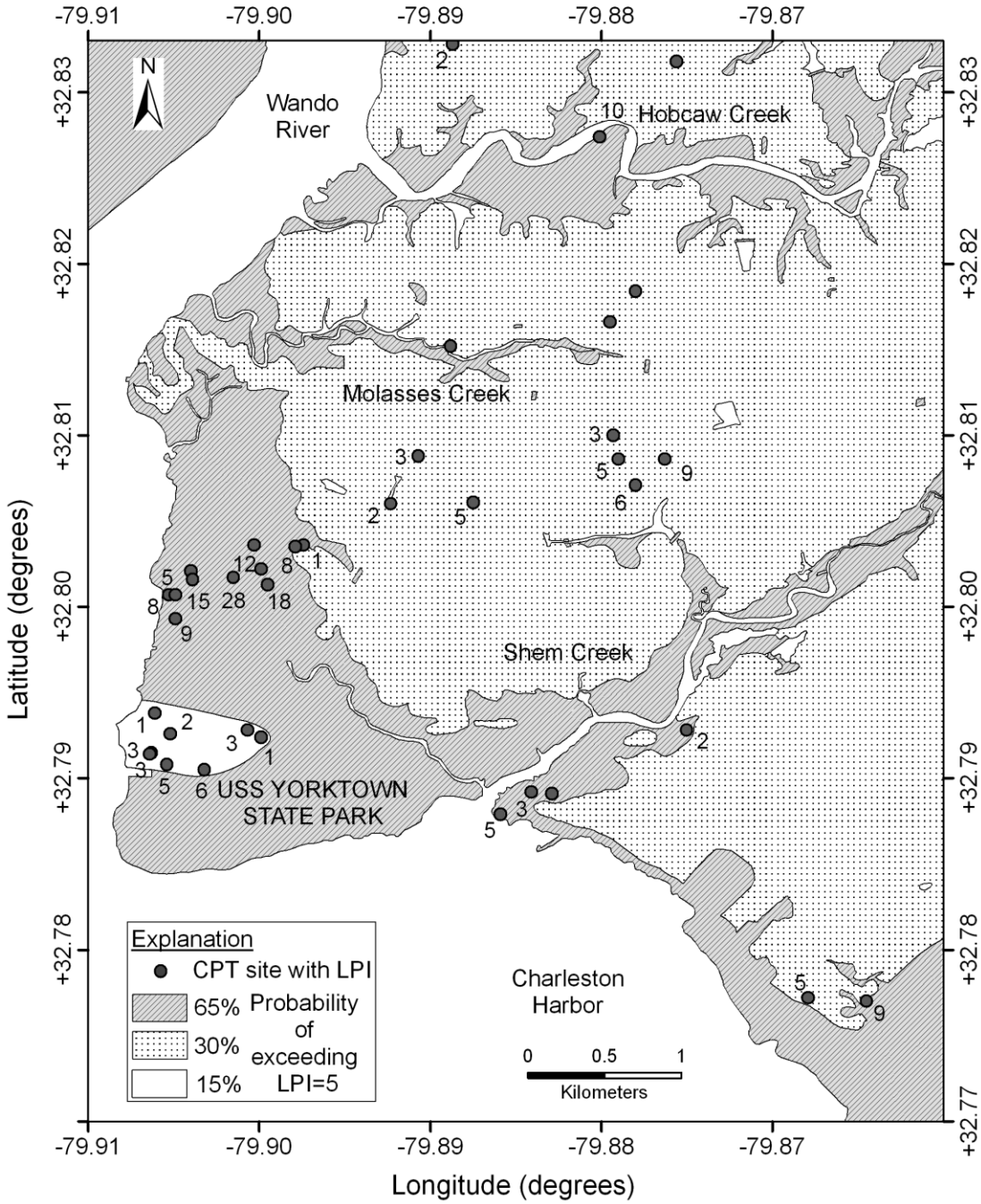

Figure 2.6 Liquefaction potential map of Mount Pleasant based on 1886 field performance data and deposit resistance-corrected LPI assuming M_w = 6.9, a_{max} = 0.25g, and $K_{DR} \neq 1$.

2.8 Conclusion

Liquefaction potential of soil deposits in Mount Pleasant was characterized through careful review of early Mount Pleasant history, comparison of 1886 ground behavior with geology, and analysis of available CPTu and V_S measurements. Based on the review of early Mount Pleasant history, four areas of af not previously mapped were identified and added to the geologic map by Weems and Lemon (1993). It was also noted that much of the Qht deposit along Mount Pleasant water front south of Shem Creek is thin and underlain by beach sand.

Eleven cases of 1886 surface effects of liquefaction and ground deformation, and four cases of no surface effects of liquefaction were located. Nine of the eleven cases of surface effects of liquefaction plotted in Qhes and younger sandy soil deposits. The four cases of no surface effects of liquefaction plotted in Qws deposits.

The finding that Qws had significantly less potential for liquefaction than Qhes and younger sands was supported by measured-to-estimated shear wave velocity ratios. The ratios indicated that Qhes/younger sands and Qws have velocities 9% and 38%, respectively, greater than typical shear wave velocities in uncemented 6-year-old sands with the same cone tip resistances.

LPI values were computed from 31 CPTu profiles, after first screening out layers not susceptible to liquefaction. The middle range M_w of 6.9 and a_{max} of 0.25 g were used for calculation of CSR. Assuming K_{DR} = 1.0 for all geology units, median LPI values for five site categories or subcategories ranged from 7 to 15, suggesting moderate to high

liquefaction potential for the entire Mount Pleasant area. Because a median LPI of 11 computed for Category E (Qws) sites did not agree with observed field behavior, the LPI calculations were repeated using K_{DR} correction factors estimated from the age/MEVR relationships proposed by Hayati and Andrus (2009). The adjusted LPI analysis resulted in median LPI values of 4 for Category E (Qws) sites and 7 for Category $D_{1\&2}$ (Qhes and younger sand deposits along streams) sites.

A liquefaction map of Mount Pleasant was created by dividing the area into three liquefaction zones characterized with 65%, 30% and 15% probability of LPI $\geq$ 5. The zone of 65% probability of exceeding LPI of 5 includes all areas covered by af, Qhes, Qhec, Qht and Qal, except an area in the south-western part of USS Yorktown State Park. The zone of 30% probability corresponds to areas where Qws is exposed at the ground surface. The zone of 15% probability includes part of the area covered by af in the USS Yorktown State Park, where thick clayey sediment deposits are present. The map provides useful information needed for mitigating liquefaction damage in future earthquakes, but should not replace site-specific evaluations for final project design. Additional CPTu data are needed to refine the liquefaction potential map.

CHAPTER THREE

LIQUEFACTION POTENTIAL OF PLEISTOCENE SANDS IN THE CHARLESTON AREA, SOUTH CAROLINA*

3.1 Introduction

Liquefaction potential of Pleistocene sand deposits in the Charleston area, South Carolina, is characterized in this chapter. The characterization involves reviewing cases of conspicuous craterlets and horizontal ground displacement that occurred in sand deposits during the 1886 Charleston earthquake, and analyzing eighty-two seismic cone soundings. Also presented for the first time is an investigation of the influence of distance to the inferred 1886 fault on MEVR and liquefaction potential for major sand deposits in the Charleston area. Liquefaction potential is computed in terms of the liquefaction potential index (LPI) originally introduced by Iwasaki et al. (1978) and using eighty-two seismic cone penetration tests with pore pressure measurements (SCPTu) from the Charleston area. The LPI approach is adopted for this study because: (1) it provides a single value of liquefaction potential for a site, rather than a profile of

---

* A similar form of this chapter has been submitted to ASCE Journal of Geotechnical and Geoenvironmental Engineering for possible publication; Heidari, T., and Andrus, R. D. (2011). "Liquefaction Potential of Pleistocene Sands in the Charleston Area, South Carolina."

potentials with depth, and (2) the results can be compared with previous studies (Holzer et al. 2006, 2009; Balon and Andrus 2006; Lenz and Baise 2007; Rix and Romero-Hudock 2007; Cramer et al. 2008; Hayati and Andrus 2008a; Heidari and Andrus 2010).

3.2 Geology and Seismology

A map of the Greater Charleston area is shown in Figure 3.1. The area is located in the outer (or lower) Atlantic Coastal Plain and includes the 1886 meizoseismal region. Based on an extensive auger drilling program, geologic maps and cross sections for eighteen 7.5-minute quadrangles in the area have been published by the U.S. Geological Survey (e.g., Weems and Lemon 1988, 1993, 1996; Weems et al. 1997). Rectangular grid lines in Figure 3.1 represent the boundaries of 7.5-minute quadrangles.

The entire study area is generally covered by a blanket of Quaternary (< 1.8 million years) sand to clay that obscures underlying Tertiary stratigraphic units (Weems and Lewis 2002). Seven Quaternary sand deposits (or facies) present in the area are: Holocene beach to barrier island sand deposits (Qhs); 33,000- to 85,000-year old beach to barrier island sand deposits called the Silver Bluff terrace (Qhes); barrier island sand facies of the 100,000-year-old Wando Formation which form the Mount Pleasant barrier system (Qws); barrier sand facies of the earlier Wando Formation which form the Awendaw barrier system (Qwls); clean sand facies of the 200,000-year-old Ten Mile Hill beds which form the Cainhoy barrier system (Qts); clean sand facies of the 400,000-year-old Ladson Formation (Qls); and clean sand facies of the > 700,000-year-old Penholoway

Formation (Qps). Deposits of Qhs and Qhes are confined to the lower lying areas adjacent to the rivers, creeks, and coast line. Deposits of Qws form the higher natural ground along the coast. Deposits of Qwls are mainly found 16 to 22 km from the coast line, and are similar in lithology to Qws. Deposits of Qts are typically found 18 to 27 km from the coast line. Deposits of Qls and Qps are mainly found 36-42 km and 42-54 km, respectively, from the coast line.

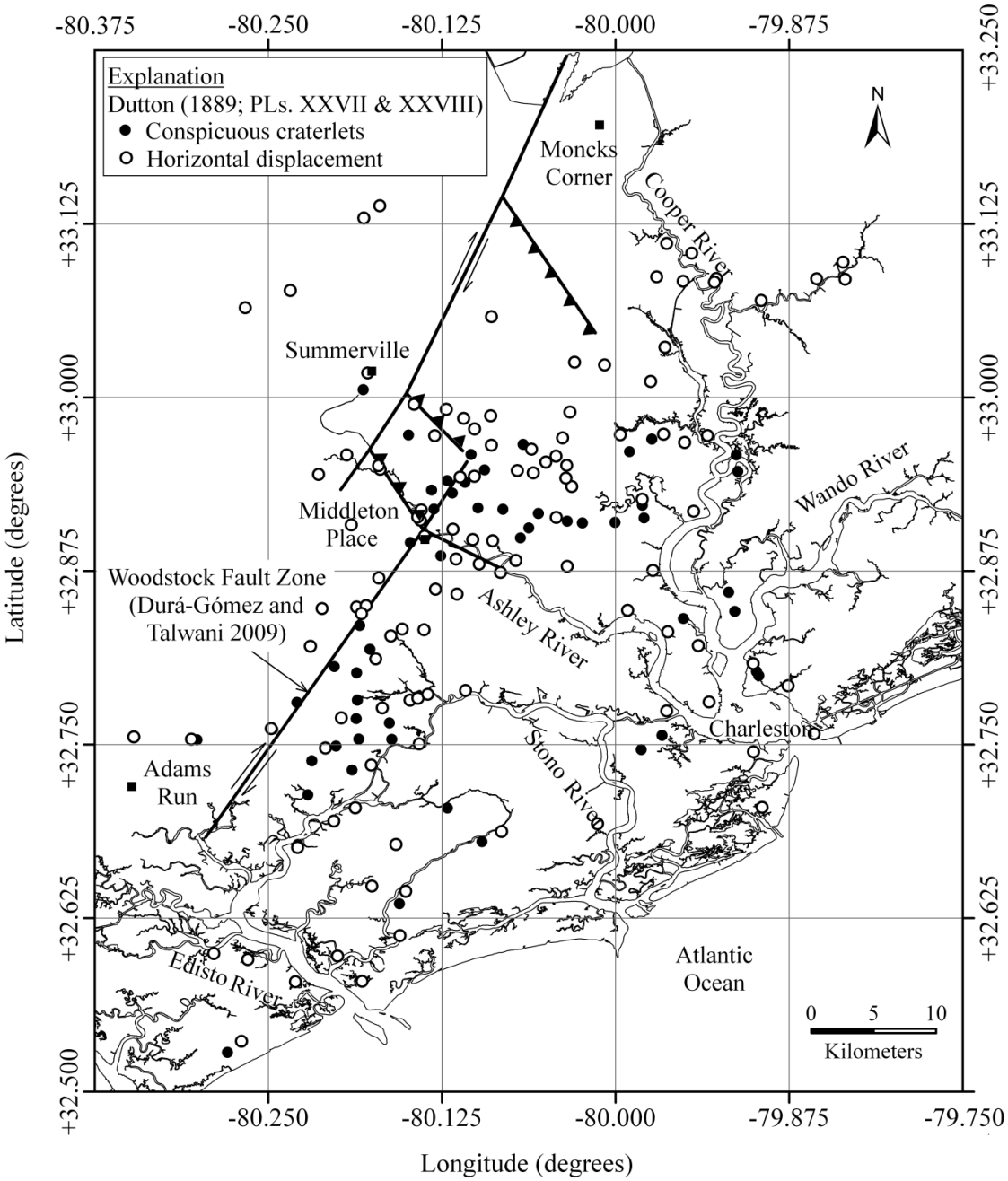

Figure 3.1 Map of the Greater Charleston area showing the inferred Woodstock fault presented in Durá-Gómez and Talwani (2009) and locations of 1886 liquefaction and ground failure from Dutton (1889).

Underlying the Quaternary deposits throughout much of the area are calcareous silts and clays of the Tertiary-age Ashley Formation of the Cooper Group. The Cooper Group is locally known as the Cooper Marl, and extends to depths of over 100 m below mean sea level. Locations where the Ashley Formation is not present in the subsurface include: an area south of the Edisto River which is underlain by the Dryton Limestone beds; an area south and west of the Stono River which is underlain by the Parker's Ferry Formation of the Cooper Group; and an area south of Moncks Corner which is also underlain by the Parker's Ferry Formation.

Durá-Gómez and Talwani (2009) provided a summary of previous seismological studies and the latest analysis of available seismic data. Shown in Figure 3.1 is the inferred trace of the Woodstock fault, the likely source of the 1886 Charleston earthquake. The fault trace was inferred from macroscopic observations following the 1886 earthquake, analysis of instrumentally recorded seismicity between 1974 and 2004, and study of displaced river channels. The Woodstock fault was characterized as a right-lateral strike slip fault oriented N30°E with an antidilatational compressional left step near Middleton Place which divides it in two parts. Both the north and the south parts of the Woodstock fault deep steeply (≥ 50º) to the northwest. Focal depths of instrumentally recorded earthquakes range from 3 to 16 km. Chapman and Beale (2010) studied reprocessed seismic refraction profiles of the area and concluded that the 1886 earthquake occurred due to compressional reactivation of a Mesozoic extensional fault in pre-Cretaceous crystalline basement rock.

Estimates of earthquake moment magnitude for the 1886 event range from 6.6 to 7.5. These estimates are based on analysis of 1886 ground shaking intensify information (Bollinger 1986; Johnston 1996; Bakun and Hopper 2004) or liquefaction case history data (Martin and Clough 1994; Talwani and Gassman 2008; Hayati and Andrus 2008a; Heidari and Andrus 2010). Paleoliquefaction studies in the South Carolina Coastal Plain suggest a recurrence rate of about 500 years for magnitude 7+ earthquakes near Charleston (Talwani and Schaeffer 2001).

3.3 1886 Liquefaction and Ground Failure

Extensive surface manifestations of liquefaction were observed throughout the Greater Charleston area in 1886 (Dutton 1889), as shown in Figure 3.1. The latitudes and longtitudes of these cases are presented in Appendix A. Presented in Tables 3.1 and 3.2 are summaries of these areas of horizontal ground displacement and conspicuous craterlets (i.e., intense ejection of sand and water), respectively, mapped by Earle Sloan (Dutton 1889, PL. XXVII and PL. XXVIII) grouped by surficial sand deposits. The range and mean/median distances to the Woodstock fault are indicated for each group. It is interesting to note in Tables 3.1 and 3.2 that the furthest distances of ground failure for each group increases with decreasing geologic age.

Plotted in Figure 3.2 are the numbers of mapped horizontal displacement and craterlet areas grouped by surficial sand deposits. Nearly half of the ground displacement and craterlet areas are associated with Qts surficial deposits. The close proximity of Qts

deposits to the Woodstock fault is a primary factor contributing to their high liquefaction potential. The fewer number of ground displacement and craterlet areas in Qws and Qwls suggests significantly lower liquefaction potentials in these deposits. Although Qwls are very similar in lithology to Qws, closer proximity to the Woodstock fault may explain the greater number of liquefaction areas in Qwls than in Qws. Although Qhes deposits are generally located farther from the fault, the greater number of ground displacement and craterlet areas suggest that their younger age may have been a factor. The fact that only one area of mapped horizontal ground displacement occurred in Qhs deposits may be explained the greater distance these deposits are from the fault.

The frequency of mapped ground failures shown in Figure 3.2 agrees well with the previous liquefaction studies of Charleston Peninsula and Mount Pleasant. Hayati and Andrus (2008a) documented twenty-seven cases of liquefaction and ground deformation located in Qhes and af/Qhes deposits. Only one case of ground deformation could be associated with Qws deposits on Charleston Peninsula. Heidari and Andrus (2010) reported ten cases of liquefaction and ground deformation in Qhes and younger sand deposits, and only one case of minimal liquefaction in Qws in Mount Pleasant.

It should be noted that Tables 3.1 and 3.2, and Figure 3.2, summarize only the areas of major ground failure mapped by Earle Sloan. Based on review of firsthand accounts of the 1886 earthquake, additional less conspicuous ground failures occurred at many other locations, including in Qps.

Table 3.1 Summary of 1886 ground displacement mapped by Earle Sloan (Dutton 1889, PL. XXVII) for seven Quaternary seven sands.

Surficial Geology	Range of geologic age (years)[a]	Number of mapped areas	Distance to Woodstock fault (km)	
			Range	Mean (Median)
Qhs	< 10 k	1	31.0	31.0 (31.0)
Qhes	33-85 k	7	13.0-27.6	17.9 (15.3)
Qws	70-130 k	3	4.7-16.5	9.1 (6.2)
Qwls	70-130 k	4	3.2-15.2	7.0 (4.8)
Qts	200-240 k	9	0.6-12.2	4.9 (4.8)
Qls	240-730 k	2	0.9-3.0	2.0 (2.0)
Qps	730-970 k	0	-	-

Table 3.2 Summary of 1886 conspicuous craterlet areas mapped by Earle Sloan (Dutton 1889, PL. XXVIII) for seven Quaternary sands.

Surficial Geology	Range of geologic age (years)[a]	Number of mapped areas	Distance to Woodstock fault (km)	
			Range	Mean (Median)
Qhs	< 10 k	0	-	-
Qhes	33-85 k	5	14.0-25.5	22.3 (24.6)
Qws	70-130 k	2	16.2 to 17.3	16.8 (16.8)
Qwls	70-130 k	4	3.0 to 6.8	4.6 (4.4)
Qts	200-240 k	14	0.2 to 12.8	6.9 (6.2)
Qls	240-730 k	0	-	-
Qps	730-970 k	0	-	-

[a] *Weems and Lemon (1993, 1996).*

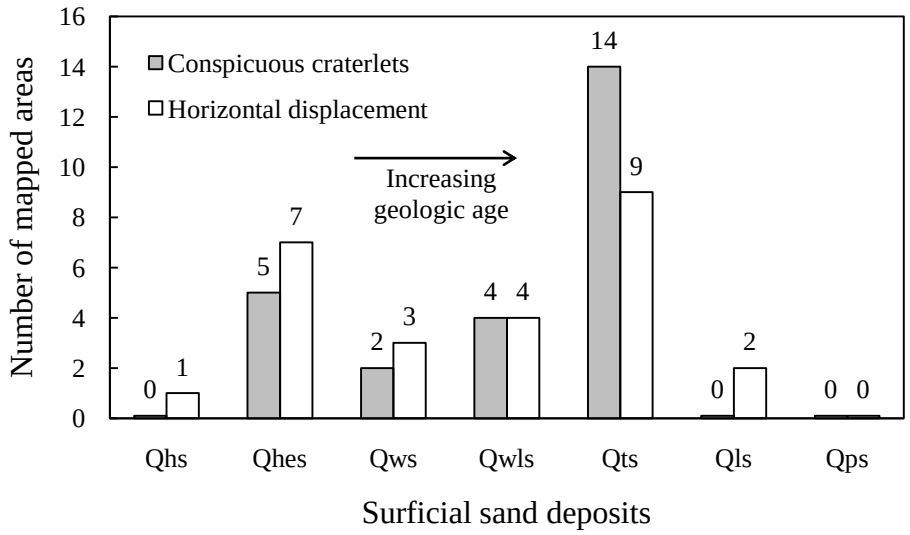

Figure 3.2 Frequency of mapped 1886 craterlet and ground displacement areas (Dutton 1889) grouped by surficial sand deposits.

3.4 SCPTu Database

Locations of the eighty-two SCPTu sites are shown in Figure 3.3. Summary information for the SCPTu sites is provided in Table 3.3. Site codes give in Table 3.3 begin with a letter representing the organization performing the test. The two digits following the initial letter indicate the year the test was conducted, and are followed by the project number and the test site designation. For example, the site code W02130-SC8 refers to a SCPTu performed by WPC in 2002 as part of project number 130 at test location SC8. SCPTu profiles for site Nos. 31-33 were published in Boller et al. (2008); and sites Nos. 70-72 and 78-82 were published in Hu et al. (2002). Latitudes and longitudes were approximated using project site address information and the GoogleEarth free software. Location accuracy of the SCPTu sites is believed to be within 100 m. The distance to inferred Woodstock fault is the shortest length between the site and the Woodstock fault shown in Figure 3.3. Electronic files for most of the SCPTu profiles are available in Fairbanks et al. (2004) and Mohanan et al. (2006).

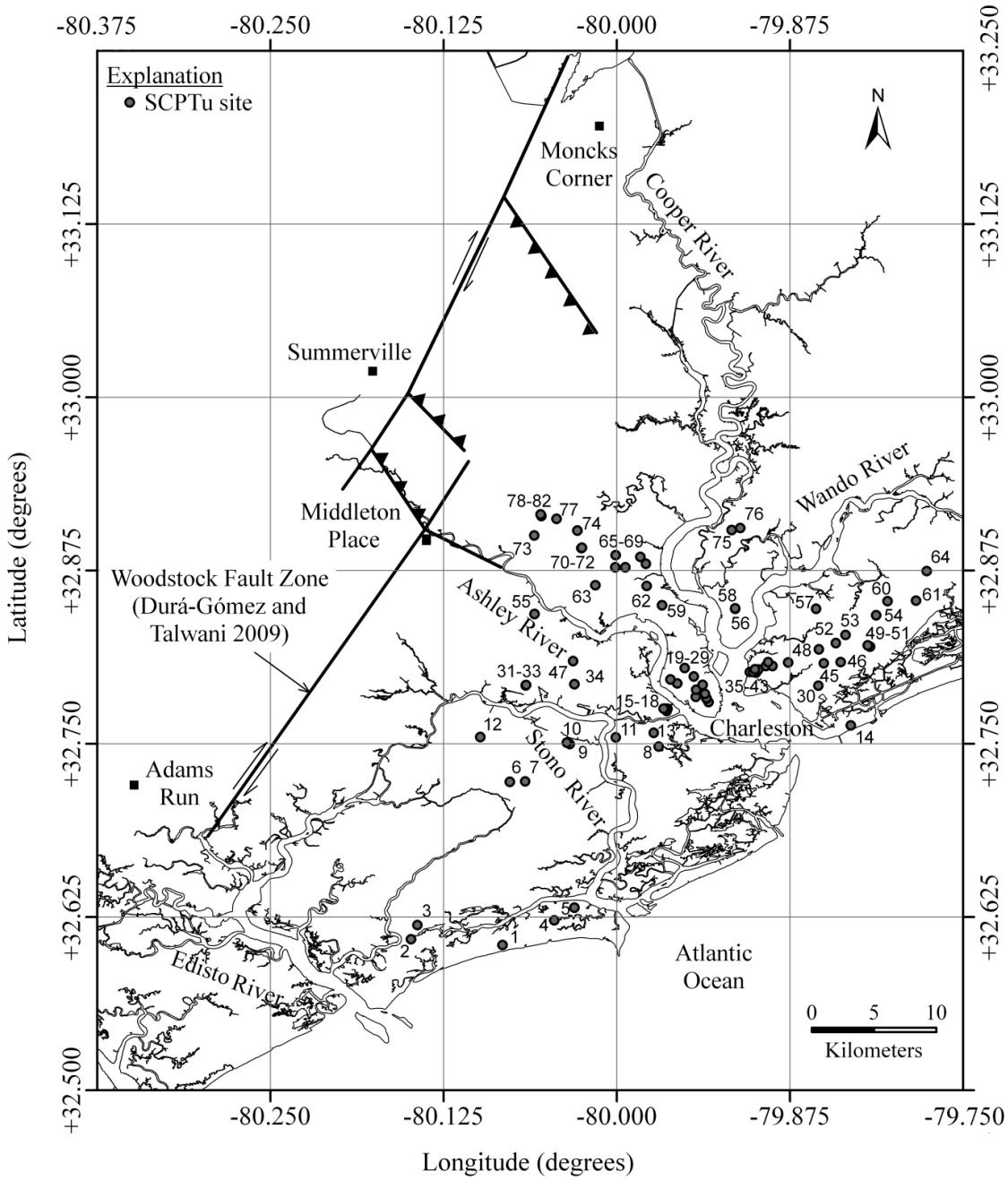

Figure 3.3 Map showing the inferred Woodstock fault presented in Durá-Gómez and Talwani (2009) and location of SCPTu sites plotted in surficial sand deposits.

Table 3.3 SCPTu soundings from the Greater Charleston area that plot in surficial sand deposits.

Site No.	Site code[a]	Latitude (deg)	Longitude (deg)	Distance to Woodstock fault (km)	Water table depth (m)	Maximum test depth (m)	Top of the Cooper Marl depth (m)	Surficial geology
1	S03305-B1	32.6047	-80.0824	21.61	1.5	14.8	18.7?	Qhes
2	W02130-SC8	32.6089	-80.1485	16.04	1.5	18.0	-	Qhes
3	W02096-SCPT1	32.6191	-80.1438	15.83	1.8	19.9	19.2	Qws
4[d]	S03304-B1	32.6225	-80.0451	23.59	1.2	20.0	18.7	Qht
5[d]	S02522-B4	32.6317	-80.0306	24.23	1.3	26.3	22.8	Qht
6	S00297-SC1	32.7225	-80.0772	15.30	1.8	14.5	14.5?[e]	Qws
7	W01339-SC1	32.7227	-80.0660	16.19	1.5	12.8	11.0?[e]	Qws
8	W03045-SC2	32.7478	-79.9697	22.50	1.8	18.0	14.2	Qws
9	W01211-SCPT9	32.7496	-80.0339	17.24	1.4	12.9	12.5	Qws
10	W01211-SCPT4	32.7508	-80.0360	17.00	1.5	11.9	11.5	Qws
11[d]	W03044-SC1	32.7546	-80.0006	19.63	1.0	11.6	12.0[b]	af
12[d]	W02212-SCPT1	32.7548	-80.0985	11.75	1.2	15.1	-	Qws
13	W04111-SC1	32.7578	-79.9732	21.65	1.8	13.7	15.2[b]	Qws
14[d]	W03071-SC1	32.7631	-79.8311	32.79	0.5	14.0	15.0[b]	af
15	W03367-SC1	32.7735	-79.9639	21.22	1.6	15.0	13.6	Qws
16	W03088-SC1	32.7751	-79.9634	21.50	0.6	14.0	12.7	Qhes
17	W03337-SC1	32.7752	-79.9649	21.32	1.5	13.7	13.7?[c]	Qws
18	W04131-SC1	32.7753	-79.9661	21.45	1.6	13.7	13.6	Qws
19	W00363-SCPT1	32.7799	-79.9337	23.56	2.3	18.9	17.9	Qws
20	S02457-B2	32.7824	-79.9352	22.32	1.8	21.6	>21.3	Qws
21	S02457-B1	32.7828	-79.9352	23.30	1.4	25.3	22.5	Qws
22	S02578-B1	32.7839	-79.9429	22.59	1.5	20.4	21.9	Qhes
23	S03462-S1	32.7858	-79.9363	23.02	0.9	30.4	28.3	Qws
24	W02288-SC2	32.7889	-79.9427	22.60	2.3	16.7	15.5	Qhes
25	W04030-SC1	32.7924	-79.9380	22.50	2.5	19.8	17.1	Qws
26	S01039-B4	32.7934	-79.9563	20.97	2.0	22.8	15.0	Qws
27	S01317-B2	32.7964	-79.9613	20.40	2.1	22.8	15.2	Qws
28[d]	S99876-CHS20	32.7985	-79.9443	21.65	2.3	40.0	19.8	af
29	W02100-SCPT1	32.8045	-79.9509	20.78	2.5	18.9	17.0	Qws
30	W03454A-SC1	32.7918	-79.8544	29.35	1.6	16.9	14.3	Qws
31	S071081-SC6	32.7920	-80.0656	12.27	1.0	11.8	6.6	Qws
32	S071081-SC1	32.7922	-80.0656	12.27	0.8	27.8	5.9	Qws
33	S071081-SC3	32.7923	-80.0654	12.27	1.0	10.7	6.5	Qws
34[d]	W02195-SC1	32.7929	-80.0305	15.04	1.9	10.9	-	Qhec
35[d]	S99634-MPE5	32.8013	-79.8995	25.13	0.5	18.3	14.9	af
36[d]	S99634-C27	32.8016	-79.9039	24.75	1.2	27.5	20.5	af
37[d]	S99634-DS1	32.8017	-79.9015	24.95	0.3	36.6	12.6	af
38	S01772-CPT3	32.8035	-79.8979	25.15	1.7	25.8	12.6	Qhes
39[d]	S04709-C4	32.8036	-79.9003	24.95	0.6	24.4	13.4	af
40	S05196-C1	32.8060	-79.8923	25.47	2.4	15.3	14.9	Qws
41	W02182-SC1	32.8061	-79.8875	25.87	1.3	15.9	16.2?[c]	Qws

Table 3.3. SCPTu soundings from the Greater Charleston area that plot in surficial sand deposits. (Continued).

Site No.	Site code[a]	Latitude (deg)	Longitude (deg)	Distance to Woodstock fault (km)	Water table depth (m)	Maximum test depth (m)	Top of the Cooper Marl depth (m)	Surficial geology
42	S01018-B1	32.8086	-79.8763	26.66	0.5	24.3	14.7	Qws
43	W02103-SC3	32.8088	-79.8907	25.46	3.0	16.9	16.4	Qws
44	W04204-SC13	32.8034	-79.7393	38.24	1.6	18.1	-	Qhs
45	W01179-SC1	32.8079	-79.8505	28.81	1.5	15.2	15.0	Qws
46	S01143-B1	32.8088	-79.8384	29.76	0.9	30.4	24.0	Qws
47	W04137-SC1	32.8096	-80.0315	14.01	0.6	12.9	11.0	Qws
48	W02237-SC1	32.8181	-79.8541	27.98	2.1	17.9	17.9	Qws
49	S02891-B2	32.8200	-79.8173	30.90	0.9	20.0	12.5	Qws
50	W01219-SC1	32.8200	-79.8171	30.92	1.2	11.3	11.5[b]	Qws
51	S02902-C13	32.8210	-79.8188	30.72	0.9	22.9	12.7	Qws
52	W04225-SC1	32.8226	-79.8418	28.75	2.6	17.8	16.2	Qws
53	W03436-SC1	32.8284	-79.8348	29.02	0.9	16.0	18.2[b]	Qws
54	W01239-SC3	32.8427	-79.8128	30.16	2.0	18.9	-	Qws
55[d]	W04130-SC1	32.8435	-80.0594	9.84	1.7	9.2	7.0?	Qws
56	S01049-F10	32.8472	-79.9145	21.47	2.4	22.9	14.6	Qws
57	W02236-SC1	32.8473	-79.8561	26.28	2.7	15.9	17.0[b]	Qws
58	S01049-F1	32.8476	-79.9145	21.47	0.9	22.0	15	Qws
59[d]	W03065-SC1	32.8499	-79.9673	17.00	1.8	12.0	-	Qws
60	W04028-SC1	32.8528	-79.8046	30.43	3.0	23.9	22.4	Qws
61	W03046-SC1	32.8531	-79.7840	32.22	0.5	24.9	24.0	Qws
62	W04016A-SCPT6	32.8637	-79.9784	17.44	2.0	25.8	25.0	Qwls
63	S03508-CPT1	32.8643	-80.0154	12.26	1.5	18.3	10.0	Qwls
64	S02784-SBA	32.8745	-79.7762	32.17	0.3	24.3	20.9	Qws
65	W02218-SC1	32.8773	-80.0010	12.76	1.5	14.9	13.4	Qwls
66	W04337-SCPT3	32.8773	-79.9938	13.35	1.3	14.9	13.9	Qwls
67	W02127-SC1	32.8798	-79.9789	14.44	1.5	14.0	12.8	Qwls
68	W02301-SC1	32.8847	-79.9829	13.86	1.8	14.9	13.0	Qwls
69	W02115-SC5	32.8860	-80.0007	12.00	2.1	8.8	7.4	Qwls
70	B96-Ten01	32.8910	-80.0255	10.02	1.5	9.1	6.0	Qts
71	B96-Ten02	32.8912	-80.0253	10.03	1.5	9.1	6.1	Qts
72	B96-Ten03	32.8914	-80.0251	10.03	1.5	12.1	6.2	Qts
73	W01292-SC1	32.9003	-80.0595	6.73	3.0	12.9	12.0	Qts
74	W05043-SC1	32.9038	-80.0284	9.11	1.5	9.6	7.2	Qts
75	W02104-SC1	32.9042	-79.9170	18.60	8.0[f]	27.9	26.1	Qts
76	S03172-B4	32.9055	-79.9108	19.12	4.0	28.2	-	Qts
77	W04320-SCPT1	32.9123	-80.0434	7.42	3.8	18.1	-	Qts
78	B96-Ten10	32.9143	-80.0544	6.41	3.0	9.0	11.2[b]	Qts
79	B96-Ten09	32.9146	-80.0545	6.38	3.0	9.0	11.2[b]	Qts
80	B96-Ten08	32.9149	-80.0547	6.36	2.3	9.0	11.2[b]	Qts
81	B96-Ten07	32.9152	-80.0548	6.33	2.3	9.0	11.2[b]	Qts

Table 3.3. SCPTu soundings from the Greater Charleston area that plot in surficial sand deposits. (Continued).

Site No.	Site code[a]	Latitude (deg)	Longitude (deg)	Distance to Woodstock fault (km)	Water table depth (m)	Maximum test depth (m)	Top of the Cooper Marl depth (m)	Surficial geology
82	B96-Ten06	32.9154	-80.0549	6.31	2.3	9.0	11.2[b]	Qts

[a]*First letter in site code: B= Bechtel; S = S&ME; W = WPC.*
[b]*Estimated from Weems and Lemon (1988, 1993).*
[c]*? = some uncertainty.*
[d]*Not considered in LPI analysis, because surficial deposit was not Qhes, Qws, Qwls or Qts; or measurement did not extend to at least 18 m.*
[e] *Parker's Ferry Formation (Weems and Lewis, 2002).*
[f] *Low water table due to dewatering. Assumed water table depth of 4.0 for LPI calculation.*

Representative SCPTu and geologic profiles are presented in Figure 3.4. These profiles are for SCPTu site No. 74 (See Figure 3.3). Cone tip resistances shown in Figure 3.4(a) are corrected to account for the effect of water pressure acting behind the cone tip (q_t). The friction ratio (*FR*) profile shown in Figure 3.4(b) is defined as the cone sleeve resistance (f_s) divided by q_t. Values of *FR* are usually much greater (over 1%) in clayey soils than sandy soils. In Figure 3.4(c), cone pore-water pressures (u_2) are measured by a transducer located behind the cone tip, and hydrostatic pore pressures (u_0) are assumed equal to the depth below the groundwater table multiplied by the unit weight of water. Values of u_2 close to u_0 indicate freely draining soil (e.g., sand); and values u_2 higher than u_0 indicate lower permeable soil (e.g., clay). Ranging from about 100 to 500 m/s, values of V_s shown in Figure 3.4(d) indicate low to high soil stiffnesses.

The geologic profile shown in Figure 3.4(f) was inferred from the q_t, *FR*, u_2 and V_s profiles, and the geologic map and cross sections by Weems and Lemon (1988). The materials beneath site No. 74 consist of 5.5 m of Qts underlain by 1.3 m of clayey material that is likely part of the clay facies of the Ten Mile Hill beds (Qtc). At depths greater than 6.8 m, the relatively uniform q_t profile, $u_2 > 1$ MPa, and $V_s > 300$ m/s are typical of the Cooper Marl. The higher value of V_s (nearly 500 m/s) at the top of the Cooper Marl indicates stiffer or more cemented material.

The SCPTu sites listed in Table 3.3 are grouped according to surficial geology, except for site Nos. 31, 32, and 33. Although site Nos. 31-33 plot in Holocene to Pleistocene estuarine deposits mapped by Weems and Lemon (1988), subsurface

information indicates that only Qws is present at the ground surface at these sites (Boller et al. 2008).

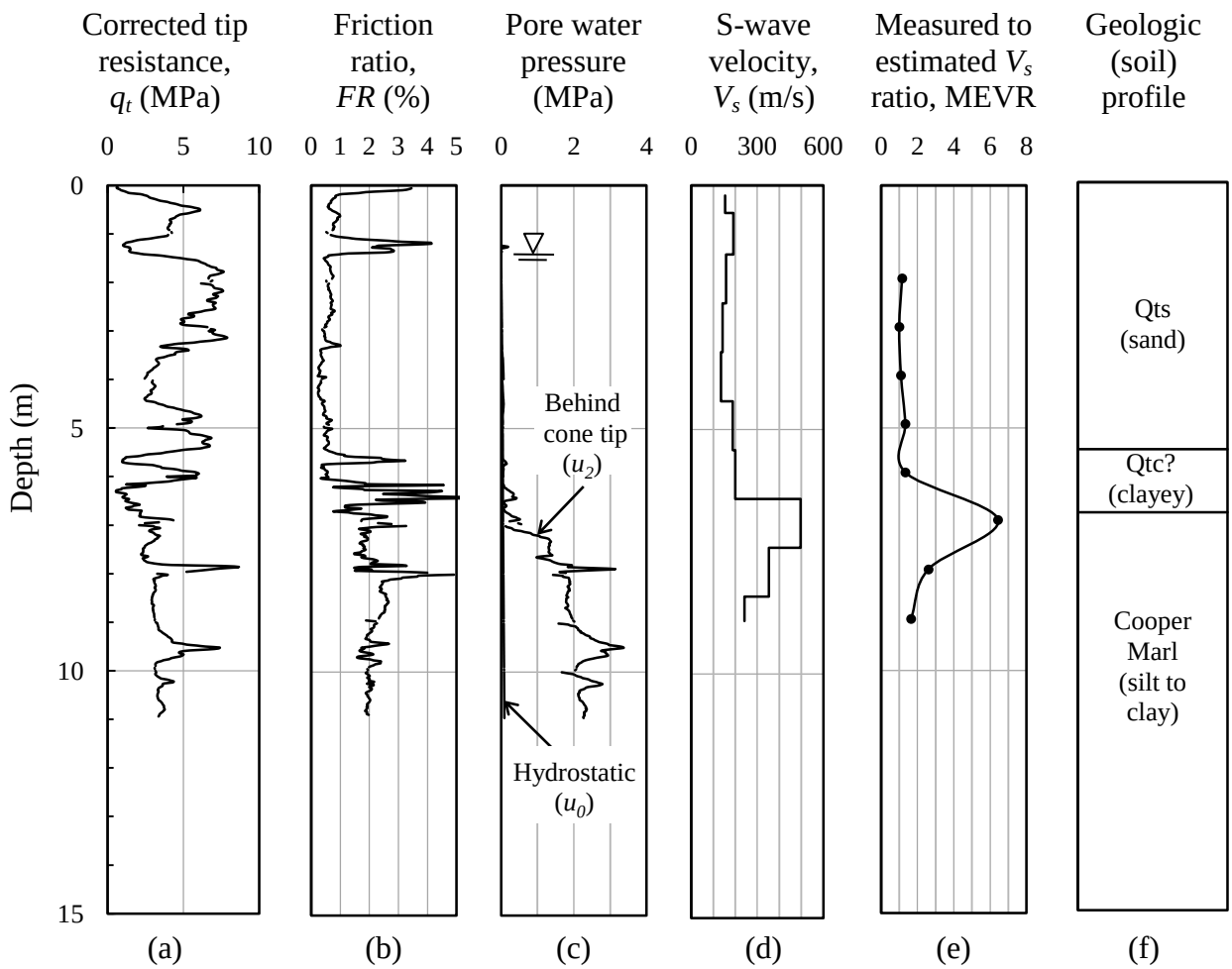

Figure 3.4 Representative profiles of cone, V_S, and geology from SCPTu site No. 74.

3.5 Measured to Estimated Velocity Ratio

Presented in Figure 3.4(e) is the profile of MEVR for site No. 74 (See Figure 3.3). MEVR is obtained by dividing corrected V_S values by estimated V_S using normalized q_t values and the following relationship with cone tip resistance (Andrus et al. 2004a):

$$(V_{s1})_{cs} = 62.6\left[(q_{t1N})_{cs}\right]^{0.231} \tag{3.1}$$

where $(V_{s1})_{cs}$ = equivalent clean-sand value of stress-corrected shear wave velocity in m/s, and $(q_{t1N})_{cs}$ = equivalent clean-sand cone tip resistance normalized to atmospheric pressure. Equation 3.1 was developed from regression analysis of $(V_{s1})_{cs}$ - $(q_{t1N})_{cs}$ data pairs from Holocene-age sand layers with FC ≤ 20% or $I_c \leq 2.25$. Many of the sand layers experienced liquefaction less than 30 years before geotechnical testing. To normalize cone tip resistances and adjust to equivalent clean-sand values, the procedures recommended by Youd et al. (2001) were used.

Considering $(V_{s1})_{cs}$ - $(q_{t1N})_{cs}$ data pairs from Holocene and older sand deposits, Andrus et al. (2009) developed the following relationship between MEVR and time since initial deposition or last critical disturbance (e.g., liquefaction):

$$\text{MEVR} = 0.0820\log_{10}(t) + 0.935 \tag{3.2}$$

where t = time in years. For MEVR = 1.0, Equation 3.2 suggests that the data pairs used in the development of Equation 3.1 are from deposits with average geotechnical age of about 6 years. Thus, MEVR greater than 1.0 in Figure 3.4(e) suggests soils that are older than 6 years and/or cemented.

Summarized in Table 3.4 are mean values of measured V_s, measured $(V_{s1})_{cs}$, estimated $(V_{s1})_{cs}$, and MEVR grouped by sand deposits. Sites located in Qhs and Qhes are grouped together because of the limited number of test sites. The criteria used for selecting the values were as follows: measurements were from below the groundwater table, measurements included at least two V_s test intervals, corresponding test intervals were within a uniform layer susceptible to liquefaction, and geology of the layer could be reasonably inferred.

Shown in Figure 3.5 are variations of MEVR with depth for four sand groups. The plots exhibit overall constant MEVR with depth. For sand deposits that liquefied in 1886 (120 years age), MEVR is expected to be around 1.11 based on Equation 3.2. The mean MEVRs of 1.11 and 1.15 for Qhs/Qhes and Qts deposits, respectively, are consistent with the greater number of mapped areas of 1886 craterlets and ground displacements in these deposits. The greater MEVRs for Qws and Qwls are consistent with the fewer number of mapped areas ground failure (see Figure 3.2).

In Figure 3.5(d), values of MEVR from site No. 71 are not included in the statistical analysis because cone tip resistances are higher than at other Qts sites. It is possible that construction activities near the Charleston Airport may have caused the atypical high q_t values at site No. 71, or ground shaking was not sufficient to trigger intense liquefaction in the 1886 earthquake.

Table 3.4 Measured to estimated V_{s1} ratios for four Quaternary sand groups.

Site No.	Depth of susceptible layers[a] (m)	Number of V_s test intervals	Measured: Mean V_s (m/s)	Measured: Mean $(V_{s1})_{cs}$[b] (m/s)	Estimated: Mean $(V_{s1})_{cs}$[c] (m/s)	Range of MEVR value	Mean of MEVR value
Qhs/Qhes							
1	2.6-6.7	4	183	222	184	0.73-1.59	1.22
2	2.8-5.4	3	207	262	177	1.02-1.81	1.54
4	1.8-8.9	7	162	196	179	0.97-1.21	1.10
5	3.4-8.5	5	192	216	202	0.90-1.47	1.09
11	1.4-7.4	6	163	207	179	1.04-1.30	1.16
14	0.5-2.4	2	141	231	189	0.98-1.52	1.25
16	2.4-4.4	2	145	201	166	1.11-1.30	1.21
22	1.5-3.6	2	131	175	168	1.00-1.08	1.04
35	1.4-7.4	6	133	176	170	0.81-1.14	1.04
36	1.4-3.4	2	155	213	203	1.05	1.05
37	4.0-8.0	4	165	204	169	1.12-1.38	1.21
38	1.7-7.4	6	143	177	174	0.88-1.22	1.02
39	4.3-11.0	6	157	177	184	0.45-1.33	0.96
44	1.6-7.4	6	179	220	218	0.85-1.19	1.01
Qws							
3	3.7-6.7	3	183	220	177	0.93-1.62	1.26
6	3.9-5.9	2	182	214	211	0.99-1.04	1.02
7	1.5-8.6	7	270	327	209	0.73-2.91	1.64
9	2.7-10.7	8	194	220	187	0.96-1.54	1.18
10	1.7-6.7	5	178	225	195	0.90-1.51	1.16
12	1.5-13.5	12	237	304	186	0.75-3.01	1.65
13	1.8-3.4	2	195	260	184	1.30-1.55	1.42
15	1.6-4.4; 6.4-10.4	7	187	228	169	1.15-1.80	1.35
16	6.4-8.4	2	203	239	163	1.30-1.65	1.48
17	1.5-3.3	2	168	229	188	1.16-1.28	1.22
18	1.6-4.4	3	200	277	176	1.36-2.17	1.57
19	2.6-4.6	2	239	318	175	1.68-1.97	1.81
20	2.5-5.5	3	167	212	178	1.08-1.30	1.19
21	1.4-8.4	6	215	273	187	1.23-1.74	1.46
23	2.0-4.1; 9.3-12.4	2;3	207	234	176	0.91-1.61	1.33
25	2.5-5.4	3	178	218	185	0.93-1.34	1.18
26	6.5-9.5	3	204	220	172	1.19-1.34	1.27
27	2.4-5.4; 7.4-11	3;4	222	263	173	0.99-1.90	1.53
28	2.4-5.4; 8.5-11.2	3;3	243	281	176	1.30-2.18	1.59
29	2.7-4.4; 5.7-9.7	2; 5	209	230	174	1.10-2.00	1.31
30	1.6-6.4	5	172	215	203	0.91-1.28	1.07
31	1.4-4.3	3	168	240	174	1.29-1.54	1.38
32	1.3-4.3	3	182	257	197	1.06-1.51	1.32
33	1.3-4.3	3	182	249	199	1.11-1.42	1.25
34	2.5-7.5	5	198	232	200	0.87-1.46	1.17
35	7.8-9.4	2	228	252	189	1.09-1.57	1.33
37	10.1-12.1	2	257	283	173	1.53-1.73	1.63
41	1.5-6.5	5	214	275	190	1.07-1.75	1.45

Table 3.4 Measured to estimated V_{s1} ratios for four Quaternary sand groups (Continued).

Site No.	Depth of susceptible layers[a] (m)	Number of V_s test intervals	Measured Mean V_s (m/s)	Measured Mean $(V_{s1})_{cs}$[b] (m/s)	Estimated Mean $(V_{s1})_{cs}$[c] (m/s)	Range of MEVR value	Mean of MEVR value
Qws							
42	1.3-5.1	4	157	220	186	1.10-1.30	1.18
43	3.0-5.7	3	219	266	181	1.17-1.76	1.47
45	1.7-6.7	5	203	268	182	1.08-1.79	1.48
46	1.4-9.5	8	202	247	172	1.01-1.81	1.42
47	0.6-4.6	4	162	243	167	1.08-1.83	1.44
48	2.5-4.5	2	188	248	190	1.00-1.66	1.33
49	1.8-3.8	2	163	223	186	0.98-1.42	1.20
50	1.5-4.5	3	190	252	244	0.84-1.23	1.04
51	1.8-4.8	3	188	251	207	0.90-1.49	1.22
52	2.4-5.3	3	239	281	191	1.25-1.74	1.47
53	1.4-3.4	2	268	433	204	1.54-2.71	2.12
54	4.5-6.5	2	216	260	172	1.26-1.80	1.53
55	1.5-3.4	2	175	241	176	0.99-1.74	1.36
59	2.4-5.4	3	171	216	174	1.09-1.39	1.23
60	3.5-6.5	3	168	190	178	0.92-1.30	1.07
61	1.6-13.2	3	230	302	178	1.57-1.90	1.70
Qwls							
62	2.4-6.4	4	205	251	197	1.07-1.54	1.28
63	2.7-4.9	2	264	353	208	1.55-1.87	1.71
65	2.5-4.5	2	141	179	182	0.93-1.04	0.99
66	4.4-6.4	2	229	348	174	0.94-2.97	1.95
67	1.4-4.4	3	234	319	180	1.45-1.97	1.79
68	3.5-6.5	3	181	226	166	1.1-1.48	1.34
Qts							
71	1.5-3.2	2	308	422	227	1.00-2.64	1.82
73	3-5.6	3	168	197	176	0.98-1.30	1.12
74	1.4-5.4	4	156	201	176	1.00-1.33	1.15
75	8.5-16.5	8	231	214	173	0.97-1.87	1.24
76	7.6-10.7; 11.7-18.9	10	219	211	180	0.98-1.58	1.17
77	3.4-9.4	6	180	193	175	0.83-1.33	1.10
78	3.2-7.8	5	156	176	168	0.94-1.22	1.05
79	3.0-6.0	3	153	177	173	0.88-1.16	1.02
80	2.3-6.0	4	156	190	168	0.94-1.32	1.13
81	2.3-6.0	4	164	201	167	0.98-1.36	1.19
82	2.3-5.0	3	153	192	164	1.04-1.32	1.17

[a] *Considered susceptible if $I_c < 2.6$ and below the groundwater table.*

[b] $(V_{s1})_{CS} = K_{CS} V_s (\frac{P_a}{\sigma'_{V0}})^{0.25}$ *where K_{CS} = correction factor for fines content, P_a = 100 kPa, and σ'_{v0} = initial effective vertical stress (Robertson et al. 1992; Juang et al. 2002).*

[c] *Estimated* $(V_{s1})_{CS} = 62.6\left[(q_{c1N})_{CS}\right]^{0.231}$ *(Andrus et al. 2004a).*

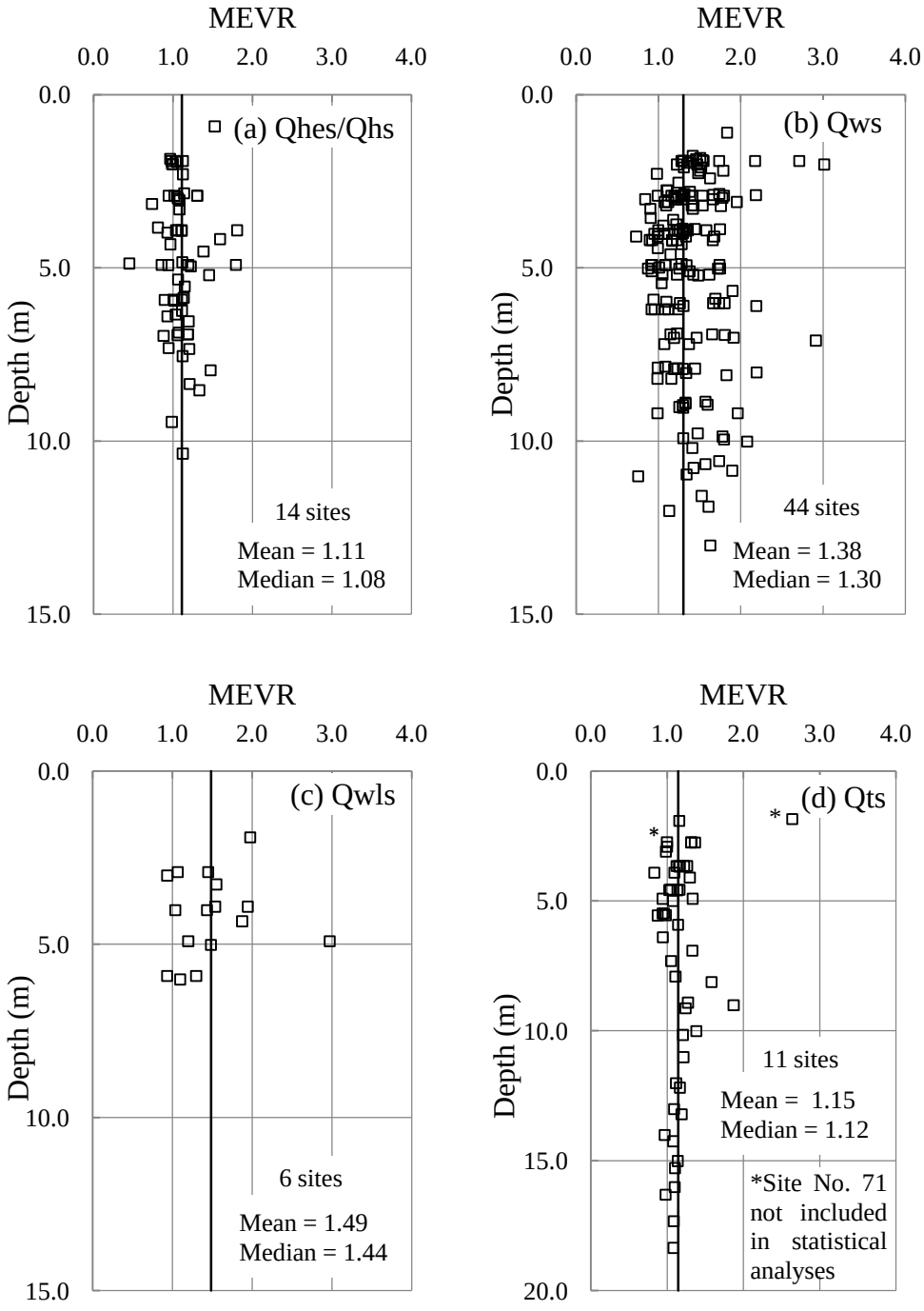

Figure 3.5 Variation of MEVR with depth for four sand groups.

To investigate the possible influence that strong shaking might have had on MEVR, site mean values listed in Table 3.4 are plotted in Figure 3.6 with respect to distance to the Woodstock fault (see Figure 3.3). As can be seen in Figure 3.6, the data do not exhibit significant correlations (coefficient of determination, $R^2 < 0.2$) between the site mean MEVRs and the distance to the fault for the three youngest sand groups (Qhs/Qhes, Qws, and Qwls). On the other hand, the mean MEVRs for Qts sites indicate a slight increase with increasing distance from the fault. The increase in mean MEVRs with increase in distance to fault suggests that the degree of liquefaction in Qts decreased away from the fault. It should be mentioned that the correlation coefficient in Figure 3.6(d) is lower (< 0.1) when median MEVRs are used instead of mean values. More data are needed to investigate the variation of MEVR with distance to the fault.

The MEVRs in Figure 3.6 suggest that Qhs/Qhes and Qts deposits are 60-420 years old, which is consistent with liquefaction occurring 120 years ago. The MEVRs for Qws and Qwls deposits suggest ages ranging from 28,000 to 6 M years, which is roughly consistent with their age of about 100,000 years.

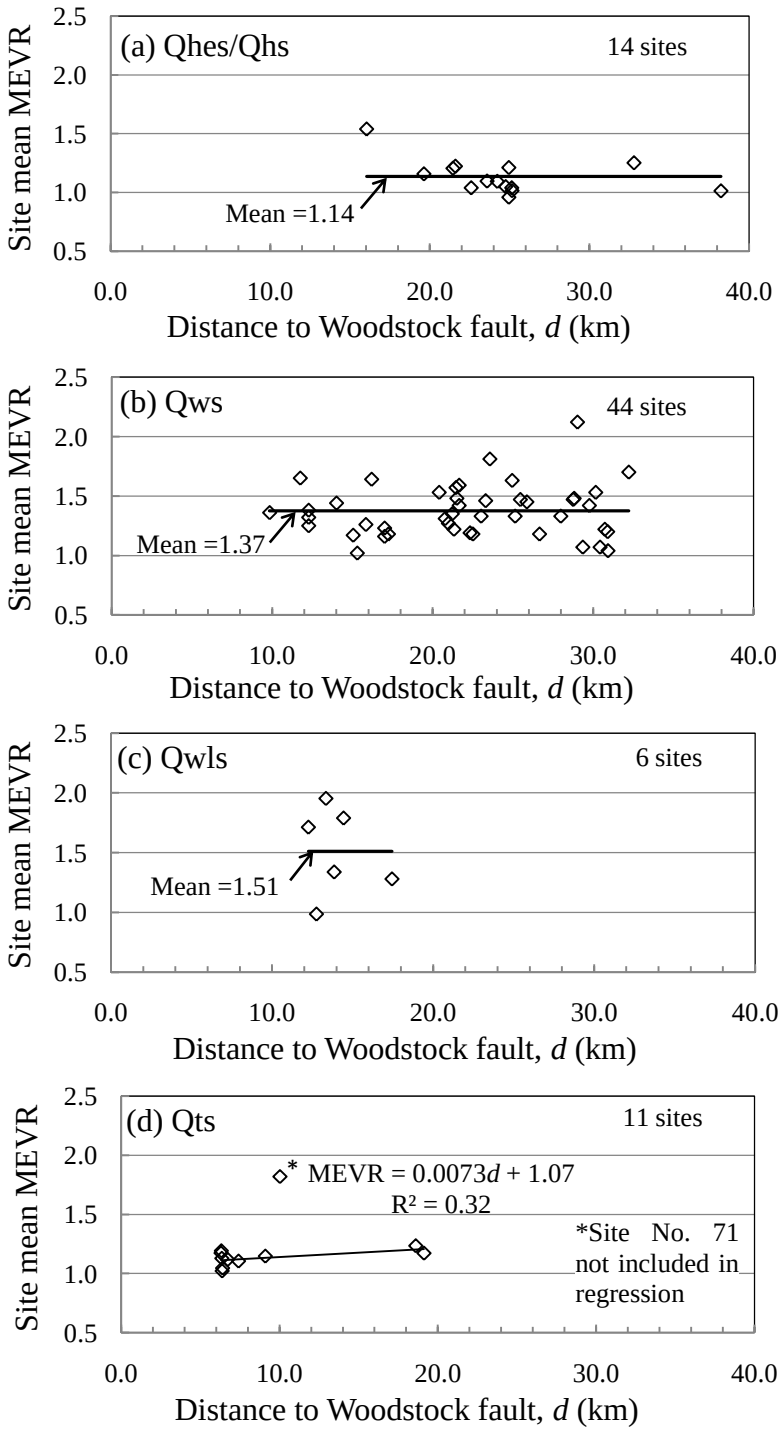

Figure 3.6 Variation of site mean MEVR with distance to inferred Woodstock fault for four Quaternary sand groups.

3.6 Liquefaction Potential Calculation

Liquefaction potential can be evaluated in terms of factor of safey against liquefaction (*FS*) or liquefaction potential index (LPI) originally proposed by Iwasaki et al. (1978). The procedure to calculate LPI has been modified by several investigators (Holzer et al. 2006; Li et al. 2006; Juang et al. 2008, 2009). The CPTu-based LPI approach adopted for this study follows the procedure of Holzer et al. (2006) so that the results can be compared with previous studies (Holzer et al. 2006, 2009; Balon and Andrus 2006; Lenz and Baise 2007; Rix and Romero-Hudock 2007; Cramer et al. 2008; Hayati and Andrus 2008a; Heidari and Andrus 2010).

The liquefaction potential index is defined as (Iwasaki et al. 1978):

$$\text{LPI} = \int_0^{20} Fw(z)dz \tag{3.3}$$

where F = a function of factor of safety against liquefaction (FS) defined as $F = 1 - FS$ for $FS \leq 1$ and $F = 0$ for $FS > 1$; z = depth in meters; and $w(z)$ = a depth-weighting factor equal to $10 - 0.5z$. LPI values calculated using Equation 3.3 theoretically could range from 0 to 100. The minimum value of 0 is obtained where $FS > 1$ over the entire 20 m depth. The maximum value of 100 is obtained where $FS = 1$ over the entire 20 m depth. LPI weighs factor of safety and thickness of potentially liquefiable layers according to the proximity of layers to the ground surface.

To screen out clay-rich layers not susceptible to liquefaction before LPI is calculated, the cone penetration test (CPT)-based criterion proposed by Robertson and

Wride (1998) is used. According to their criterion, a layer with soil behavior type index, I_c, more than 2.6 is too plastic to be susceptible to liquefaction. I_c is defined as (Lunne et al. 1997):

$$I_c = [(3.47 - log_{10}Q)^2 + (log_{10}F + 1.22)^2]^{0.5} \tag{3.4}$$

where Q = normalized cone tip resistance, and F = normalized friction ratio. Youd et al. (2001) recommended the $I_c > 2.6$ criterion for engineering practice, but noted that soils with I_c between 2.4 and 2.6 may also be too clay rich to liquefaction. For soils with $2.4 \leq I_c < 2.6$, Youd et al. (2001) suggested the soil be sampled and tested. The $I_c > 2.6$ criterion is initially used in this study to screen out non-susceptible clayey Quaternary soil layers.

The Cooper Marl is considered non-susceptible to liquefaction (Li et al. 2007; Hayati and Andrus 2008a,b). SCPTu profiles are considered acceptable for LPI analysis if the cone soundings extended to depths ≥ 20 m, or extended into the Cooper Marl, or extended within two meter above the Cooper Marl. If SCPTu soundings are less than 20 m and extended within two meter above the Marl, the missing portion of the profile above the Marl is assumed to be the same as in the last 2 m of the measured profile. The one exception is site No. 1, which extends to a depth 3.9 m above the Marl. For site No.1, the missing portion of the SCPTu profile about the Marl is assumed to be the same as an adjacent SCPTu profile (site No. 4).

Factor of safety is defined as CRR divided by the cyclic stress ratio. Cyclic stress ratio (CSR) represents the seismic loading on the soil and can be expressed as (modified from Seed and Idriss 1971):

$$\mathrm{CSR} = 0.65\left(\frac{a_{\max}}{g}\right)\left(\frac{\sigma_v}{\sigma_v'}\right)(r_d)/(MSF) \tag{3.5}$$

where a_{max} = peak horizontal acceleration at the ground surface; g = acceleration of gravity; σ_v and σ_v' = total and effective vertical overburden stresses, respectively; r_d = stress reduction coefficient; and MSF = magnitude scaling factor that accounts for effects of shaking duration. The procedures recommended by Youd et al. (2001) to calculate each variable in Equation 3.5 are followed in this study. MSF is computed using $\mathrm{MSF} = 10^{2.24}/M^{2.56}$ where M = moment magnitude.

For computing CRR from CPT measurements, the following relationship developed by Robertson and Wride (1998) and recommended by Youd et al. (2001) is used:

$$\text{If } (q_{t1N})_{CS} < 50, \qquad \mathrm{CRR} = 0.833\left(\frac{(q_{t1N})_{CS}}{1000}\right) + 0.05 \tag{3.6a}$$

$$\text{If } 50 \le (q_{t1N})_{CS} < 160, \qquad \mathrm{CRR} = 93\left(\frac{(q_{t1N})_{CS}}{1000}\right)^3 + 0.08 \tag{3.6b}$$

Because Equation 3.6 is based on fairly young sand deposits, the following correction is applied to the computed CRR:

$$\mathrm{CRR}_k = \mathrm{CRR} \times K_{DR} \tag{3.7}$$

where CRR_k = deposit resistance-corrected CRR, and K_{DR} = correction factor to capture the influence of diagenetic processes on CRR. The correction factor K_{DR} can be estimated using the following relationships (Hayati and Andrus 2009):

$$K_{DR} = 1.08\mathrm{MEVR} - 0.08 \tag{3.8}$$

where MEVR is based on estimated velocity using Equation 3.1.

Because Equation 3.1 and 3.8 were derived using data from sandy soils (with I_c < 2.25) and diagenesis may be different in fine-grained soils, both equations should be used cautiously in soils with 2.25 < I_c < 2.6. It is also recommended that Equation 3.8 be used only for MEVR > 1, because Equation 3.6 is based on sites where MEVR is generally around 1.0.

Toprak and Holzer (2003) used CPT data from sites shaken by the 1989 Loma Prieta California earthquake to calibrate LPI with the severity of surface manifestations of liquefaction. For computing *FS*, they applied the procedure recommended by Youd et al. (2001). Toprak and Holzer (2003) found that sites in the Monterey Bay region with LPI values of 5 and 15 correspond to probabilities of showing surface manifestations of liquefaction of 58% and 93%, respectively. They concluded that LPI = 5 generally represents the threshold for sand boil generation. These findings are consistent with the severity scale proposed by Iwasaki et al. (1982) based on standard penetration blow counts at Japanese sites.

3.7 Liquefaction Potential Based on a Scenario Shaking

The scenario shaking assumed for the initial LPI calculations is defined by M_w of 6.9 and a_{max} of 0.25g. These values of M_w and a_{max} are assumed to allow direct comparison with the liquefaction study of Mount Pleasant by Heidari and Andrus (2010). Using a single set of M_w and a_{max} values also allows for evaluation of the influence of distance to Woodstock fault on LPI.

Presented in Figure 3.7 is an example of the LPI calculations applied to site No. 74 assuming M_w of 6.9, a_{max} of 0.25g, and $I_c > 2.6$ as the criterion for non-susceptible clay-rich soils. Profiles of q_t and I_c versus depth are plotted in Figures 3.7(a) and 3.7(b), respectively. Figure 3.7(c) depicts the calculated CSR and CRR values versus depth. Values of *FS* versus depth are presented in Figure 3.7(d). The shaded sections in Figures 3.7(c) and 3.7(d) are the layers considered non-susceptible to liquefaction and screened out before the LPI calculation. Presented in Figure 3.7(e) is the accumulation of LPI with depth. The K_{DR}-corrected LPI and uncorrected LPI obtained for site No. 74 are 6 and 10, respectively. A LPI value of 6 is slightly greater than the threshold for sand boil generation (LPI = 5), which somewhat agrees with widespread liquefaction in Qts.

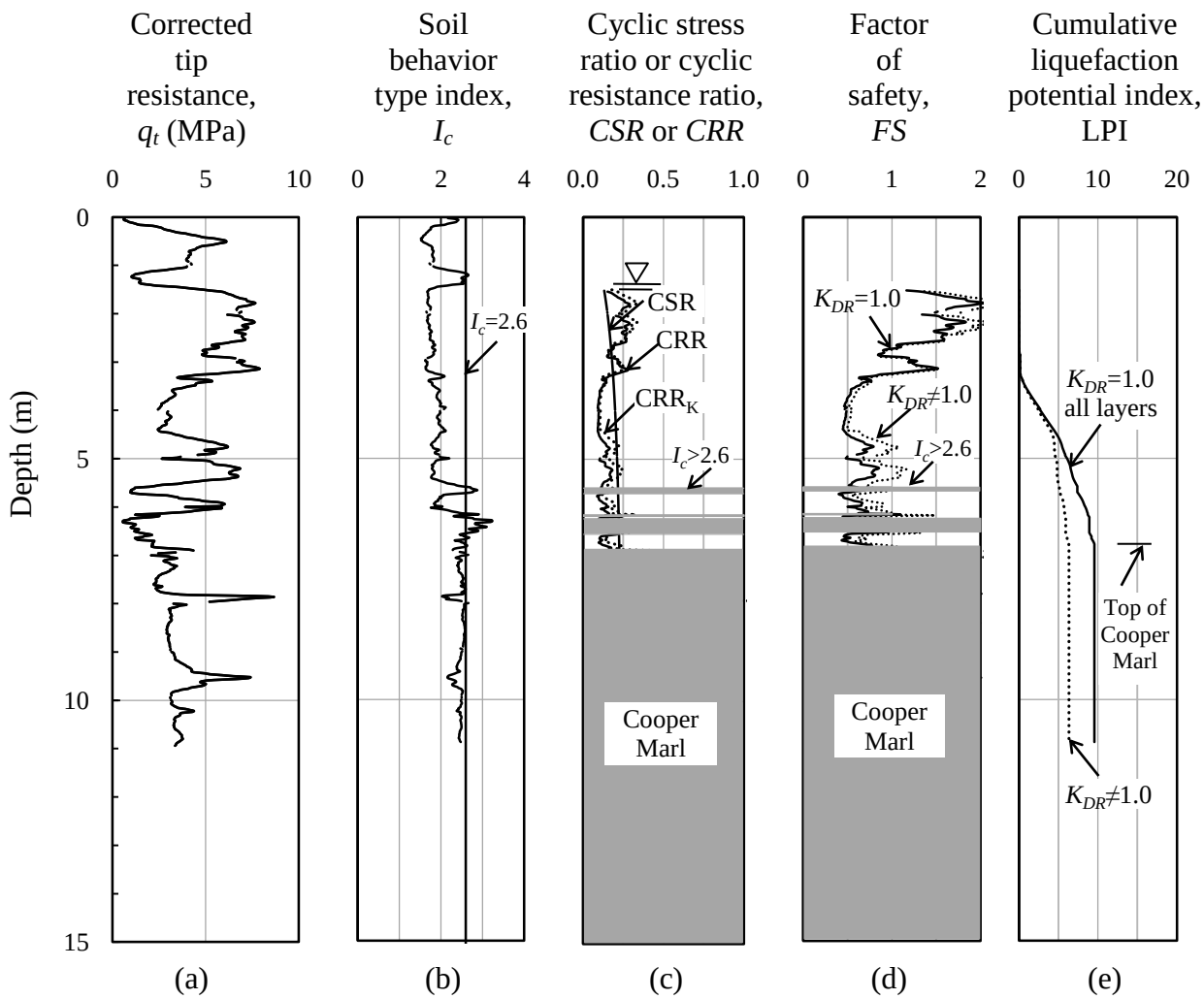

Figure 3.7 Calculation of LPI for SCPTu site No. 74 based on M_w = 6.9, a_{max} = 0.25g, and I_c > 2.6 as the criterion for non-susceptible clay-rich soils.

Shown in Figure 3.8 are variations of LPI values with distance to the Woodstock fault for the four sand groups assuming M_w of 6.9 and a_{max} of 0.25g for all sites. Sites Nos. 70-72 are not considered in the liquefaction potential analysis of Qts (Figure 3.8d), because high cone tip resistances in the sand layers below the groundwater table at these sites are not consistent with other Qts sites. As can be seen in Figure 3.8, there are no significant correlations (coefficient of determination, $R^2 < 0.1$) between the LPI values and the site-to-fault distance for the Qhs/Qhes, Qws, and Qwls groups. On the other hand, the LPI values for the Qts sites indicate a decrease with increasing distance to the fault. The decrease in LPI values with increase in distance to the fault is consistent with the trend in mean MEVRs [see Figure 3.6(d)]. Because of the correlation between LPI and distance to fault, SCPTus in Qts within 9 km of the fault are grouped together for the analysis of LPIs.

Summarized in Table 3.5 are mean, median and standard deviation of LPI values for the four sand groups. The LPI values in each group are assumed to be from lognormally distributed populations, and the Lilliefors test (Lilliefors 1967) supports this assumption. The population mean, μ, is estimated by the sample mean, $\overline{X}$. The uncertainty associated with μ can be calculated by dividing the population standard deviation, σ, by the square root of the sample size, $\sqrt{n}$. Because σ is unknown, the sample standard deviation, *S*, is used to calculate the standard error. Considering μ as the mean LPI value, the point estimate of μ are 10, 6, 5, and 9 and their standard errors are

±2, ±1, ±1, and ±2 for Qhs/Qhes, Qws, Qwls and Qts, respectively, when soils with I_c > 2.6 are assumed non-susceptible.

Because the cutoff I_c can have a significant impact on liquefaction potential calculations, values of LPI computed assuming I_c > 2.4 are also listed in Table 3.5. Based on a comparison of I_c values with Atterburg limits values obtained from sampling of soils in the Santa Clara Valley, California, Holzer et al. (2009) adopted I_c of 2.4 as the cutoff value for soils susceptible to liquefaction. Considering I_c > 2.4 as the criteria to screen out clay-rich soil layers, the mean LPI values decrease to 8, 5, 4, 8 for Qhs/Qhes, Qws, Qwls and Qts, respectively. The impact of the cutoff I_c value is particularly significant for a few of the SCPTu profiles. For example, in Figure 3.8(b), the outlier LPI value of 23 (site No. 46) dramatically decreases to 12 when cutoff I_c of 2.4 is assumed. This decrease in LPI from 23 to 12 occurs mainly in a 3-m thick clayey layer with low q_t, high u_2, and I_c between 2.55 and 2.6.

The values of LPI summarized in Table 3.5 for Qhs/Qhes and Qws agree well with values obtained in the previous study of Mount Pleasant by Heidari and Andrus (2010). In that study, mean (median) values for Qhs/Qhes and Qws groups were 7 (10) and 4 (5), respectively. The LPI values in Table 3.5 also agree with the mapped areas of ground displacement and conspicuous craterlets (see Figure 3.2).

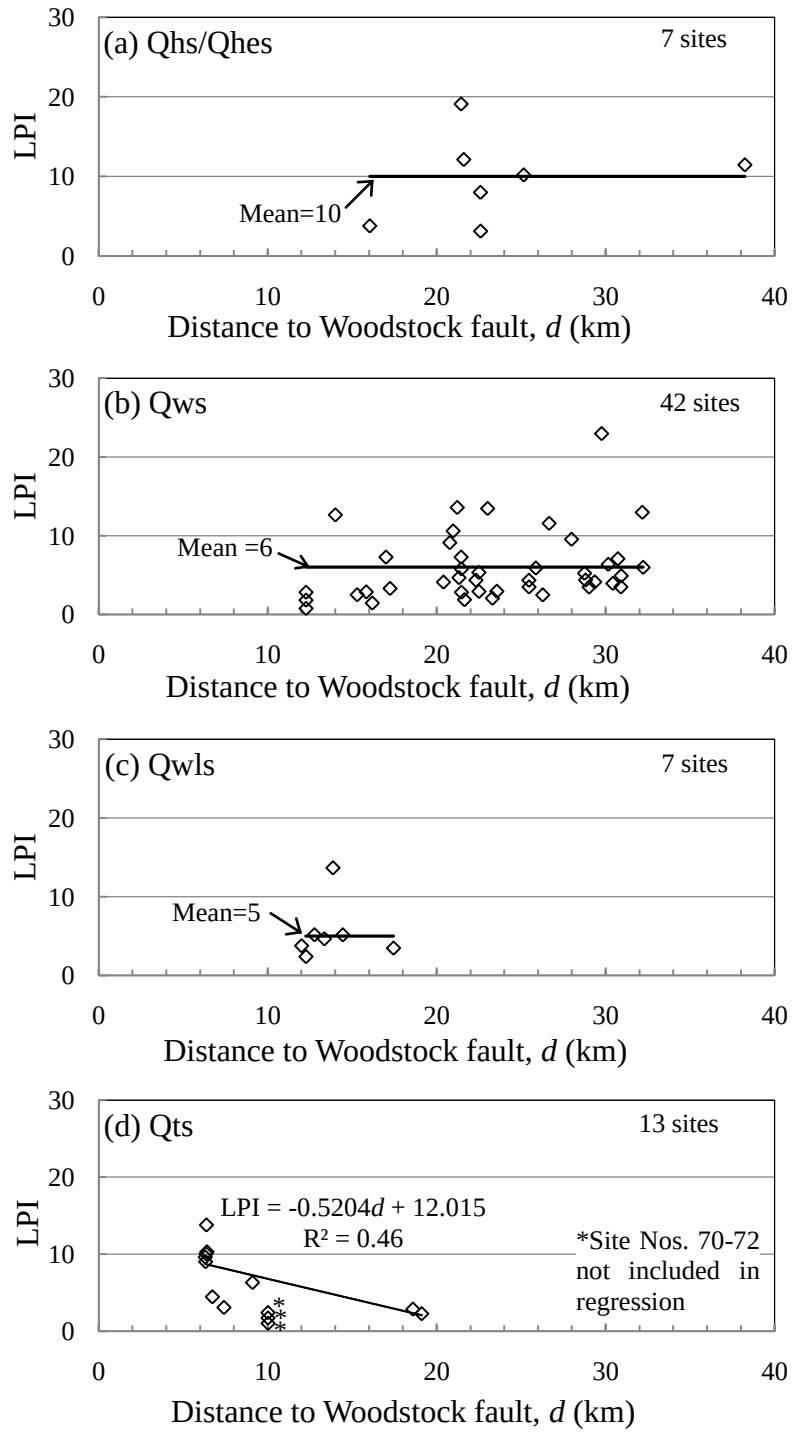

Figure 3.8 Variation of K_{DR}-corrected LPI with distance to inferred Woodstock fault for four Quaternary sand groups assuming M_w=6.9, a_{max}=0.25g, and I_c > 2.6 as the criterion for non-susceptible clay-rich soils.

Table 3.5 Statistic of LPI assuming M_w = 6.9 and a_{max}= 0.25g for four Quaternary sand groups.

		Cut off I_c value of 2.6			Cut off I_c value of 2.4		
Surficial geology	Number of CPTus	Mean (Median) LPI[a]	±1 Standard deviation[a]	Uncertainty of mean[a]	Mean (Median) LPI[a]	±1 Standard deviation[a]	Uncertainty of mean[a]
Qhs/Qhes(16-38 km[b])	7	10 (8)	4-15	±2	8 (7)	3-12	±2
Qws (12-32 km[b])	42	6 (5)	2-9	±1	5 (3)	1-7	±1
Qwls (12-17 km[b])	7	5 (5)	3-8	±1	4 (4)	2-7	±1
Qts (6-9 km[b])	8	9 (8)	5-12	±2	8 (7)	4-11	±2

[a]*Assuming log-normal distribution.*
[b]*Distance of SCPTu to Woodstock fault.*

3.8 Liquefaction Probability Curves

The methodology proposed by Holzer et al. (2006, 2009) and Rix and Romero-Hudok (2007) is followed to compute liquefaction potential probability curves for any value of a_{max}/MSF. Considering LPI of 5 as the threshold for sand boil generation, the probability of LPI $\geq$ 5 is derived from complementary log-normal cumulative distribution of LPI values in each group for various values of a_{max} and M_w. The liquefaction probability curve is estimated as a function of a_{max} for a specific earthquake magnitude by repeating the calculation for 0.1g $\leq a_{max} \leq$ 0.5g in 0.05g increments and a given M_w. Repeating the calculation for $5.0 \leq M_w \leq 7.5$ in 0.5 magnitude increments, the probability of LPI $\geq$ 5 as a function of a_{max}/MSF can be obtained.

Shown in Figure 3.9 are liquefaction probability curves for the four sand groups. The mean probability curves are derived considering the LPI values are lognormally distributed when a_{max}/MSF is greater than about 0.12 (denoted by circles in Figure 3.9). When a_{max}/MSF is less than about 0.12, some LPI values are zero and the assumption that LPI values are from a lognormally distributed population is not correct. The probability of LPI $\geq$ 5 for a_{max}/MSF < 0.12 is computed using the experimental cumulative distribution of LPI values for each group (denoted by triangles in Figure 3.9).

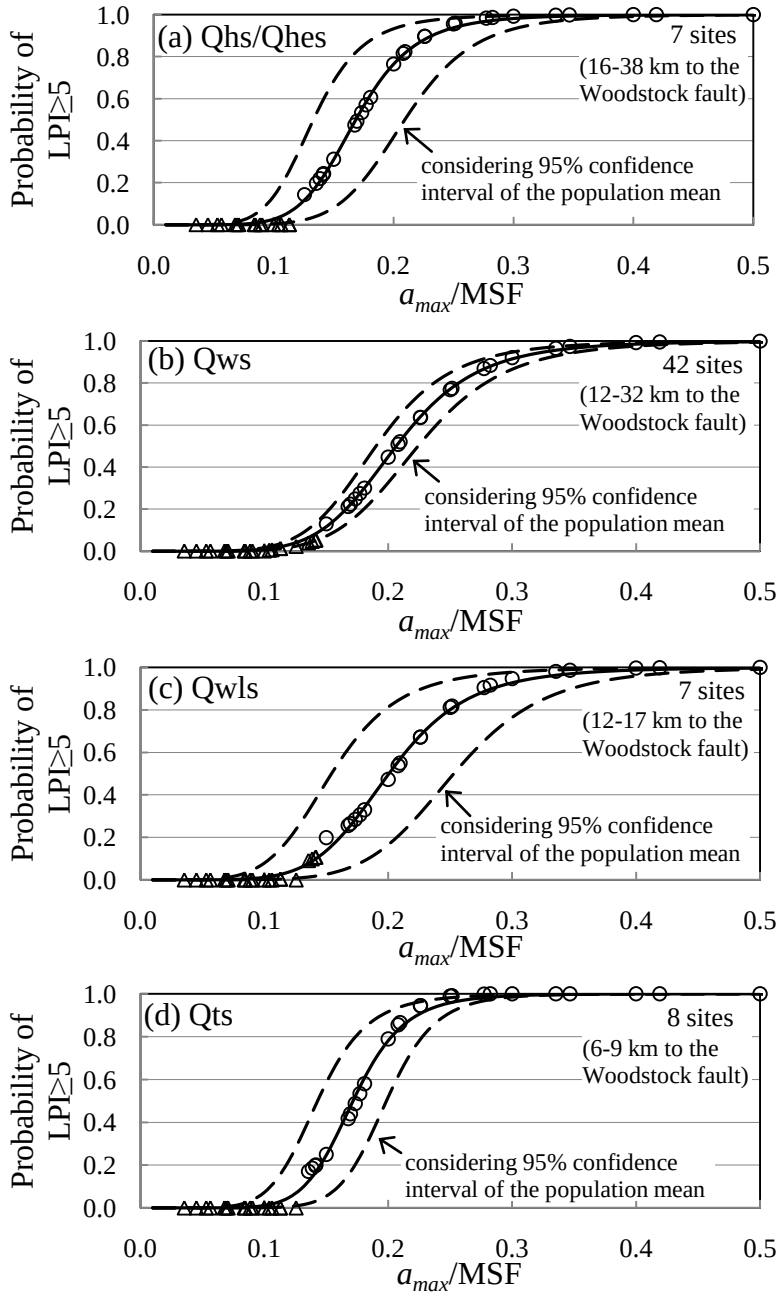

Figure 3.9 Liquefaction probability curves for four Quaternary sand groups, assuming I_c > 2.6 as the criterion for non-susceptible clay-rich soils. Note that the circles in the figure represent probability based on lognormal distribution, and the triangles represent probability based on experimental cumulative distribution.

The 95% confidence interval of the probability of LPI ≥ 5 shown in Figure 3.9 are derived from the lognormal cumulative distribution function assuming mean value equal to the upper and lower limit of 95% confidence interval of the population mean. The 95% confidence interval estimate of the mean LPI value can be calculated by $\overline{X} \pm t_{0.025} S / \sqrt{n}$, where $t_{0.025}$ is the 97.5% quantile of student's t distribution with n-1 degrees of freedom (Schiff and D'Agostino 1996). The 95% confidence interval for the mean probability curve of Qws sites [Figure 3.9(b)] is fairly narrow because of the large number of sites available. The broader confidence intervals shown in Figure 3.9(a), 3.9(c), and 3.9(d) are the result of fewer SCPTu sites available in Qhs/Qhes, Qwls, and Qts, respectively. More SCPTu data are needed to reduce the uncertainty associated with the liquefaction probability curves for these groups.

Because LPI values in Qts exhibit correlation with the distance to the Woodstock fault, the sites located in Qts with the distance 6-9 km to the fault are grouped together to calculate the probability of LPI ≥ 5. Site Nos. 64 and 65 that are 19 km away from the fault are not considered in the development of the liquefaction probability curve for Qts.

Presented in Figure 3.10 is a comparison of the mean liquefaction probability curves for the four sand groups. Liquefaction probability curves for Qws and Qwls are very similar. It is expected that Qwls deposits 12 to 17 km from the fault have the same probabilities of surface manifestation of liquefaction as Qws deposits 12 to 17 km from the fault. For Qwls deposits with distance < 12 km to the fault, the curve shown in Figure 3.10 likely underestimates the probability of liquefaction. Therefore, it is

recommended that liquefaction probability curves between the Qts and Qws curves be adopted for distances < 12 km. Similarly, the curves for Qts in Figure 3.10 may be overly conservative for sites in Qts located more than 9 km from the fault. The similar probability curves for Qhs/Qhes and Qts deposits is consistent with the computed MEVR values, and agrees with the observations of greater liquefaction in these two deposits in 1886.

The probability curves presented in Figures 3.9 and 3.10 can be combined with geologic maps to create liquefaction hazard maps of the Greater Charleston area. Liquefaction maps are used to identify areas where specific investigations for liquefaction hazard are needed or should be required prior to project development. Liquefaction hazard maps are also useful for regional planning and mitigation studies.

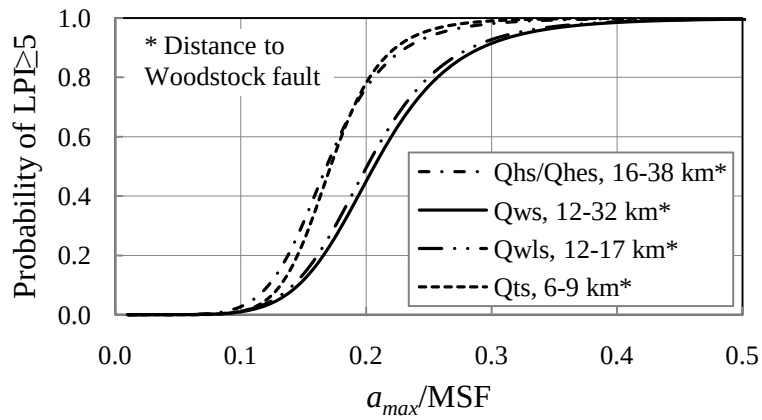

Figure 3.10 Comparison of liquefaction probability curves for four Quaternary sand groups, assuming $I_c > 2.6$ as the criterion for non-susceptible clay-rich soils.

3.9 Conclusion

Liquefaction potential of Pleistocene sand deposits in the Charleston area was characterized through reviewing mapped cases of 1886 ground failure, and analyzing eighty-two SCPTu profiles. Grouping cases of ground failure by surficial sand deposits, it was found that 45% of the ground failure cases were associated with the 200,000-year-old Ten Mile Hill beds (Qts) located within 13 km of the Woodstock fault. About 25% of the cases were associated with the 100,000-year-old Wando Formation (Qws, Qwls) located within 17 km of the fault. About 25% cases were associated with the Holocene to late Pleistocene deposits (Qhs/Qhes) that lie adjacent to the harbor, rivers, and creeks located within 31 km of the fault. The remaining cases were associated with the 400,000-year-old Ladson Formation (Qls) located within 3 km of the fault.

Ratios of measured-to-estimated shear wave velocity were calculated using the SCPTu profiles. Mean MEVRs computed for Qhs/Qhes and Qts were found to be 1.11 and 1.15, respectively, which are consistent with severe liquefaction observed in these deposits. Mean MEVRs for the Qws and Qwls deposits located > 12 km from the inferred fault were 1.38 and 1.49, respectively, which agree with the observation of little or no liquefaction in these areas.

Variation of MEVRs with distance to the Woodstock fault for Qts indicated a slight increase with increasing distance, suggesting that the degree of liquefaction in Qts deposits decreased away from the fault. No significant correlations between MEVR and distance to the fault were observed for the three younger sands groups.

LPI values were computed for the SCPTu profiles, after screening out layers not susceptible to liquefaction and correcting CRR for the influence of digenetic processes. Considering a constant level of shaking (a_{max}= 0.25g) for all the sites regardless of distance to the fault, variation of LPIs with distance to the fault were examined. Only the LPIs for Qts sites exhibited a decrease with increasing distance to the fault, which is consistent with the variation of MEVR values.

Liquefaction probability curves were developed for four major sand groups considering the effect of distance to the fault. The probability curves for Qhs/Qhes and Qts located 16-38 km and 6-9 km from the fault, respectively, predict significantly higher potentials than the probability curves for Qwls and Qws deposits located over 12 km from the fault. Additional SCPTu data are needed to decrease the large uncertainties associated with liquefaction probability curves for Qhs/Qhes, Qwls and Qts. The results of this study can be used in probabilistic liquefaction hazard mapping of the Charleston area.

CHAPTER FOUR

CHARACTERIZING THE LIQUEFACTION POTENTIAL OF THE PLEISTOCENE-AGE WANDO FORMATION IN THE CHARLESTON AREA, SOUTH CAROLINA*

4.1 Introduction

The 1886 Charleston earthquake, with a moment magnitude of about 7, is the largest historic seismic event to have occurred in the eastern United States (Bollinger 1977). A major cause of damage was liquefaction-induced ground failure (Dutton 1889). A map of the Greater Charleston area is shown in Figure 4.1. The area is located in the Atlantic Coastal Plain and includes the 1886 meizoseismal region. The probable source of the 1886 earthquake is the Woodstock fault zone. As illustrated in Figure 4.1, the Woodstock fault has been characterized as a right-lateral strike slip fault with an antidilatational compressional left step near Middleton Place (Durá-Gómez and Talwani 2009).

Most of the study area is covered by a blanket of Quaternary (< 1.8 million years) sand to clay that obscures underlying Tertiary stratigraphic units (Weems and Lewis

* A similar form of this chapter has been submitted in the form of a conference paper; Heidari, T., Andrus, R. D., Moysey, S. M. J. (2011). "Characterizing the Liquefaction Potential of the Pleistocene-age Wando Formation in the Charleston Area, South Carolina." *Risk Assessment and Management in Geoengineering, GeoRisk*, to be hold in Atlanta, GA.

2002). The sand facies of the 100,000-year-old Wando Formation (Qws) form the higher natural ground near the coast. The Cooper Group is a major Tertiary marine deposit that underlies the entire area and extends to depths > 100 m below mean sea level. The Cooper Group is locally known as the Cooper Marl, and consists of calcareous silts and clays.

The primary objective of this study is to characterize the liquefaction potential of Qws surficial deposits. This chapter extends the characterization of Qws deposits presented in Hayati and Andrus (2008a), Heidari and Andrus (2010, 2011) and Chapter 3 to include an analysis of the influence of depth to the groundwater table and depth to the Cooper Marl on liquefaction potential based on seismic cone penetration tests with pore pressure measurements (SCPTu). Locations of forty-two SCPTu sites considered in this study are plotted in Figure 4.1. Details of each SCPTu are given in Chapter 3.

4.2 Liqefaction Potential

The liquefaction potential index is defined as (Iwasaki et al. 1978):

$$\text{LPI} = \int_0^{20} Fw(z)dz \tag{4.1}$$

where F = a function of factor of safety against liquefaction (FS) defined as $F = 1 - FS$ for $FS \leq 1$ and $F = 0$ for $FS > 1$; z = depth in meters; and $w(z)$ = a depth-weighting factor given by Iwasaki et al. as $10 - 0.5z$. The LPI values calculated using Equation 4.1 could

theoretically range from 0 to 100. LPI weighs factor of safety and thickness of potentially liquefiable layers according to the proximity of layers to the ground surface.

To screen out clay-rich layers not susceptible to liquefaction before LPI calculation, the cone penetration test-based criterion proposed by Robertson and Wride (1998) is used. According to their criterion, a layer with soil behavior type index (I_c) more than 2.6 is too plastic to be susceptible to liquefaction. This criterion is applied to layers in the Quaternary deposits. It should be noted that Robertson (2009) provides an update to Robertson and Wride (1998) recommending that samples be taken where $I_c > 2.6$ regardless of normalized friction ratio. This recommendation, however, does not apply easily to mapping liquefaction potential over large areas. Thus, the screening out criterion I_c of 2.6 is applied here. Although I_c is often < 2.6 in the Tertiary-age Cooper Marl, it is considered non-susceptible to liquefaction (Li et al. 2007; Hayati and Andrus 2008a,b).

SCPTu profiles are considered acceptable for LPI analysis if the cone soundings extend to depths ≥ 20 m, extend into the Cooper Marl, or extend within two meters above the Cooper Marl based on available geologic maps. If SCPTu soundings are less than 20 m and extend within two meters above the Marl, the missing portion of the profile above the Marl is assumed to be the same as in the last two meters of the measured profile.

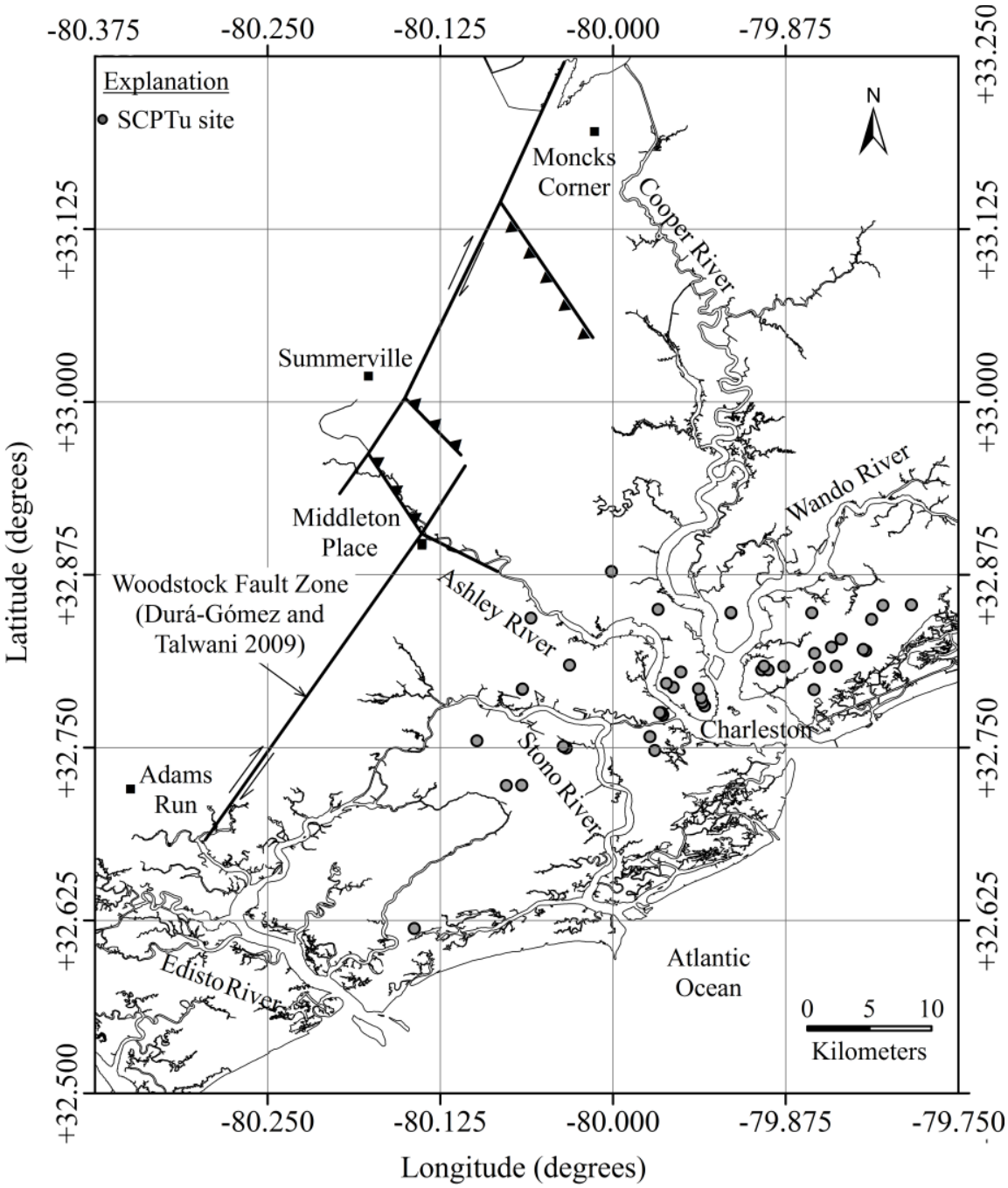

Figure 4.1 Map of the Greater Charleston area showing the Woodstock fault zone (Durá-Gómez and Talwani 2009) and the locations of SCPTu sites plotted in Qws.

The factor of safety is defined as the cyclic resistance ratio divided by the cyclic stress ratio. The cyclic stress ratio (CSR) represents the seismic loading on the soil and can be expressed as (modified from Seed and Idriss 1971):

$$\text{CSR} = 0.65(\frac{a_{\max}}{g})(\frac{\sigma_v}{\sigma_v'})(r_d) / (\text{MSF}) \tag{4.2}$$

where a_{max} = peak horizontal acceleration at the ground surface; g = acceleration of gravity; σ_v and σ_v' = total and effective vertical overburden stresses, respectively; r_d = stress reduction coefficient; and MSF = magnitude scaling factor that accounts for the effects of shaking duration. The procedures recommended by Youd et al. (2001) to calculate each variable in Equation 4.2 are followed in this study. MSF is computed using $\text{MSF} = 10^{2.24} / M_w^{2.56}$ where M_w = moment magnitude.

Cyclic resistance ratio (CRR) represents the resistance of the soil to liquefaction. For computing CRR from cone measurements, the following relationship developed by Robertson and Wride (1998) and recommended by Youd et al. (2001) is used:

$$\text{If } (q_{t1N})_{CS} < 50, \quad \text{CRR} = 0.833\left(\frac{(q_{t1N})_{CS}}{1000}\right) + 0.05 \tag{4.3a}$$

$$\text{If } 50 \le (q_{t1N})_{CS} < 160, \ \text{CRR} = 93\left(\frac{(q_{t1N})_{CS}}{1000}\right)^3 + 0.08 \tag{4.3b}$$

where $(q_{t1N})_{cs}$ = equivalent clean-sand cone tip resistance normalized to atmospheric pressure.

Because Equation 4.3 is based on fairly young sand deposits or deposits that liquefied in the recent past, the following correction is applied to the computed CRR:

$$\mathrm{CRR}_k = \mathrm{CRR} \times K_{DR} \tag{4.4}$$

where CRR_k = deposit resistance-corrected CRR, and K_{DR} = correction factor to capture the influence of diagenetic processes on CRR. The correction factor K_{DR} can be estimated using the following relationship (Hayati and Andrus 2009):

$$K_{DR} = 1.08\mathrm{MEVR} - 0.08 \tag{4.5}$$

where MEVR is the measured shear wave velocity corrected for overburden stress and fine content divided by the estimated velocity defined by (Andrus et al. 2004a):

$$(V_{s1})_{cs} = 62.6\left[(q_{t1N})_{cs}\right]^{0.231} \tag{4.6}$$

where $(V_{s1})_{cs}$ = equivalent clean-sand value of stress-corrected shear wave velocity in m/s. It should be noted that Equations 4.5 and 4.6 were derived using data from sandy soils (with $I_c < 2.25$) and diagenesis may be different in fine-grained soils. Therefore, both equations should be used cautiously in soils with $2.25 < I_c < 2.6$. It is also recommended that Equation 4.5 be used only for MEVR > 1, because Equation 4.3 is based on sites where MEVR is generally around 1.0.

4.3 Liquefaction Potential Based on a Scenario Earthquake

The scenario shaking assumed for the initial LPI calculations is defined by M_w of 6.9 and a_{max} of 0.25g. Using a single set of M_w and a_{max} values allows for an evaluation of the influence of distance to the Woodstock fault, depth to top of the Cooper Marl, and depth to the groundwater table on LPI within the original forty-two SCPTu profiles.

Presented in Figure 4.2 are variations of LPI values with distance to the Woodstock fault (*D*), depth to top of the Cooper Marl (*C*), and depth to the groundwater table (*W*). As it can be seen in Figure 4.2(a), there are no statistically significant correlations (coefficient of determination, $R^2 < 0.1$) between the LPI values and the site-to-fault distance and the trend suggested by the regression equation is opposite to what would be expected. On the other hand, R^2 is greater than 0.1 between the LPI values and *C* or *W*. The LPI values indicate a slight increase with increasing *C* values, and a slight decrease with increasing *W* values. These trends are consistent with the definition of LPI.

To further evaluate the significance of the three predictor variables (*D*, *C*, and *W*) the following regression equation is applied to the LPI data:

$$\mathrm{LPI} = \beta_0 + \beta_1 D + \beta_2 C + \beta_3 W \tag{4.7}$$

where *D* in km, *C* and *W* in m. From regression analysis, β_0 = 3.16±5.94 (95% confidence interval), β_1 = 0.033±0.250, β_2 = 0.366±0.314, and β_3 = -2.34±1.73. The coefficient of multiple regression, R^2, and the standard deviation of the residuals (or error), s, associated with this regression are 0.285 and 3.867, respectively. The *P*-value,

the probability that the current result would have been found if the coefficient was equal to 0, for the estimated coefficient of β_1, β_2, and β_3 are 0.791, 0.023, and 0.009, respectively, further indicating that the site-to-fault distance is not related to LPI for sites located within 12-32 km of the fault, while *C* and *W* are significantly related to LPI.

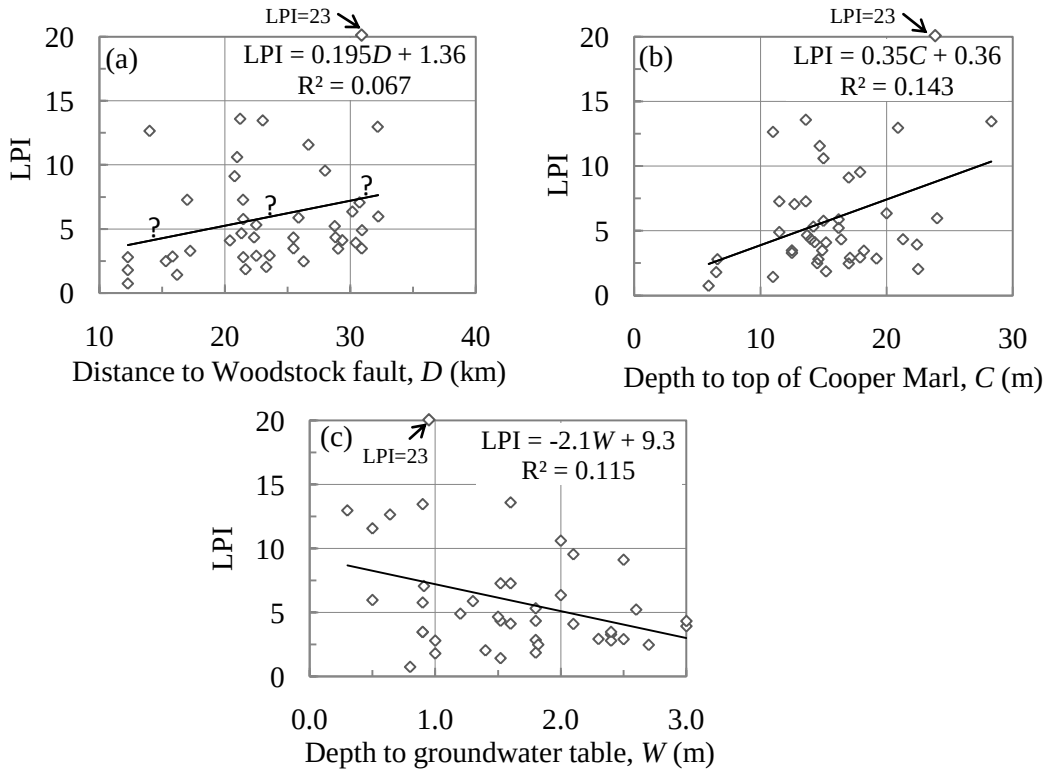

Figure 4.2 Variation of K_{DR}-corrected LPI with (a) distance to the Woodstock fault, (b) depth to top of the Cooper Marl, and (c) depth to the groundwater table for 42 SCPTu sites plotted in Qws assuming M_w=6.9, a_{max}=0.25g.

4.4 Liquefaction Probability Curves

The methodology proposed by Holzer et al. (2006, 2010), and Rix and Romero-Hudok (2007) is followed to develop liquefaction potential probability curves for any value of a_{max}/MSF. Considering LPI of 5 as the threshold for sand boil generation, (Toprak and Holzer 2003), the probability of LPI $\geq$ 5 is derived from complementary cumulative distribution of LPI values for various values of a_{max} and M_w. The probability of LPI $\geq$ 5 is estimated as a function of a_{max} for a specific earthquake magnitude by repeating the calculation for 0.1g, 0.15g, 0.2g, 0.25g, 0.3g, 0.4, 0.5g. Repeating the calculation for $5.0 \leq M_w \leq 7.5$ in 0.5 magnitude increments, the probability of LPI $\geq$ 5 as a function of a_{max}/MSF can be obtained.

Shown in Figure 4.3 are liquefaction probability curves developed for the Qws surficial deposits considering the influence of depth to top of the Cooper Marl and depth to the groundwater table. The probability of LPI $\geq$ 5 for a given a_{max}/MSF is derived assuming that the LPI values are lognormally distributed (denoted by circles in Figure 4.3) except when LPI values for some sites are calculated zero and the assumption that LPI values are from a lognormally distributed population is not correct. The probability of LPI $\geq$ 5 for the set of LPI analysis with LPI values of zero is computed using the experimental cumulative distribution of LPI values (denoted by triangles in Figure 4.3).

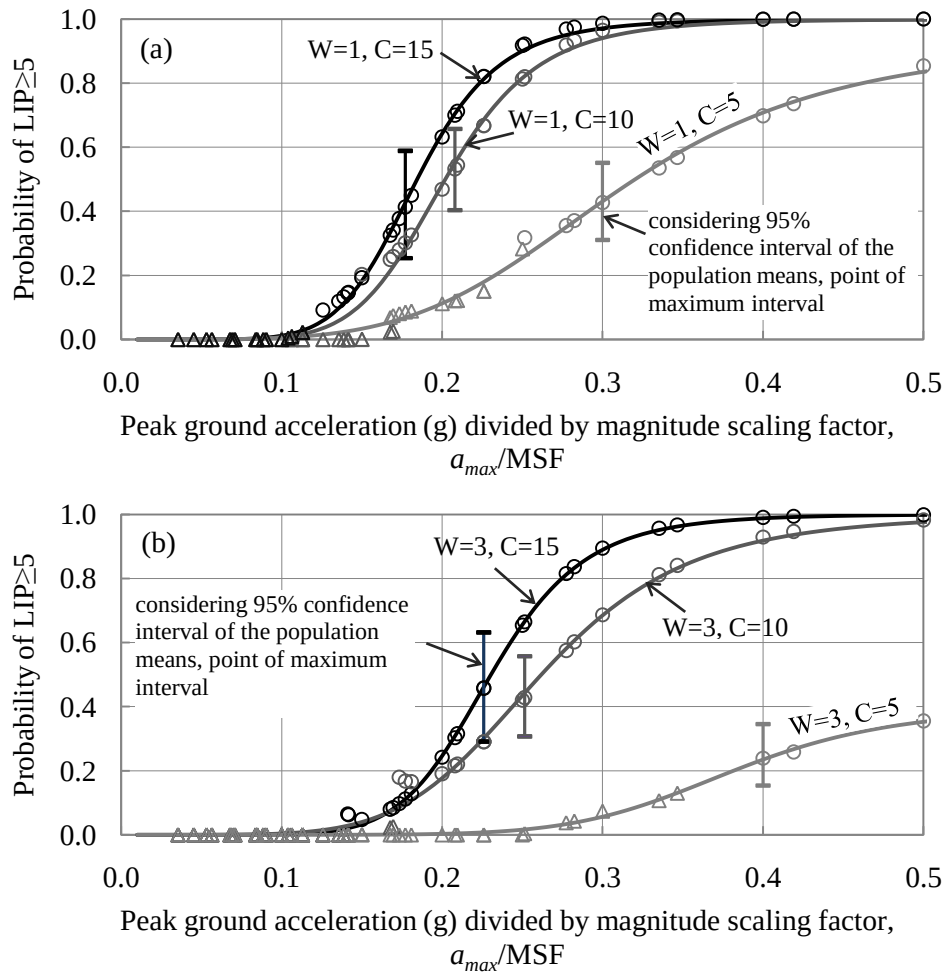

Figure 4.3 Liquefaction probability curves assuming various depths to the groundwater table (a) 1 m and (b) 3 m, and depth to top of Cooper Marl of 5, 10, 15 m for Qws surficial deposits in the Charleston area. Note that the circles in the figure represent probability based on lognormal distribution, and the triangles represent probability based on experimental cumulative distribution.

The following equation is fitted to the calculated points plotted in Figure 4.3 representing the probability of LPI ≥ 5 as a function of a_{max}/MSF:

$$P_{LPI>5} = \frac{\mathrm{a}}{\mathrm{b} + (\frac{a_{max} / \mathrm{MSF}}{\mathrm{c}})^{\mathrm{d}}} \tag{4.8}$$

where a, b, c and d are curve fitting coefficients. The probability curves developed assuming depth to top of the Cooper Marl at 5, 10, and 15 m, are based on 42, 39 and 22 SCPTu sites, respectively. The curves for *C*=10-15 m are in good agreement with the average curve derived by Heidari and Andrus (2011) and Chapter 3 using the 42 SCPTu profiles directly, and in general agreement with curves derived by Holzer et al. (2010) for South Carolina Pleistocene beach sands. Presented in Table 4.1 are the coefficients of Equation 4.8 for each set of LPI analysis.

The 95% confidence interval of the probability of LPI ≥ 5 for the point of maximum interval shown along each curve in Figure 4.3 is derived from the lognormal cumulative distribution function assuming a population mean equal to the upper and lower limit of 95% confidence interval of the sample mean. The 95% confidence interval estimate of the mean LPI value can be calculated by $\overline{X} \pm t_{0.025} S / \sqrt{n}$, where n is the number of sites and $t_{0.025}$ is the 97.5% quantile of student's t distribution with n-1 degrees of freedom (Schiff and D'Agostino 1996).

Table 4.1 Coefficients of the fitted liquefaction probability curves based on values for Qws surficial deposits.

Depth to groundwater table (m)	Depth to top of Cooper Marl (m)	a	b	c	d
1	5	29.337	31.493	0.664	-4.529
1	10	30.560	30.559	0.330	-6.984
1	15	30.559	30.559	0.296	-7.241
3	5	17.585	44.121	0.631	-7.511
3	10	30.472	30.457	0.477	-5.704
3	15	30.611	30.610	0.356	-7.891

4.5 Conclusion

The liquefaction potential of areas covered by Qws in the Charleston area was characterized in this paper. The characterization involved analyzing forty-two seismic cone soundings. LPI values were computed for SCPTu profiles after screening out layers not susceptible to liquefaction and correcting CRR for the influence of diagenetic processes using MEVR. The influence of distance to the Woodstock fault, depth to top of the Cooper Marl, and depth to the groundwater table on LPI was investigated. It was found that LPI values, computed assuming a scenario shaking, are independent of the distance to the Woodstock fault. Liquefaction probability curves are developed considering the influence of depth to the groundwater table and depth to the non-liquefiable Cooper Marl. These curves can be used for mapping liquefaction potential of Qws near Charleston. Liquefaction potential maps are useful tools for planners, engineers, and scientists working to mitigate damage during future earthquakes.

CHAPTER FIVE

LIQUEFACTION POTENTIAL OF ARTIFICIAL FILL AREAS IN THE CHARLESTON AREA, SOUTH CAROLINA

5.1 Introduction

Liquefaction potential of areas covered by artificial fill (af) around Charleston, South Carolina, are characterized in this chapter. The characterization involves reviewing cases of conspicuous craterlets and horizontal ground displacement that occurred in areas now covered by af material during the 1886 Charleston earthquake, reviewing previous liquefaction studies in the area, analyzing twenty-three seismic cone soundings, and developing liquefaction probability curves from the results.

Deposits of af consist of sand or clayey sand of diverse origin, and include fills used for roads, dams, and other construction. Most of the af areas mapped by the U.S. Geological Survey (Weems and Lemon 1988, 1989, and 1993) are located in the coastal area near the cities of Charleston and North Charleston, large spoils areas at Daniel Island and Drum Island, and the USS Yorktown State Park in Mount Pleasant. These fills have been created during the past 300 years in the low-lying areas adjacent to the harbor and rivers to allow the cities of Charleston and North Charleston to be constructed to the water's edge. On Daniel Island and Drum Island, the extensive areas of af are the result

of heaping of spoils during periodic dredging of the Charleston harbor (Weems and Lemon 1993). The thickness of af materials typically ranges from 1 to 3 m.

5.2 1886 Liquefaction and Ground Failure

Based on the report by Dutton (1889), extensive surface manifestations of liquefaction were observed throughout the Greater Charleston area in 1886. Among the 168 cases of horizontal ground displacement and conspicuous craterlet mapped by Earl Salon there are seven cases in areas that are now covered with af materials. The locations of these seven cases are plotted on the map presented in Figure 5.1. All of the cases, except one, are located in the cities of Charleston and North Charleston. It is likely that most of these areas were not covered by af in 1886.

In the recent liquefaction studies by Hayati and Andrus (2008) and Heidari and Andrus (2010), the 1886 liquefaction and ground failure cases on the Peninsula of Charleston and around the town of Mount Pleasant were carefully reviewed. Sixteen cases of liquefaction and permanent ground deformation summarized by Hayati and Andrus (2008) on the Charleston Peninsula plot in af where Qhes is believed to be in the subsurface, and four cases plot close to the contact between af and Qhes. Six cases of liquefaction surface effects in Mount Pleasant summarized by Heidari and Andrus (2010) plot in af, where Qhes or younger sand deposits are present in the subsurface.

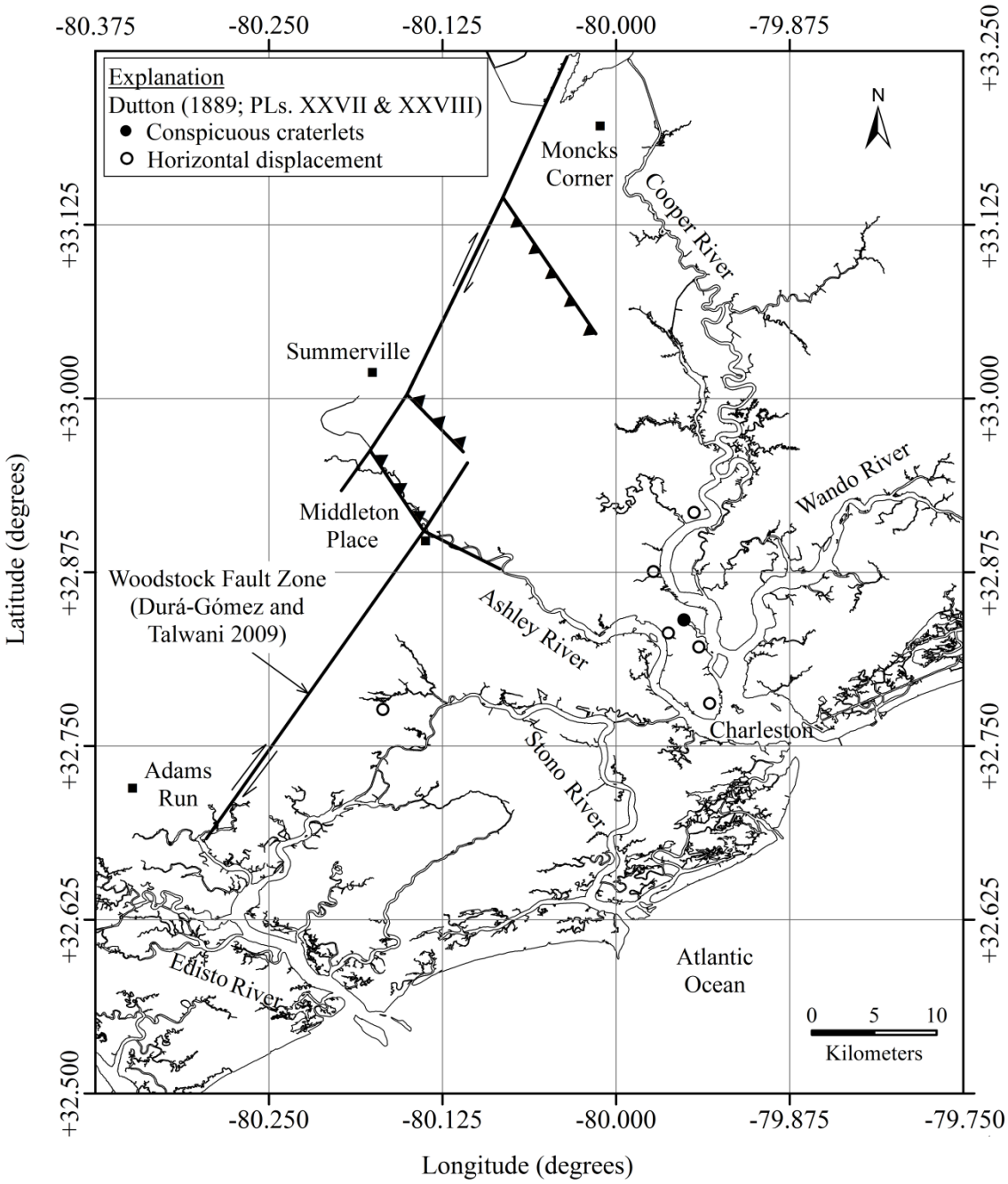

Figure 5.1 Map of the Greater Charleston area showing the Woodstock fault presented in Durá-Gómez and Talwani (2009) and the locations of 1886 liquefaction and ground failure in af areas from Dutton (1889).

5.3 SCPTu Database

Locations of the twenty-three SCPTu sites in af areas are shown in Figure 5.2. Summary information for the SCPTu sites is provided in Table 5.1. Site codes given in Table 5.1 begin with a letter representing the organization performing the test. The two digits following the initial letter indicate the year the test was conducted, and are followed by the project number and the test site designation. For example, the site code W03044-SC1 refers to the SCPTu performed by WPC in 2003 as part of project number 44 at test location SC1. Latitudes and longitudes were approximated using project site address information and the GoogleEarth free software. Location accuracy of the SCPTu sites is believed to be within 100 m. Electronic files for most of the SCPTu profiles are available in Fairbanks et al. (2004) and Mohanan et al. (2006).

Due to the wide range of variation in geology underlain by af, SCPTu sites mapped in af are grouped into three additional categories (af I, af II, af III) based on dominant geology in the top 10 m (see last column of Table 5.1). Category af I comprises sites where af is present at the ground surface and overlies Qht deposits that extend to depths ≥ 10 m. Category af II comprises sites where af is present at the ground surface and overlies Qht deposits that extend to depths < 10 m. Category af III includes sites where Qhes or younger sands are present within the top 10 m.

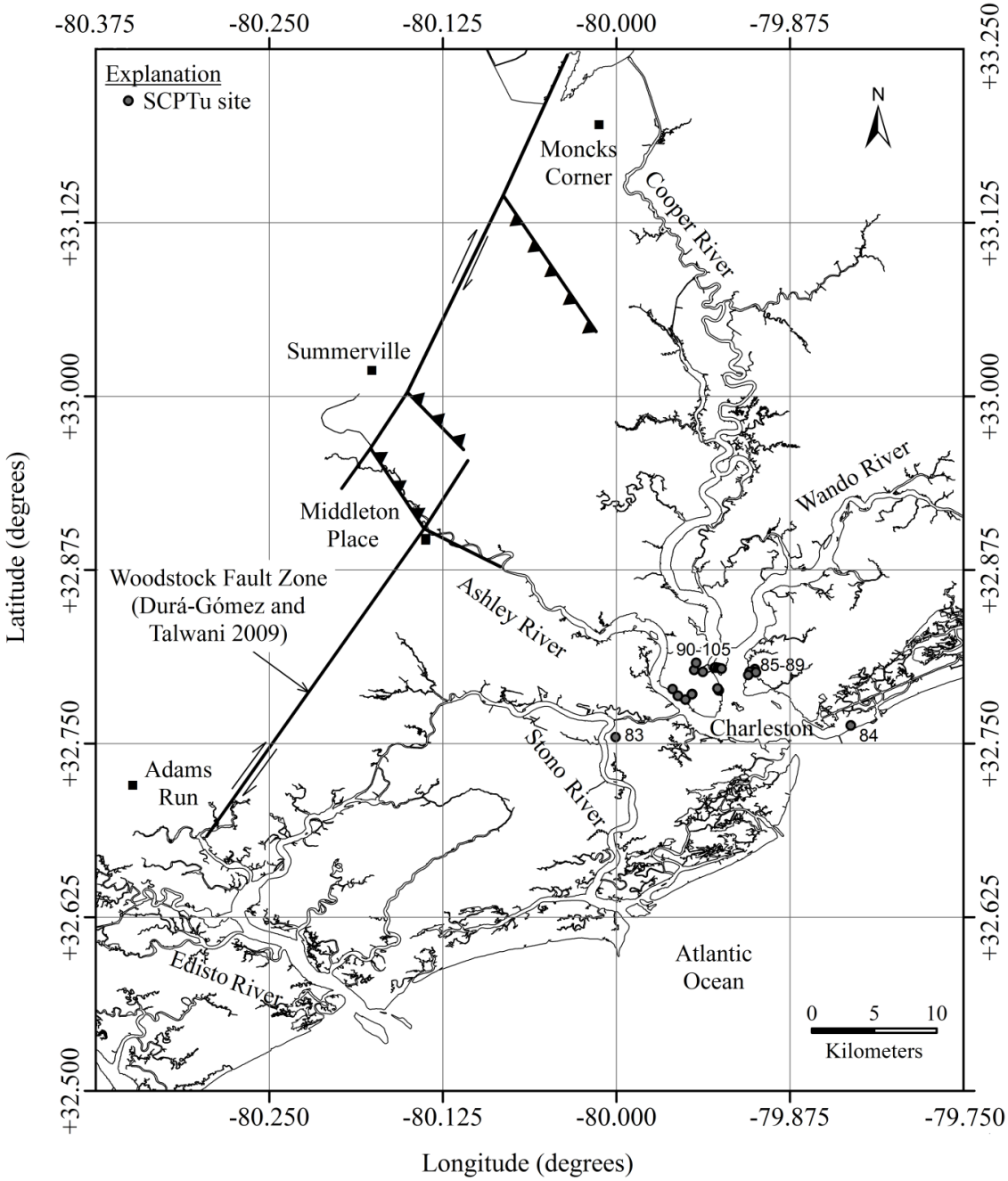

Figure 5.2 Map of the Greater Charleston area showing the Woodstock fault presented in Durá-Gómez and Talwani (2009) and the locations of SCPTu sites in areas of af.

Table 5.1 SCPTu soundings from the Greater Charleston area that plot in areas of af.

Site No.	Site Code[a]	Latitude (deg)	Longitude (deg)	Water Table Depth (m)	Maximum Test Depth (m)	Top of the Cooper Marl Depth (m)	Inferred Geology in Top 10 m	Near-surface Geology Category[d]
83	W03044-SC1	32.75459	-80.00055	1.0	11.6	11.9[b]	af/Qhec/Qhes/Qws	af III
84	W03071-SC1	32.76306	-79.83113	0.5	14.0	13.7[b]	af/Qhs/Qht/Qhec	af III
85	S04709-C4	32.8036	-79.9003	0.6	24.4	13.4	af/Qht/Qhes	af III
86	S99634-DS1	32.8017	-79.9015	0.3	36.6	12.6	af/Qht/Qhes/Qws	af III
87	S99634-C27	32.8016	-79.9039	1.2	27.5	20.5	af/Qhes/Qhec	af III
88	S99634-MPE5	32.8013	-79.8995	0.5	18.3	14.9	af/Qhes/Qws	af III
89	S04832-B1	32.7993	-79.9049	0.3	26.8	22.5	af/Qht/Qhec/Qhes	af III
90	S02105-B2	32.7883	-79.9262	1.2	22.8	18.2	af/Qht	af I
91	W99175-SCPT1	32.7897	-79.9271	1.0	37.8	24.6	af/Qht	af I
92	W03114-SC2	32.7856	-79.9455	1.6	25.3	24.3	af/Qht/Qws	af II
93	S02354-B4	32.7853	-79.9456	1.2	30.4	25.2	af/Qht/Qhec/Qws	af II
94	S01369-A5	32.7816	-79.9503	3.1	24.3	17.9	af/Qht/Qhes	af III
95	S01369-B2	32.7816	-79.9503	3.1	24.3	17.6	af/Qht/Qws	af II
96	W01352-SC1	32.7844	-79.9557	1.1	20.7	18.9	af/Qht	af I
97	S01420-S1	32.7892	-79.9595	0.9?	22.5	13.7	af/Qht	af I
98	S99876-CHS26	32.8029	-79.944	0.6	38.7	16.7	af/Qht/Qhes	af III
99	W01343-SCPT1	32.8081	-79.9425	2.7	21.9	19.8	af/Qht/Qhes	af III
100	W02092-SCPT1	32.8015	-79.9377	1.5	18.9	15.2	af/Qht	af I
101	S99876-ML15	32.8045	-79.9292	0.6	16.4	16.1	af/Qht	af I
102	S99876-ML16	32.8048	-79.9285	3.5	21.3	22.5	af/Qht	af I
103	S99876-ML18	32.8044	-79.9267	5.3	21.3	22.5	af/Qht	af I
104	S99876-ML22	32.8042	-79.9255	0.9	23.6	13.7	af/Qht	af I
105	S99876-ML24	32.8039	-79.9242	0.6	48.4	16.1	af/Qht	af I

[a]*First letter in site code: S = S&ME; W = WPC.*

[b]*Estimated from Weems and Lemon (1988, 1993).*

[c]*? = some uncertainty.*

[c]af I = *af at ground surface underlain by Qht extending to depth ≥ 10 m;* af II = *af at grounf surface underlain by Qht extending to depth < 10 m;* af III = *af at ground surface with Qhs or Qhes within the top 10 m and below the groundwater table.*

5.4 Liquefaction Potential based on a Scenario Earthquake

Liquefaction potential is expressed in terms of the liquefaction potential index (LPI) and corrected for the influence of diagenetic processes using the ratio of measured to estimated shear wave velocity (MEVR). The LPI calculations are performed according to the procedure outlined in Chapter 3. The $I_c > 2.6$ criterion is used to screen out non-susceptible clayey Quaternary soil layers above the Cooper Marl. The Cooper Marl is considered non-susceptible to liquefaction (Li et al. 2007; Hayati and Andrus 2008b).

The scenario shaking assumed for the LPI calculations is defined by M_w of 6.9 and a_{max} of 0.25g. These values of M_w and a_{max} are assumed to allow direct comparison with the liquefaction study of Mount Pleasant by Heidari and Andrus (2010). In addition, using a single set of M_w and a_{max} values allows for evaluation of the influence of distance to the Woodstock fault, depth to top of the Cooper Marl, and depth to the groundwater table on LPIs.

Summarized in Table 5.2 are mean, median and standard deviation of LPI values for af deposits grouped into four surficial geology categories. The LPI values in each group are assumed to be from lognormally distributed populations, and the Lilliefors test (Lilliefors 1967) supports this assumption. Considering μ as the mean LPI value, the point estimates of μ are 8, 4, 3 and 13, and their standard errors are ±2, ±1, ±2 and ±2 for categories all af, af I, af II, and af III, respectively.

The mean LPI value for category af III is considerably greater than for categories af I and af II. The greater LPI values in category af III are likely due to the contribution of Qhes or younger sand deposits that underlie af. The values of LPI summarized in Table 5.2 for category af III agree with values obtained in the previous study of Mount Pleasant by Heidari and Andrus (2010). In that study, the mean and median LPI values for af sites with Qhes or younger sands present below the groundwater table were 14 and 13, respectively. Also, the greater LPI values for category af III agree with the fact that all the cases of the 1886 ground failure occurred in af areas on Charleston Peninsula and around Mount Pleasant where Qhes or younger sand deposits are believed to be in the subsurface.

Presented in Figure 5.3, 5.4, and 5.5 are plots showing the variations of LPI with distance to the Woodstock fault (*D*), depth to the top of the Cooper Marl (*C*), and depth to the groundwater table (*W*) for categories all af, af I, and af III, respectively. As can be seen in these figures, the LPIs are not significantly correlated with the site-to-fault distance and depth to top of the Cooper Marl, or the correlation are highly effected by the outliers. However, LPI values indicate a slight decrease with increasing *W* values for categories all af and af III. These trends are consistent with the definition of LPI.

Table 5.2 Statistic of LPI assuming M_w = 6.9 and a_{max}= 0.25g for the af sites grouped by surficial geology.

Near-surface Geology Category	Number of SCPTus	Mean (Median) LPI[a]	±1 Standard deviation[a]	Uncertainty of mean[a]
All af	23	8 (5)	2-13	±2
af I	10	4 (3)	2-7	±1
af II	3	3 (2)	1-4	±2
af III	10	13 (11)	7-19	±2

[a]*Assuming log-normal distribution.*

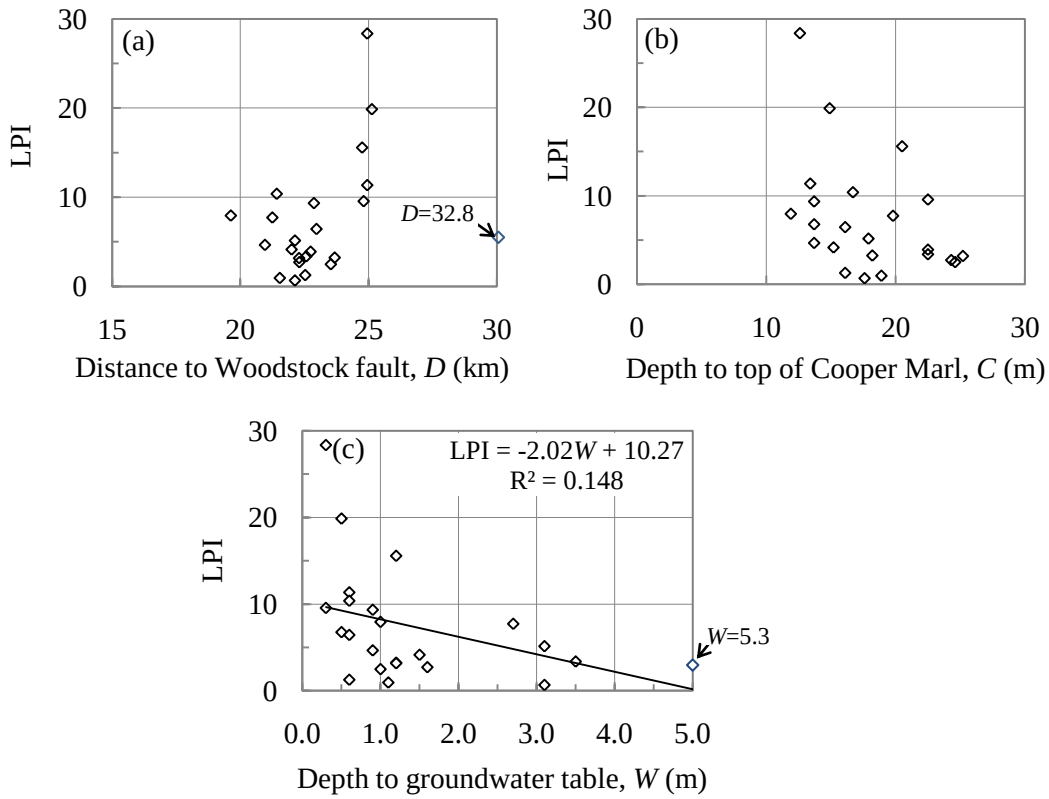

Figure 5.3 Variation of K_{DR}-corrected LPI with (a) distance to the Woodstock fault, (b) depth to top of the Cooper Marl, and (c) depth to the groundwater table for all 23 SCPTu sites in af assuming M_w = 6.9, a_{max} = 0.25g.

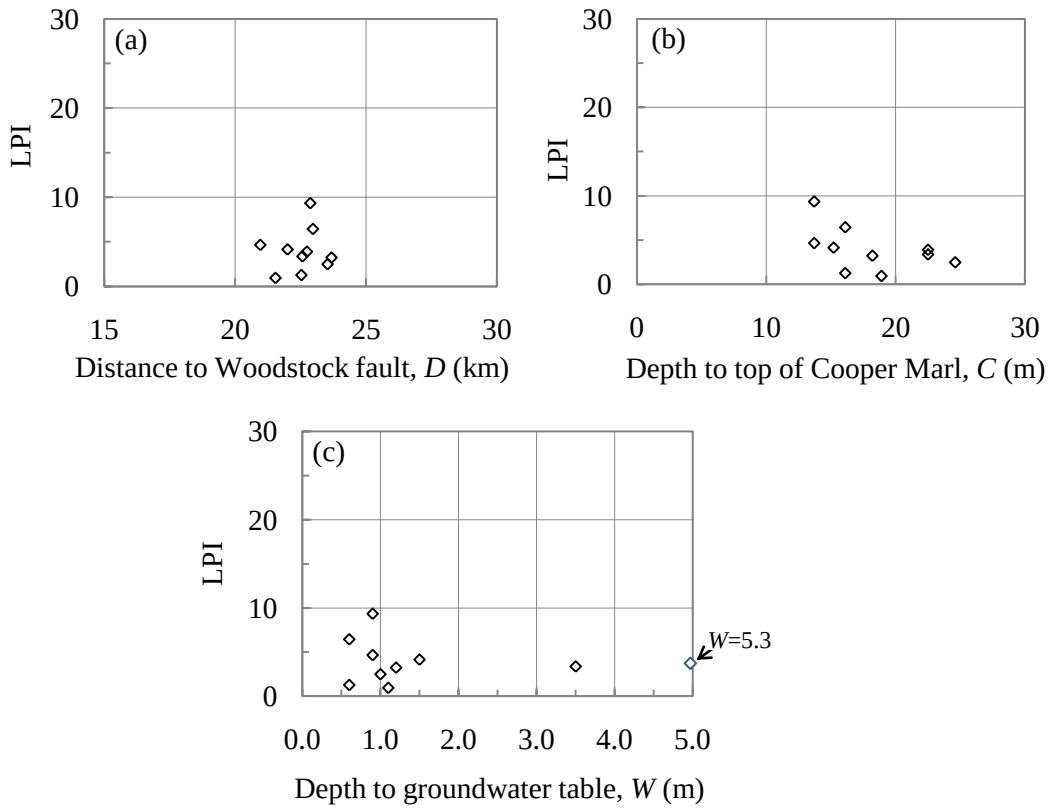

Figure 5.4 Variation of K_{DR}-corrected LPI with (a) distance to the Woodstock fault, (b) depth to top of the Cooper Marl, and (c) depth to the groundwater table for the 10 SCPTu sites of group af I assuming M_w = 6.9, a_{max} = 0.25g.

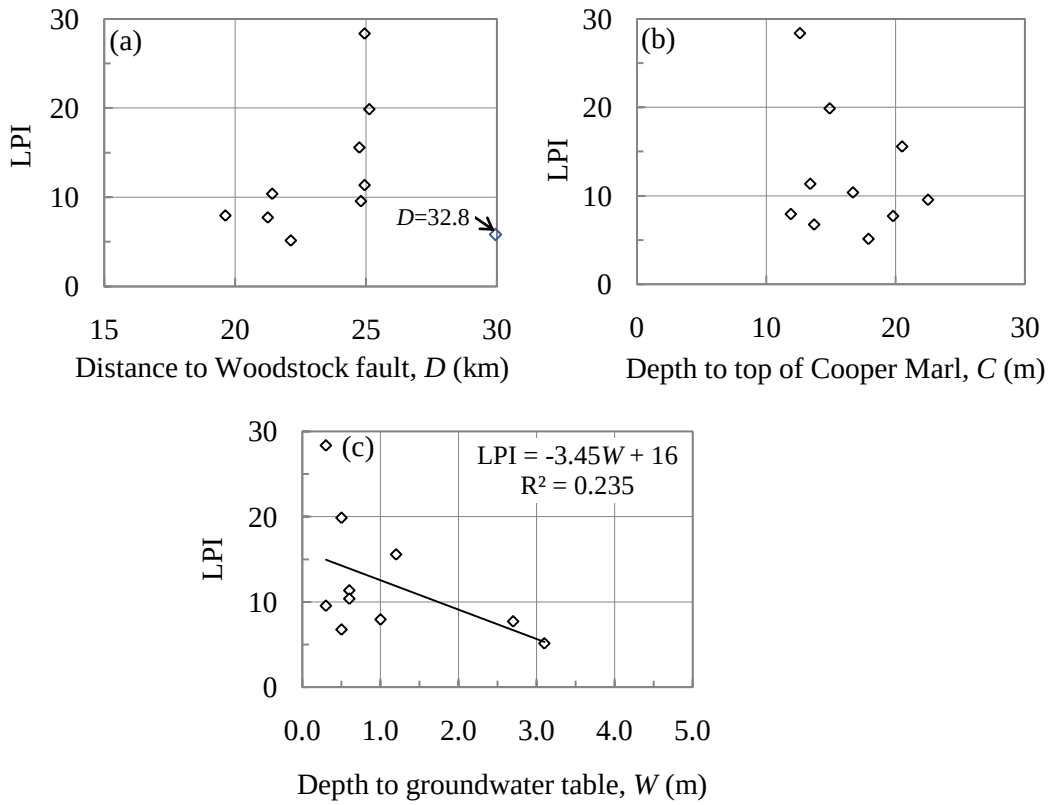

Figure 5.5 Variation of K_{DR}-corrected LPI with (a) distance to the Woodstock fault, (b) depth to top of the Cooper Marl, and (c) depth to the groundwater table for the 10 SCPTu sites of group af III assuming M_w = 6.9, a_{max} = 0.25g.

5.5 Liquefaction Probability Curves

The procedure explained in Chapter 3 is followed to compute liquefaction potential probability curves for any value of a_{max}/MSF. Shown in Figure 5.6 are liquefaction probability curves developed for the categories all af, af I, and af III. Because of the limited SCPTu sites included in category af II, no curve is developed for this category.

The 95% confidence interval of the probability of LPI ≥ 5 for the point of maximum interval shown in Figure 5.6 are derived from the lognormal cumulative distribution function assuming mean value equal to the upper and lower limit of the 95% confidence interval of the population mean. The 95% confidence interval estimate of the mean LPI value can be calculated by $\overline{X} \pm t_{0.025} S / \sqrt{n}$, where n is the number of sites and $t_{0.025}$ is the 97.5% quantile of student's t distribution with n-1 degrees of freedom (Schiff and D'Agostino 1996). The large uncertainties may be the result of limited data and/or significant variability in LPI values or af deposits.

The mean liquefaction probability curves for the three categories are compared in Figure 5.7. The probabilities of liquefaction predicted for categories af I and af III are considerably different. For area of af underlain by Qhes and younger sands, the curve for the af III category is recommended. For the areas covered by af where the subsurface geology cannot be reasonably inferred, it is recommended that liquefaction probability curve for the all af category be adopted.

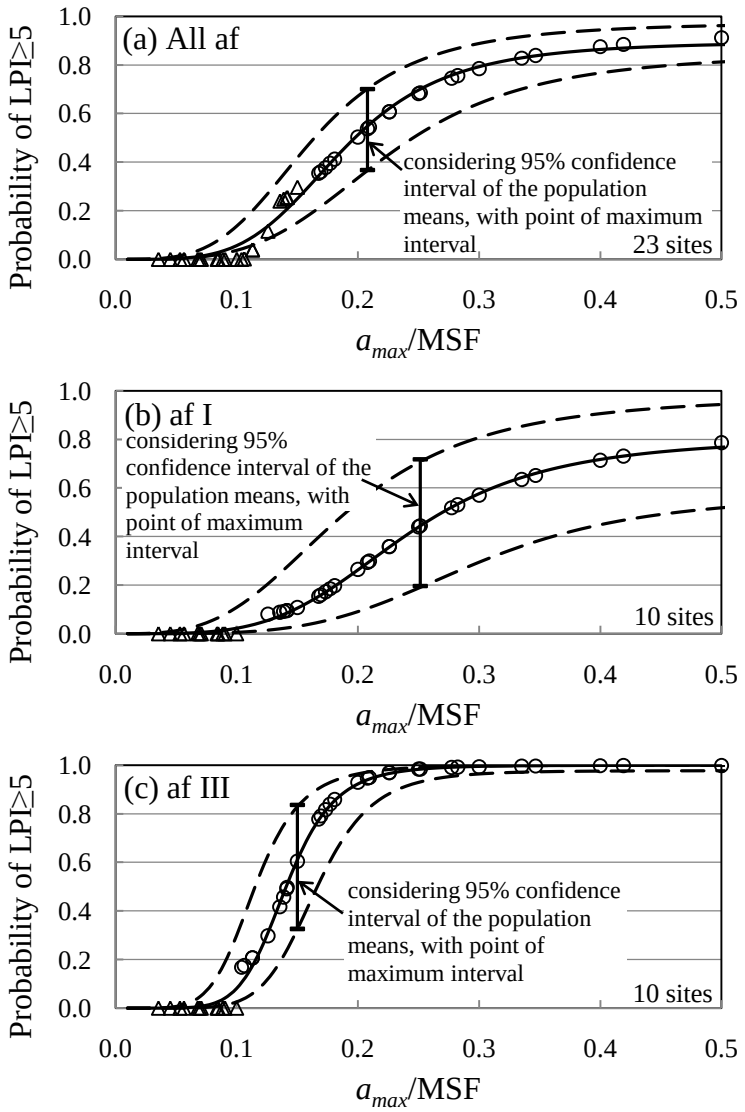

Figure 5.6 Liquefaction probability curves for (a) all af sites, (b) af I sites, and (c) af III sites. Note that the circles in the figure represent probability based on lognormal distribution, and the triangles represent probability based on experimental cumulative distribution.

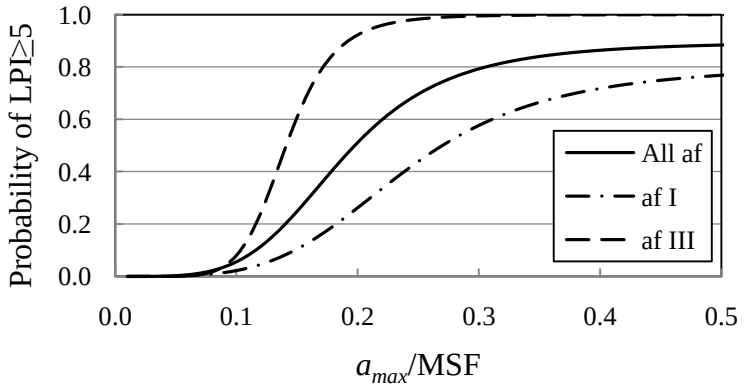

Figure 5.7 Comparison of liquefaction probability curves for three af categories.

Shown in Figure 5.8 and 5.9 are liquefaction probability curves developed for the categories af and af III considering the influence of depth to top of the Cooper Marl and depth to the groundwater table. These curves are useful for developing liquefaction potential maps for the area. The probability curves are developed assuming depths to top of the Cooper Marl of 5, 10, and 15 m, and depths to the groundwater table of 1 and 2 m. If the depth to top of the Cooper Marl is less than 15 m, the missing portion of the profile is assumed to be same as in the last portion of the measured profile.

The following equation is fitted to the calculated points in Figure 5.8 and 5.9 representing the probability of LPI ≥ 5 as a function of a_{max}/MSF:

$$P_{LPI>5} = \frac{\mathrm{a}}{\mathrm{b} + (\frac{a_{max} / \mathrm{MSF}}{\mathrm{c}})^{\mathrm{d}}} \tag{5.1}$$

where a, b, c, and d are curve fitting coefficients. Presented in Table 5.3 are the coefficients of Equation 5.1 for each set of LPI values in categories af and af III.

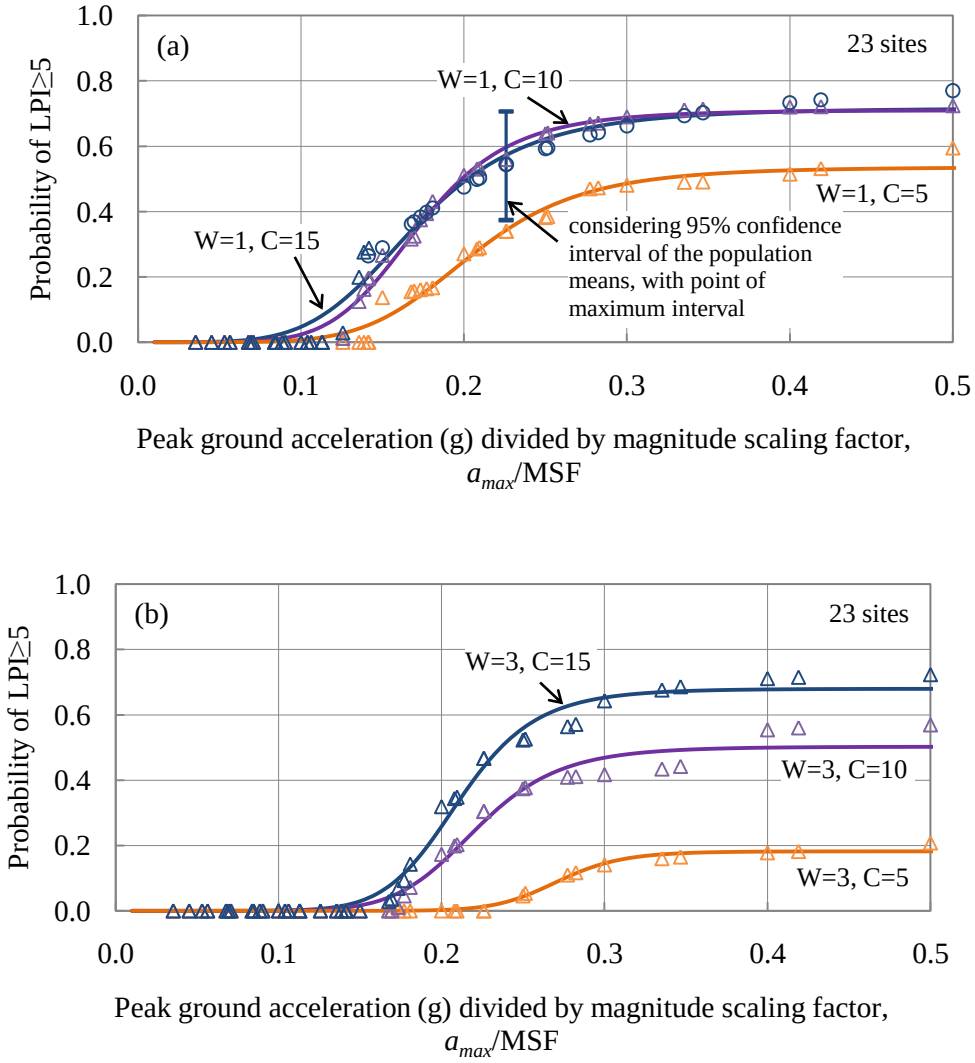

Figure 5.8 Liquefaction probability curves assuming depths to the groundwater table of (a) 1 m and (b) 3 m, and depths to top of the Cooper Marl of 5, 10, 15 m for **af** surficial deposits in the Charleston area. Note that the circles in the plots represent probability based on lognormal distribution, and the triangles represent probability based on experimental cumulative distribution.

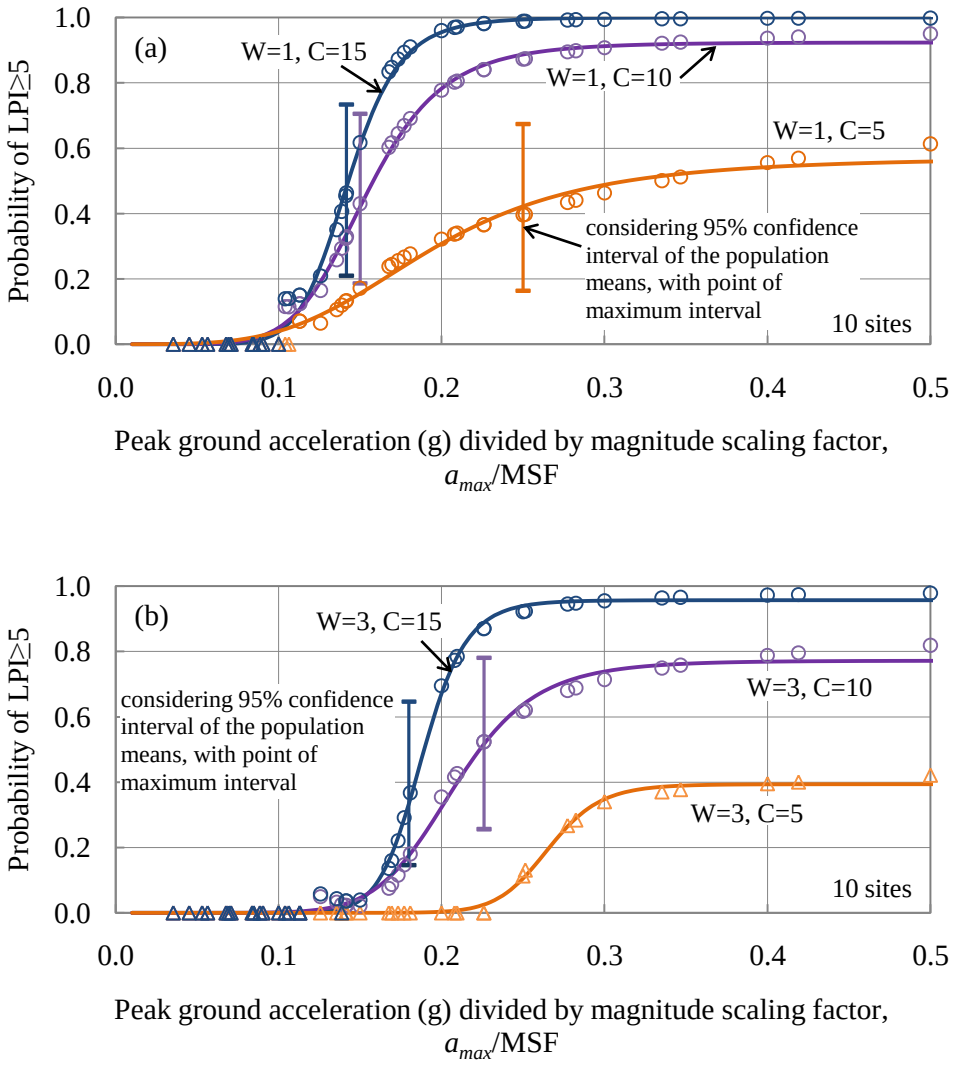

Figure 5.9 Liquefaction probability curves assuming depths to the groundwater table of (a) 1 m and (b) 3 m, and depths to top of the Cooper Marl of 5, 10, 15 m for **af III** surficial deposits in the Charleston area. Note that the circles in the plots represent probability based on lognormal distribution, and the triangles represent probability based on experimental cumulative distribution.

Table 5.3 Coefficients of the fitted liquefaction probability curves based on values for af and af III categories.

Depth to groundwater table (m)	Depth to top of Cooper Marl (m)	a	b	c	d
(a) all af category					
1	5	20.423	38.107	0.377	-5.971
1	10	24.914	35.072	0.307	-6.164
1	15	25.104	35.050	0.350	-4.955
3	5	7.973	43.704	0.357	-13.858
3	10	19.484	38.734	0.338	-8.664
3	15	24.192	35.574	0.313	-9.047
(b) af III category					
1	5	21.791	38.077	0.482	-3.961
1	10	29.357	31.778	0.261	-6.580
1	15	30.490	30.490	0.208	-9.064
3	5	16.259	41.252	0.332	-16.630
3	10	26.543	34.376	0.316	-8.461
3	15	29.109	30.403	0.240	-13.991

5.6 Conclusion

The liquefaction potential of areas covered by af in the Charleston area was characterized in this chapter. The characterization involved reviewing 1886 liquefaction and ground failure cases that plot in af and analyzing twenty-three seismic cone soundings. All the cases of 1886 ground failure that now plot in af areas on Charleston Peninsula and around Mount Pleasant appeared to be located where Qhes or younger sand deposits are believed to be in the subsurface.

LPI values were computed for twenty-three SCPTu profiles after screening out layers not susceptible to liquefaction and correcting CRR for the influence of diagenetic processes using MEVR. Liquefaction probability curves were developed for three categories. The probability curves for category af III, where Qhes or younger sand deposits is present within the top 10 m, predict significantly higher potentials than the probability curve for category af I, where Qht extends to depths > 10 m. It is recommended that the probability curves for af III (Figure 5.9) be used in areas of af where Qhes and younger sands are likely present in the subsurface. In areas where Qhes and younger sands are less likely, the probability curves for all af (Figure 5.8) are suggested.

CHAPTER SIX

LIQUEFACTION POTENTIAL OF SURFICIAL CLAYEY DEPOSITS IN THE CHARLESTON AREA, SOUTH CAROLINA

6.1 Introduction

Liquefaction potential of areas covered by clayey deposits in the Charleston area, South Carolina, are characterized in this chapter. The characterization involves reviewing cases of conspicuous liquefaction craterlets and horizontal ground displacement that occurred in surficial clayey deposits during the 1886 Charleston earthquake, reviewing previous liquefaction studies in the area, analyzing thirty-two seismic cone soundings, and developing liquefaction probability curves from the results.

6.2 Geology

A map of the Greater Charleston area is shown in Figure 6.1. Nearly all of the study area is covered by a blanket of Quaternary (< 1.8 million years) sand to clay that obscures underlying Tertiary stratigraphic units (Weems and Lewis 2002). According to the geologic maps and cross sections for eighteen 7.5-minute quadrangles in the area published by the U.S. Geological Survey (e.g., Weems and Lemon 1988, 1993, 1996; Weems et al. 1997), six Quaternary clayey deposits (or facies) present in the area are: Holocene tidal-marsh deposits (Qht); fluvial-estuarine silty to sandy clay deposits of the

33,000- to 85,000-year-old Silver Bluff terrace (Qhec); fluvial-estuarine clayey sand and clay facies of the 100,000-year-old Wando Formation (Qwc); fluvial-estuarine clayey sand and clay facies of the 200,000-year-old Ten Mile Hill beds (Qtc); fluvial-estuarine clayey sand and clay facies of the 400,000-year-old Ladson Formation (Qlc); and fluvial-estuarine clayey sand and clay facies of the > 700,000-year-old Penholoway Formation (Qpc). Also, considered in this chapter are modern to few thousand years old freshwater swamp deposits (Qhm) and Holocene alluvium deposits (Qal), which are commonly veneered by thin mucks and peats at their surface.

Deposits of Qht support marsh grass along the coast line and are confined to the lower lying areas adjacent to the modern rivers and creeks. Deposits of Qhec formed in tidal marshes that formerly extended up the river estuaries farther than the modern tidal marshes. Deposits of Qwc and Qtc form the higher natural ground with surficial clayey deposits along the coast. Deposits of Qwc are mainly found 27 to 46 km from the coast line and mostly are exposed in the western part of the study area. Deposits of Qtc are typically found 20 to 47 km from the coast line. Deposits of Qlc and Qpc are mainly found 30 to 41 km and 43 to 66 km, respectively, from the coast line. Peat and mud deposits of Qhm are accumulated in ovoid-shaped depressions on the surface of the Ten Mile Hill beds, the Ladson Formation, and the Penholoway Formation. Alluvium deposits of Qal are present along the upper reaches of the Ashley River and the Sawmill Branch, along and behind the Goose Creek Reservoir, and along the Cyprus swamp and the Four Hill swamp.

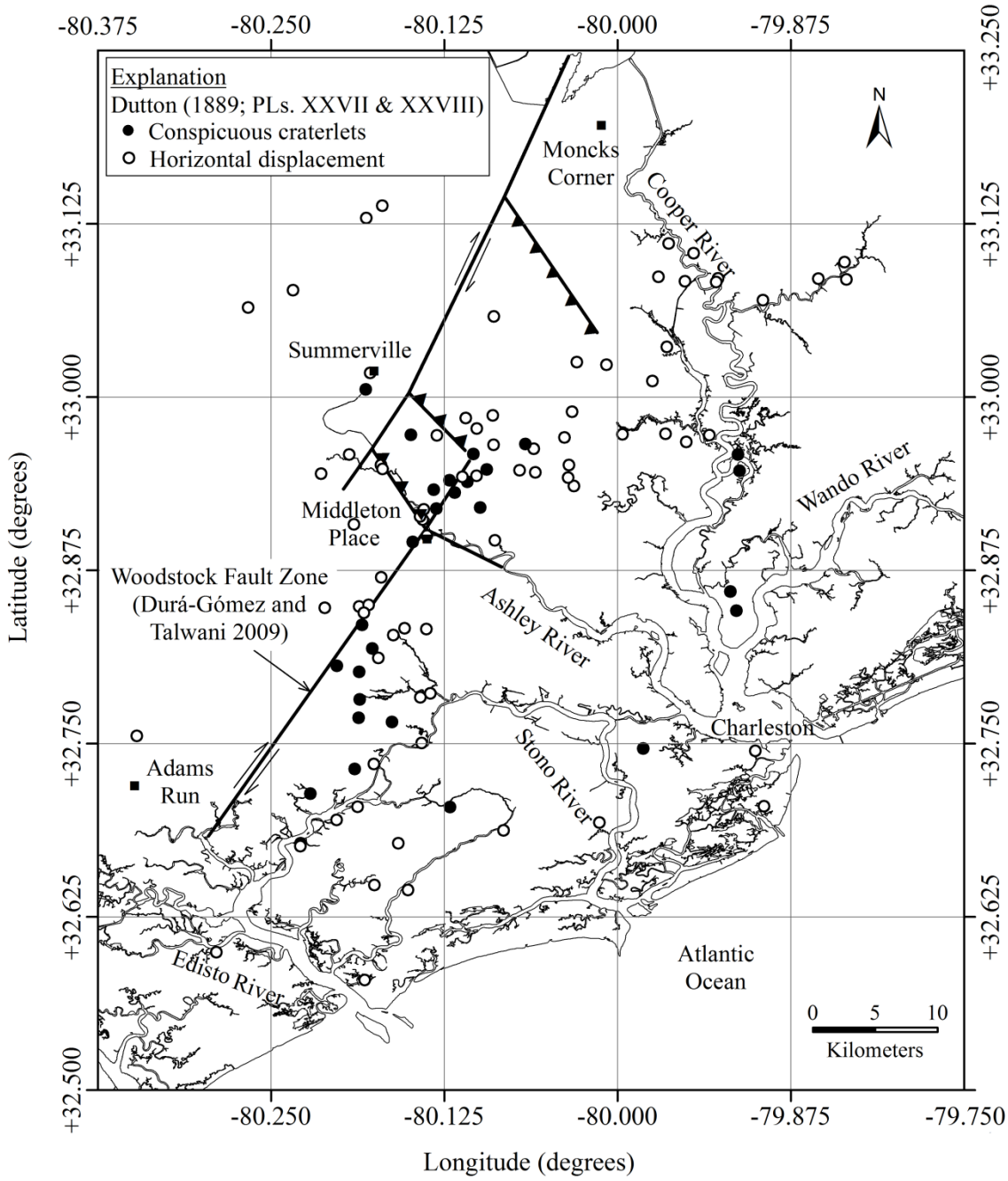

Figure 6.1 Map of the Greater Charleston area showing the Woodstock fault as presented in Durá-Gómez and Talwani (2009) and the locations of 1886 liquefaction and ground failure from Dutton (1889) that plot in surficial clayey deposits.

6.3 1886 Liquefaction and Ground Failure

As presented in Chapter 3, extensive surface manifestations of liquefaction were observed throughout the Greater Charleston area in 1886 (Dutton 1889). Shown in Figure 6.1 are the locations of areas of horizontal ground displacement and conspicuous craterlets (i.e., intense ejection of sand and water) mapped by Earle Sloan (Dutton 1889, PL. XXVII and PL. XXVIII) that plot in one of the surficial clayey deposits. Somewhat surprising is that more than sixty percent of the total mapped ground displacements and craterlets plot in the surficial clayey deposits. The large number of 1886 ground failures that plot in surficial clayey deposits may be more closely associated with the fluvial facies of the deposits, than with the estuarine facies, or where Qhes and/or younger beach sands are in the subsurface.

Summarized in Tables 6.1 and 6.2 are the areas of horizontal ground displacement and conspicuous craterlets, respectively. Plotted in Figure 6.2 are the frequencies of 1886 horizontal displacement and craterlet areas grouped by surficial clayey deposits. Sixty-five percent of the ground displacement and craterlet areas that plot in surficial clayey deposits are associated with Qhm/Qal, Qht, and Qhec. It is believed that Qhes and younger sands underlay these surficial clayey deposits at many of the locations. The large number of 1886 liquefaction manifestation cases plotted in Qht, Qhm and Qhec is comparable with the number of cases plotted in Qhes and younger sand deposits (see Chapter 3). The other thirty-five percent of the ground displacement and craterlet areas plot in mapped areas of surficial clayey deposits that are more than 100,000 years old

with the mean distance to the Woodstock fault of 4.8 m. The large number of 1886 liquefaction manifestation cases that plot in Qtc is similar to number of cases that plot in clean sand facies of the Ten Mill Hill beds (Qts). The number of 1886 liquefaction cases plotted in Qlc and Qpc are greater than the number of cases that plot in Qls and Qps surficial deposits.

The finding that the surficial sand and clayey deposits have similarly high liquefaction potential agree with the previous study by Balon and Andrus (2006), who characterized the liquefaction potential of seven surficial deposits, including three surficial clayey deposits, based on analyzing cone penetration test data. Balon and Andrus (2006) found that LPI values for the surficial clayey deposits were just as high as the LPI values for the surficial sand deposits. A new analysis of LPI values corrected for diagenetic process (or MEVR) is presented in the rest of the chapter to further evaluate the liquefaction potential of the surficial clayey deposits.

Table 6.1 Summary of 1886 ground displacement areas mapped by Earle Sloan (Dutton 1889, PL. XXVII) for eight surficial clayey deposits.

Surficial geology	Range of geologic age (years)[a]	Number of mapped areas	Distance to Woodstock fault (km)	
			Range	Mean (Median)
Qal	?	0	-	-
Qht	< 5 k	23	0.5-31.0	12.8 (13.8)
Qhm	< 34 k	8	0.1-11.3	3.1 (1.3)
Qhec	33-85 k	16	1.1-23.9	9.7 (10)
Qwc	70-130 k	1	6.6	6.6 (6.6)
Qtc	200-240 k	14	0.4-14.0	5.5 (4.6)
Qlc	240-730 k	9	0.2-10.3	5.1 (4.0)
Qpc	730-970 k	4	3.0-12.6	7.7 (7.6)

[a] *Weems and Lemon (1993, 1996).*

Table 6.2 Summary of 1886 conspicuous craterlet areas mapped by Earle Sloan (Dutton 1889, PL. XXVIII) for eight surficial clayey deposits.

Surficial Geology	Range of geologic age (years)[a]	Number of mapped areas	Distance to Woodstock fault (km)	
			Range	Mean (Median)
Qal	?	1	2.7	2.7 (2.7)
Qht	< 5 k	6	3.9-18.3	10.8 (9.4)
Qhm	< 34 k	6	0.3-1.4	0.7 (0.6)
Qhec	33-85 k	8	1.8-21.6	10.1 (5.0)
Qwc	70-130 k	0	-	-
Qtc	200-240 k	7	0.2-11.0	2.4 (0.9)
Qlc	240-730 k	1	4.0	4.0 (4.0)
Qpc	730-970 k	0	-	-

[a] *Weems and Lemon (1993, 1996).*

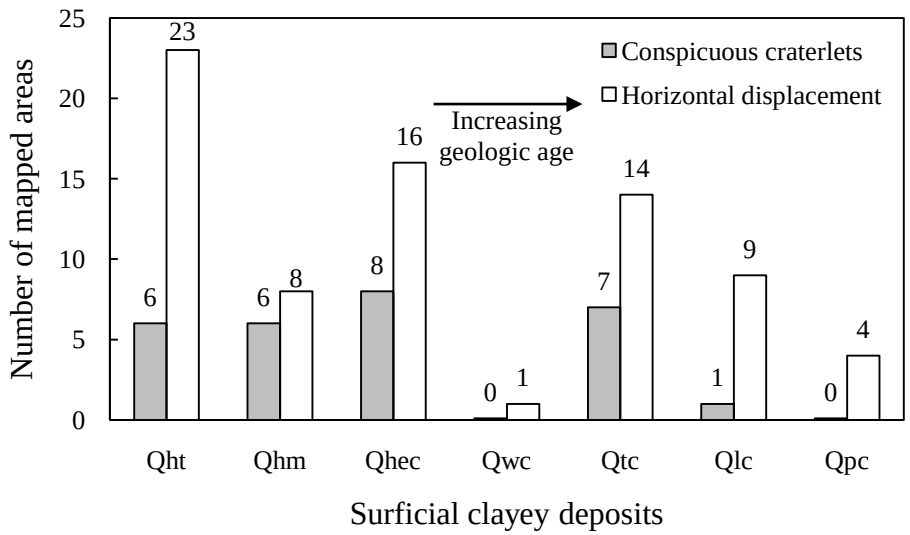

Figure 6.2 Frequency of 1886 ground displacement and craterlet areas (Dutton 1889, PLs. XXVII & XXVIII) grouped by surficial clayey deposits.

6.4 SCPTu Database

Locations of the thirty-two seismic cone (SCPTu) sites located in the surficial clayey deposits are shown in Figure 6.3. Summary information for the SCPTu sites is provided in Table 6.3. Site codes given in Table 6.3 begin with a letter representing the organization performing the test. The two digits following the initial letter indicate the year the test was conducted, and are followed by the project number and the test site designation. For example, the site code W02299-SC1 refers to a SCPTu performed by WPC in 2002 as part of project number 299 at test location SC1. Latitudes and longitudes were approximated using project site address information and the GoogleEarth free software. Location accuracy of the SCPTu sites is believed to be within 100 m. Electronic files for most of the SCPTu profiles are available in Fairbanks et al. (2004) and Mohanan et al. (2006).

The SCPTu sites are grouped into the four surficial clayey deposit categories of Qhec, Qtc, Qlc, and Qpc. Of the 32 SCPTu sites with available electronic files, there are 13, 10, 4, and 5 in the four surficial clayey deposit categories, respectively.

6.5 Liquefaction Potential based on a Scenario Earthquake

Liquefaction potential is expressed in terms of the liquefaction potential index (LPI) and corrected for the influence of diagenetic processes using the ratio of measured to estimated shear wave velocity (MEVR). The LPI calculations are performed according to the procedure outlined in Chapter 3. The $I_c > 2.6$ criterion is used to screen

out non-susceptible clayey Quaternary soil layers above the Cooper Marl. The Cooper Marl is considered non-susceptible to liquefaction (Li et al. 2007; Hayati and Andrus 2008b). The scenario shaking assumed for the LPI calculations is defined by M_w of 6.9 and a_{max} of 0.25g. These values of M_w and a_{max} are assumed to allow direct comparison with the liquefaction study in previous chapters.

Summarized in Table 6.4 are mean, median and standard deviation of LPI values for the four surficial clayey groups. The LPI values in each group, except Qtc, are assumed to be from lognormally distributed populations, and the Lilliefors test (Lilliefors 1967) supports this assumption. The LPI values in category Qtc are assumed to be from a normally distributed population. The population mean, μ, is estimated by the sample mean, $\bar{X}$. The uncertainty associated with μ can be calculated by dividing the population standard deviation, σ, by the square root of the sample size, $\sqrt{n}$. Because σ is unknown, the sample standard deviation, S, is used to calculate the standard error. Considering μ as the mean LPI value, the point estimates of μ are 7, 2, 2 and 3, and their standard errors are ±8, ±1, ±1 and ±7 for Qhec, Qtc, Qlc, and Qpc, respectively.

The high standard deviation and uncertainty associated with the mean LPI values for Qhec and Qpc may represent the wide range of variations in geology present beneath these areas. The mean LPI value for Qhec is greater than the mean LPI values for the older surficial clayey deposits of Qtc, Qlc, and Qpc. The greater LPI values associated with the Qhec may be due to the contribution of Qhes or younger sand deposits underlying Qhec or fluvial facies within Qhec.

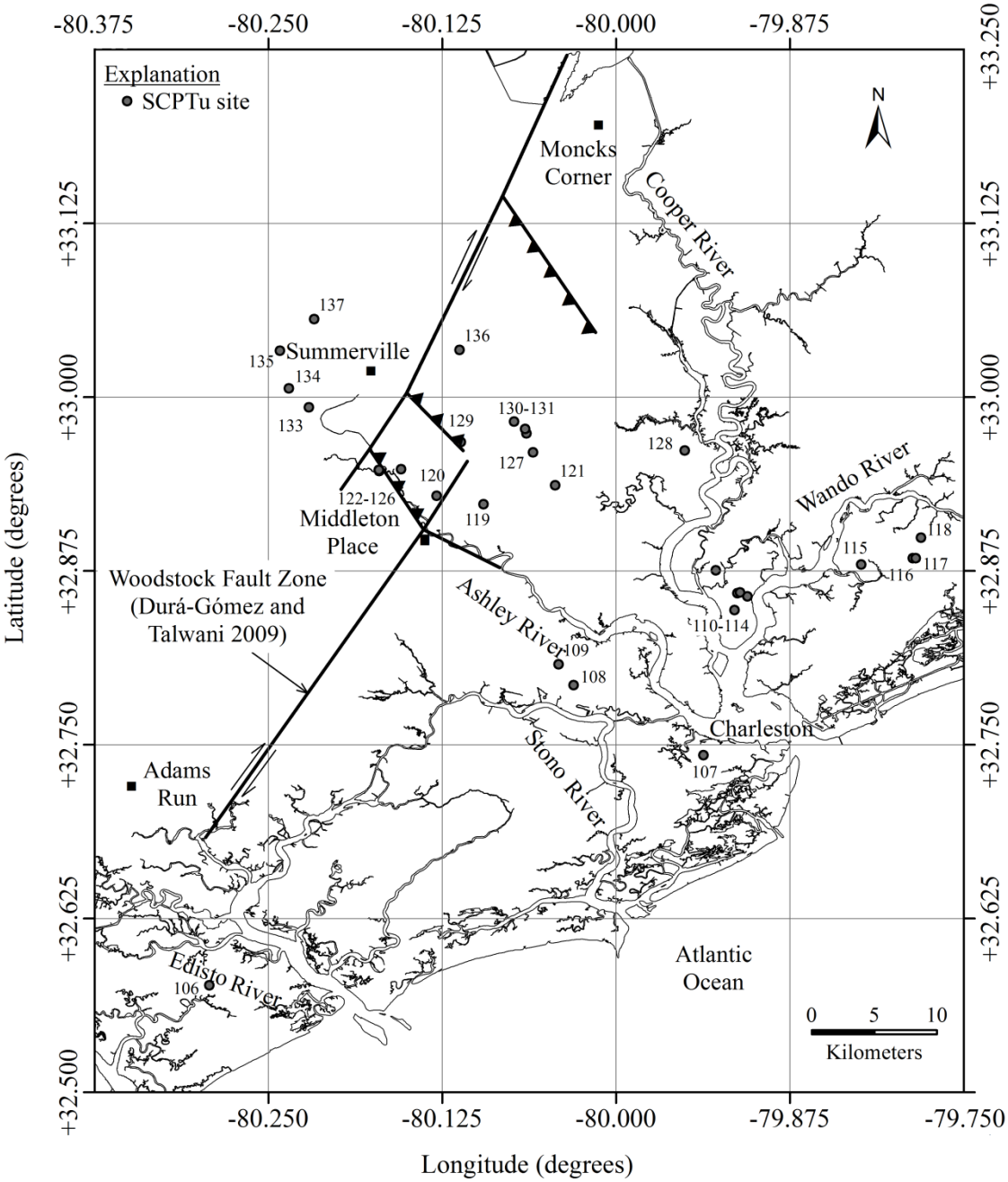

Figure 6.3 Map of the Greater Charleston area showing the Woodstock fault as presented in Durá-Gómez and Talwani (2009) and the locations of SCPTu sites that plot in surficial clayey deposits.

Table 6.3 SCPTu soundings from the Greater Charleston area that plot in surficial clayey deposits.

Site No.	Site Code[a]	Latitude (deg)	Longitude (deg)	Water Table Depth (m)	Maximum Test Depth (m)	Top of the Cooper Marl Depth (m)	Surficial Geology
106	W02299-SC1	32.57694	-80.29239	0.5	16.8	16.8	Qhec
107	W01165-SC1	32.74243	-79.93721	1.5	18.0	18.0	Qhec
108	W02195-SC1	32.79289	-80.03047	1.9	10.9	10.9	Qhec? [c]
109	S03352-B1	32.80769	-80.04131	1.1	13.1	7.0	Qhec
110	W02234-SC1	32.84670	-79.91480	2.5	15.9	15.2	Qhec
111	W04378-SC5	32.85672	-79.90557	1.2	10.9	9.5	Qhec
112	W02120-SC1	32.85889	-79.91262	1.3	11.0	8.8	Qhec
113	W03058-SC6	32.85948	-79.91084	1.7	13.0	11.7	Qhec
114	W02219-SC1	32.87530	-79.92820	1.3	10.0	7.0	Qhec
115	W01187-SC1	32.87948	-79.82359	1.2	12.8	12.8	Qhec
116	W04431-SCPT1	32.88401	-79.78659	1.8	11.8	10.2	Qhec
117	W01277-SC1	32.88406	-79.78447	1.5	8.0	10.2?	Qhec
118	W02179-SCPT1	32.89885	-79.78072	1.7	14.8	14.8	Qhec
119	W02059-B06	32.92290	-80.09520	3.5	13.0	13.0	Qtc
120	W04179-SC1	32.92894	-80.12892	1.9	10.9	5.3	Qtc
121	W01218-SC1	32.93653	-80.04378	2.0	7.3	10.3[b]	Qtc
122	S06858-FD5	32.94684	-80.17021	1.8	7.3	7.3	Qtc
123	S06858-FD4	32.94699	-80.17035	1.8	9.9	9.9	Qtc
124	S06858-FD1	32.94748	-80.17067	2.1	9.6	9.6	Qtc
125	S06858-FD2	32.94758	-80.17045	1.8	10.5	10.5	Qtc
126	W04432-SC1	32.94818	-80.15448	1.2	8.8	7.6	Qtc
127	W02073-SC6	32.96030	-80.05960	1.7	9.0	7.6	Qlc
128	S03489-B1	32.96162	-79.95056	2.4	30.3	13.4	Qtc
129	W01163-SCPT1	32.96755	-80.11156	2.3	10.0	10.0	Qlc
130	W03422-SC1	32.97389	-80.06446	1.5	10.0	9.9	Qlc
131	W03390-SC2	32.97705	-80.06534	2.0	8.2	8.2	Qlc
132	W03137-SC1	32.98238	-80.07339	1.5	9.2	9.2	Qtc
133	W02250-SC1	32.99260	-80.22080	3.1	12.8	12.8	Qpc
134	W04282-SCPT2	33.00630	-80.23520	1.7	14.9	14.9	Qpc
135	W05024-SC2	33.03326	-80.24171	0.8	3.1	6.1[b]	Qpc
136	W04390-SCPT3	33.03390	-80.11250	1.5	8.6	8.5?	Qpc
137	S02823-C1	33.05614	-80.21701	0.9	8.8	8.7?	Qpc

[a]*First letter in site code: S = S&ME; W = WPC.*
[b]*Estimated from Weems and Lemon (1988, 1993).*
[c]*? = some uncertainty.*

Table 6.4 Statistic of LPI assuming M_w = 6.9 and a_{max}= 0.25g for four surficial clayey deposits.

Near-surface geology Category	Number of SCPTus	Mean (Median) LPI[a]	±1 Standard deviation[a]	Uncertainty of mean[a]
Qhec	13	7 (2)	0-9	±8
Qtc	10	2 (1)[b]	0-5[b]	±1
Qlc	4	2 (1)	1-3	±1
Qpc	5	3 (1)	0-4	±7

[a]*Assuming log-normal distribution.*
[b]*Assuming normal distribution.*

6.6 Liquefaction Probability Curves

The procedure outlined in Chapter 3 is followed to compute liquefaction potential probability curves for any value of a_{max}/MSF for the four surficial clayey deposit groups with SCPTu data. Shown in Figure 6.4 are liquefaction probability curves developed for the four surficial clayey deposit groups. The 95% confidence interval of the probability of LPI $\geq$ 5 with the point of maximum interval shown in Figure 6.4 are also derived following the procedure explained in Chapter 3.

Considering the fact that the numbers of 1886 ground displacement and craterlet areas in Qhec and Qtc are comparable to those in Qhes and Qts deposits, the low liquefaction potentials predicted for Qhec and Qtc deposits in Figure 6.4(a) and 6.4(b) are not consistence with the 1886 observations (see Figure 6.2). The moderate liquefaction potential predicted for Qlc and Qpc in Figure 6.4(c) and 6.4(d) are generally consistent with the 1886 observations (see Figure 6.2). The broad confidence intervals shown in Figure 6.4(c) and 6.4(d) are the result of few SCPTu sites available in Qlc and Qpc, respectively, and scatter in the computed LPI values.

The mean liquefaction probability curves for the four categories are compared in Figure 6.5. Liquefaction probabilities predicted for Qhec and Qtc are less than the predicted values for the Qlc and Qpc when a_{max}/MSF is greater than about 0.3. These results do not agree with the observations of greater liquefaction in these deposits in 1886. Therefore, it is recommended that the liquefaction probability curves for Qhs/Qhes (Figure 3.9a) and Qts (Figure 3.9d) be used for estimating the liquefaction potential of

Qht/Qhec and Qtc. Shown in Figure 6.7 and 6.8 are liquefaction probability curves developed for the Qhs/Qhes and Qts considering the influence of depth to top of the Cooper Marl and depth to the groundwater table.

The liquefaction probability curves for Qlc and Qpc are similar. Therefore, it seems appropriate to develop liquefaction potential curves for the combined Qlc and Qpc group. Shown in Figure 6.6 are liquefaction probability curves developed for the combined Qlc and Qpc group considering the influence of depth to top of the Cooper Marl and depth to the groundwater table. The probability curves are developed assuming depths to top of the Cooper Marl of 5 and 10 m, and depths to the groundwater table of 1 and 3 m. If the depth to top of the Cooper Marl is less than 10 m, the missing portion of the profile is assumed to be same as in the last portion of the measured profile. These preliminary curves shown in Figure 6.6 are tentatively suggested for developing liquefaction potential maps for the mapped Qlc and Qpc areas.

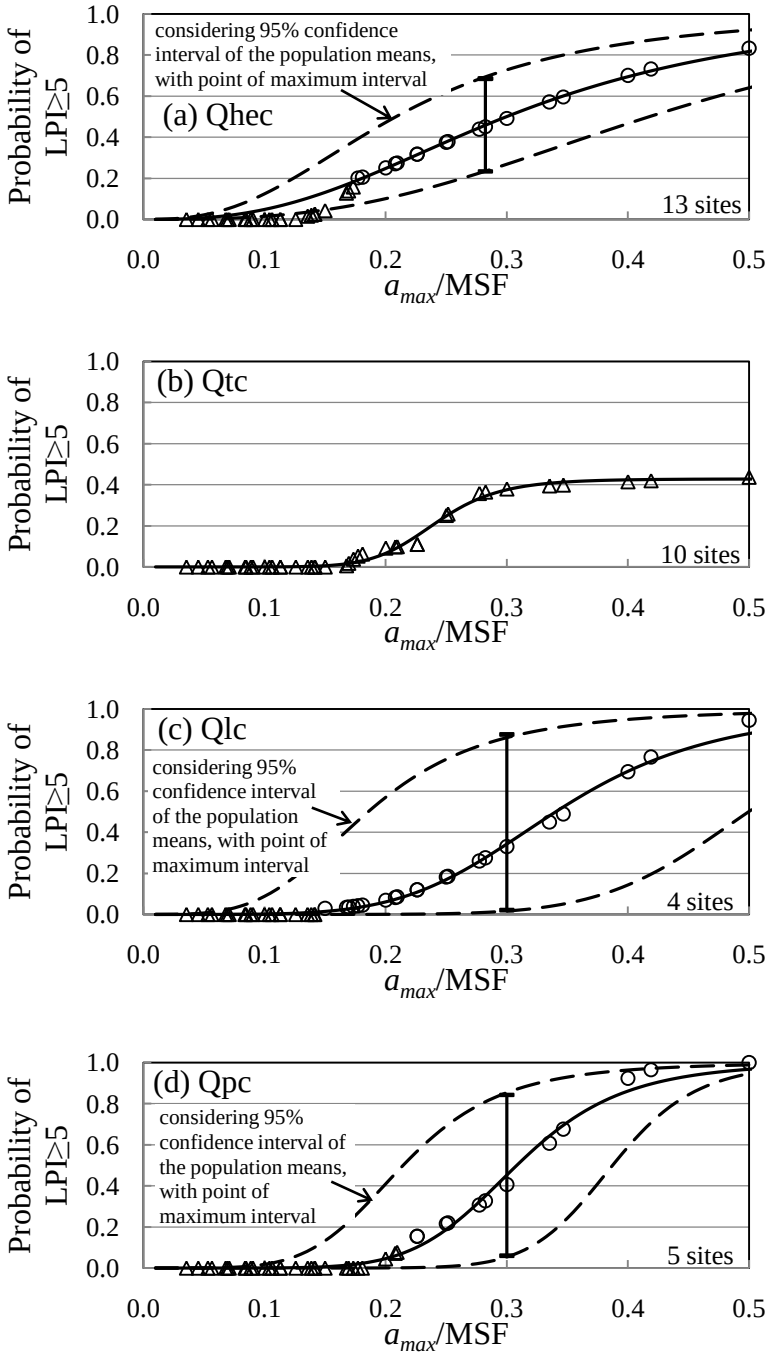

Figure 6.4 Liquefaction probability curves for four surficial clayey deposits. Note that the circles in the plots represent probability based on lognormal distribution, and the triangles represent probability based on experimental cumulative distribution.

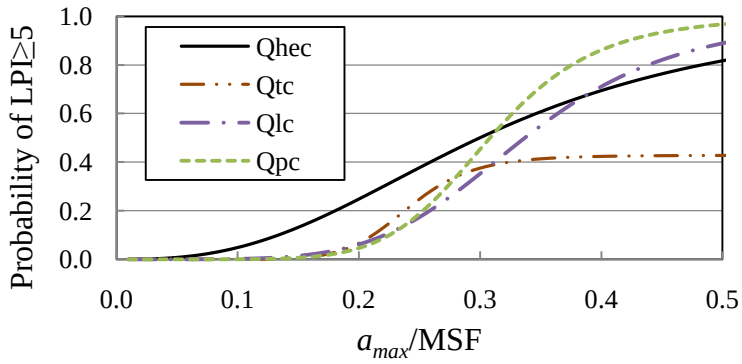

Figure 6.5 Comparison of liquefaction probability curves for four surficial clayey deposits.

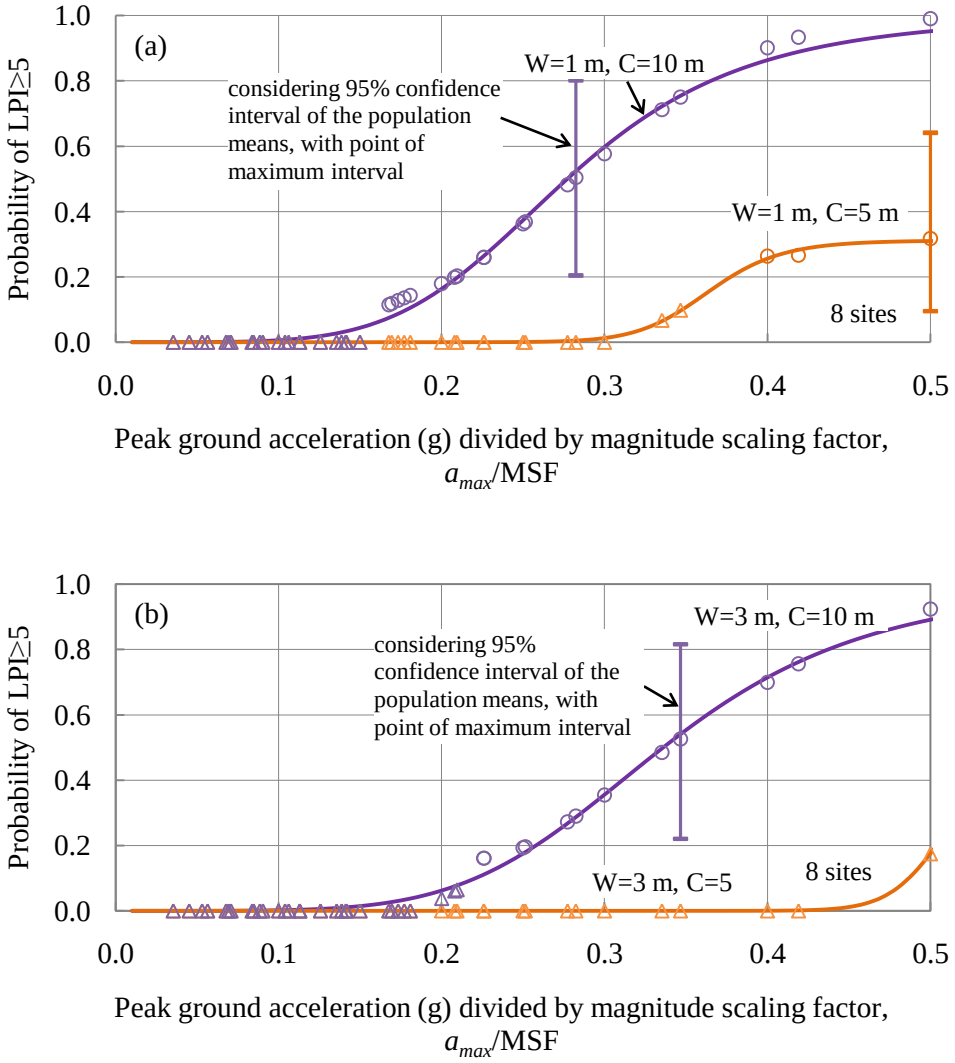

Figure 6.6 Liquefaction probability curves for the combined Qlc and Qpc surficial deposits assuming depths to the groundwater table of (a) 1 m and (b) 3 m, and depths to top of the Cooper Marl of 5 and 10 m. Note that the circles in the plots represent probability based on lognormal distribution, and the triangles represent probability based on experimental cumulative distribution.

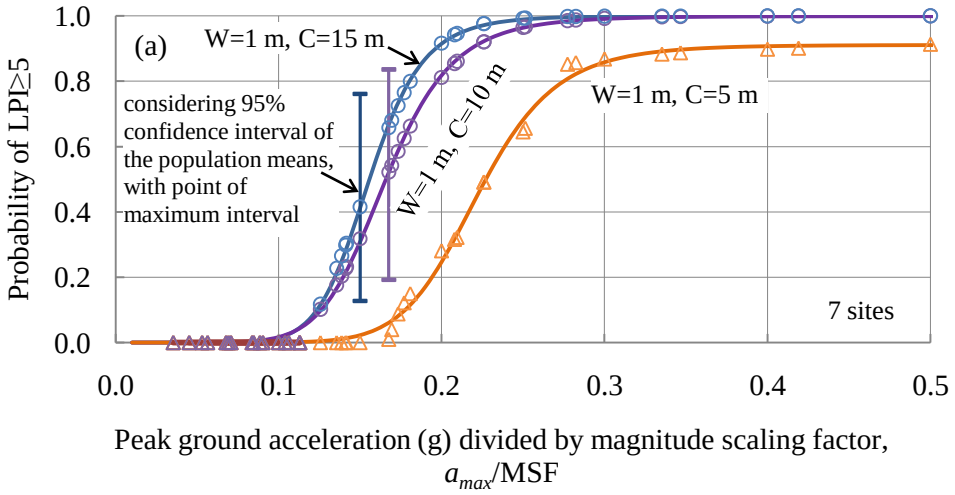

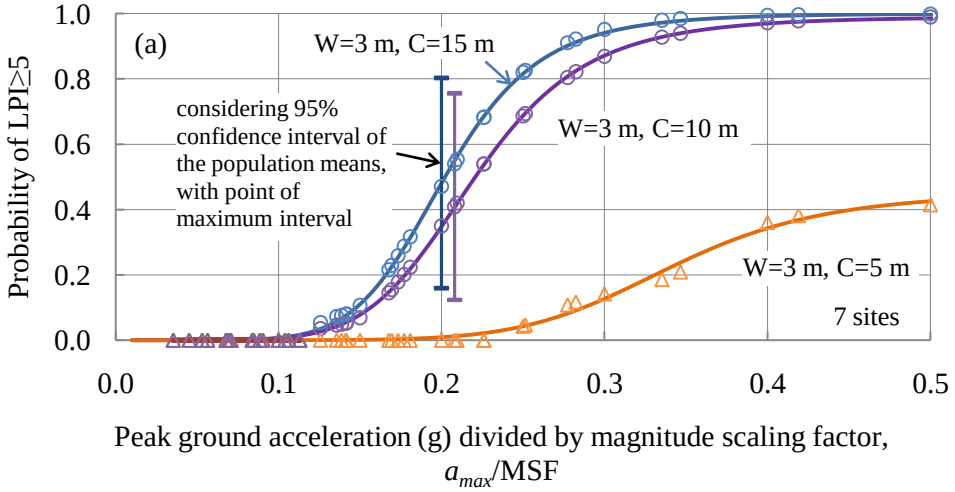

Figure 6.7 Liquefaction probability curves for Qhs/Qhes, recommended for Qht/Qhec surficial deposits, assuming depths to the groundwater table of (a) 1 m and (b) 3 m, and depths to top of the Cooper Marl of 5, 10, 15 m. Note that the circles in the plots represent probability based on lognormal distribution, and the triangles represent probability based on experimental cumulative distribution.

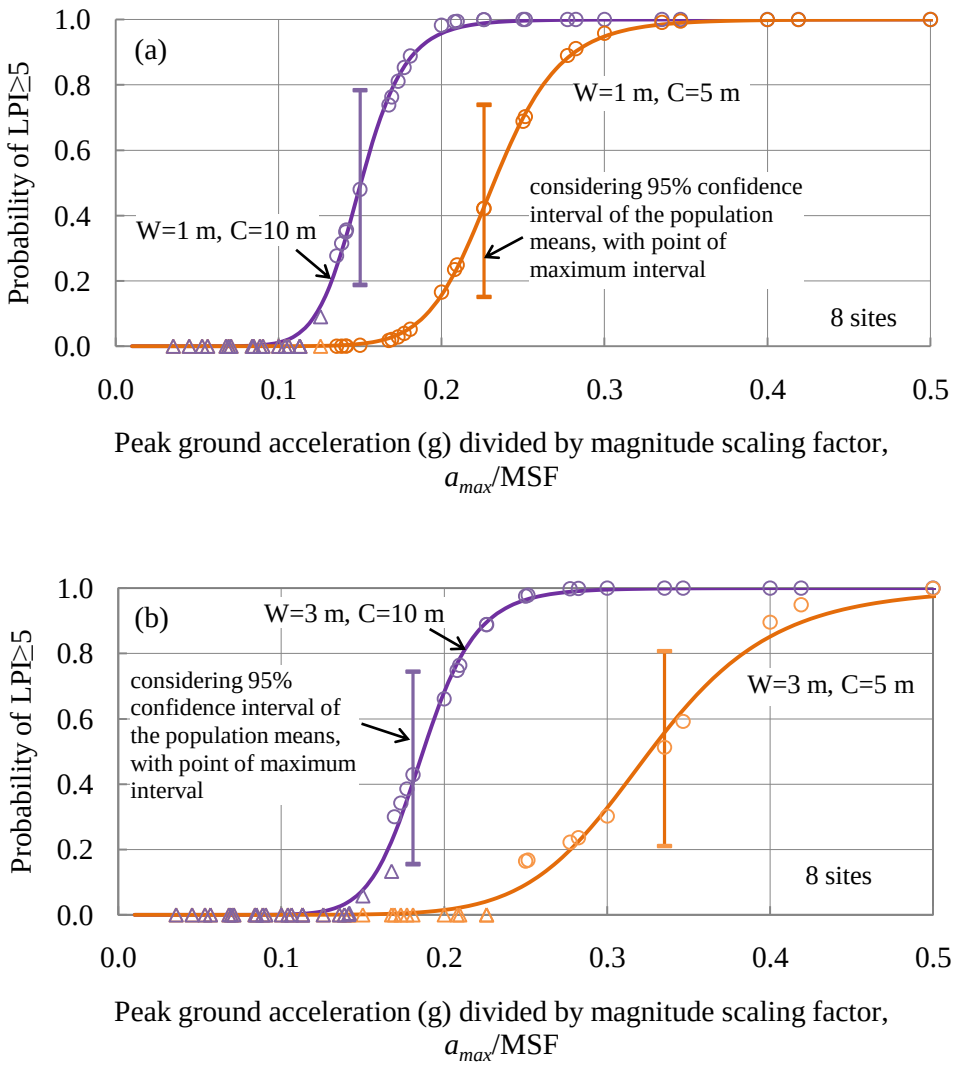

Figure 6.8 Liquefaction probability curves for Qts, recommended for Qtc surficial deposits, assuming depths to the groundwater table of (a) 1 m and (b) 3 m, and depths to top of the Cooper Marl of 5 and 10 m. Note that the circles in the plots represent probability based on lognormal distribution, and the triangles represent probability based on experimental cumulative distribution.

The following equation is fitted to the calculated points in Figure 6.6, 6.7 and 6.8 representing the probability of LPI ≥ 5 as a function of a_{max}/MSF:

$$P_{LPI>5} = \frac{\mathrm{a}}{\mathrm{b} + (\frac{a_{max} / \mathrm{MSF}}{\mathrm{c}})^{\mathrm{d}}} \tag{6.1}$$

where a, b, c, and d are curve fitting coefficients. Presented in Table 6.5 and 6.6 are the coefficients of Equation 6.1 the LPI values for the combined Qlc and Qpc group, Qht/Qhec, and Qtc.

Because no SCPTu data were available for Qhm surficial deposits and there were several cases of 1886 ground failure that plotted in these areas, the liquefaction probability curves for Qhs/Qhes (Figure 3.9a, Figure 6.7) are also recommended for Qhm surficial deposits. Because no SCPTu data were also available for Qwc surficail deposits, the liquefaction probability curve for Qws (Figure 3.9b, Figure 6.8) is recommended for Qwc surficial deposits.

Table 6.5 Coefficients of the fitted liquefaction probability curves based on values for the combined Qlc and Qpc surficial deposits.

Depth to groundwater table (m)	Depth to top of Cooper Marl (m)	a	b	c	d
1	5	15.361	49.379	0.463	-16.277
1	10	31.087	31.036	0.551	-5.003
3	5	20.885	47.681	0.576	-30.295
3	10	31.140	31.036	0.649	-5.228

Table 6.6 Coefficients of the fitted liquefaction probability curves based on values for Qhs/Qhes and Qts surficial deposits.

Depth to groundwater table (m)	Depth to top of Cooper Marl (m)	a	b	c	d
(a) Qhs/Qhes					
1	5	28.426	31.190	0.322	-9.136
1	10	30.523	30.557	0.254	-8.040
1	15	30.560	30.560	0.223	-9.480
3	5	18.697	41.285	0.572	-7.225
3	10	30.128	30.406	0.375	-6.416
3	15	30.438	30.438	0.329	-6.998
(b) Qts					
1	5	30.524	30.524	0.314	-11.322
1	10	30.524	30.524	0.206	-10.950
3	5	30.519	30.517	0.486	-8.571
3	10	30.523	30.523	0.253	-11.352

6.7 Conclusion

The liquefaction potential of areas covered by surficial clayey deposits in the Charleston area was characterized in this chapter. The characterization involved reviewing 1886 liquefaction and ground failure cases that plot in surficial clayey deposits and analyzing thirty-two seismic cone soundings. Somewhat surprising was that more than sixty percent of the total reported cases of 1886 horizontal ground displacement and conspicuous craterlets were found to plot in the surficial clayey deposits. This finding agreed with the previous study by Balon and Andrus (2006) who found the surficial clayey deposits to have just as high liquefaction potential as surficial sand deposits based on cone penetration test data without the MEVR correction.

LPI values were computed for the thirty-two SCPTu profiles after screening out layers not susceptible to liquefaction and correcting CRR for the influence of diagenetic processes using MEVR. Liquefaction probability curves developed for Qhec and Qtc were not consistence with the numbers of 1886 liquefaction cases that plot in the surficial clayey deposits. Therefore, it was recommended that the liquefaction probability curves for Qhs/Qhes (Figure 3.9a, Figure 6.7) and Qts (Figure 3.9d, Figure 6.8) be used for estimating the liquefaction potential of Qht/Qhec and Qtc. The liquefaction probability curves for Qhs/Qhes (Figure 3.9a, Figure 6.7) were also recommended for Qhm surficial deposits because no SCPTu data were available and there were several cases of 1886 ground failure that plotted in these areas. Because no SCPTu data were also available for Qwc surficail deposits, the liquefaction probability curve for Qws (Figure 3.9b, Figure

6.8) was recommended. For Qlc and Qpc, the liquefaction probability curves presented in Figure 6.6 are tentatively suggested. These recommendations are believed to be conservative. Additional SCPTu data are needed for all surficial clayey deposits to further establish the recommended curves.

CHAPTER SEVEN

CARBONATE CONTENT OF SOIL DEPOSITS IN THE GREATER CHARLESTON AREA, SOUTH CAROLINA

7.1 Introduction

Although there is general agreement that liquefaction resistance of soils improves by age (e.g., Youd and Perkins 1978, Seed 1979), mechanisms causing the aging effects are currently not well understood. Mechanisms that have been suggested include mechanical mechanisms such as particle interlocking/rearrangement (Schmertman 1991), and chemical mechanisms such as the precipitation of silica or similar bonding agents (Joshi et al. 1995). A summary of selected previous studies to identify possible mechanisms causing increase in liquefaction resistance with time is presented next. Much of this summary is based on review by Schmertmann (1991). Following the review of previous studies, the possibility of carbonate cementation in various Pleistocene sand deposits in the Greater Charleston area is investigated.

7.2 Review of Possible Soil Aging Mehanisms

Seed (1979) conducted a series of laboratory test on identical specimens of Monterey No. 0 sand subjected to sustained loads for periods ranging from 0.1 day to 100 days. The results indicated that resistance to development of a cyclic pore pressure ratio

of 100%, in terms of stress ratio, increased up to 25% with time. The increases in resistance to cyclic loading with age of samples were explained to be the result of likely "cementation or welding, which occurs at contact points between sand particles and is associated with secondary compression of the soil."

Dusseault and Mogenstern (1979) suggested a new group of engineering materials, called **locked sands,** characterized by absence of cohesion, highly quartzose mineralogy, high strength, steeply curved failure envelopes, low porosities, and considerable geological age. Locked sands were also characterized by a lack of interstitial cement, brittle behavior, residual shear strengths of 30°–35°, and exceptionally large dilation rates at failure. Dusseault and Mogenstern (1979) reported that the characteristic behavior of locked sands is the result of dilation, and the dilation is the result of an interpenetrative fabric identifiable by microscopic examination. This fabric and grain-surface rugosity develops through the action of diagenetic processes of crystal overgrowth and solution.

Mitchell and Solymar (1984) studied time-dependent behavior of clean sands following a densification program for the Jebba Hydroelectric Development in Nigeria. It was observed that penetration resistance increased substantially over a period of weeks to months following blasting or vibrocompaction densification, while pore pressures remained constant and surface settlements were negligible. Trying to explain strength gains of clean sand with age, they suggested that dissolution and precipitation of silica, in both quartz and amorphous forms, resulting in some forms of cementing bonds at

interparticle contacts may have been responsible for time-dependant behavior of sands after densification. However, no explicit evidence was presented to support this hypothesis.

Schmertmann (1987) presented two more possible explanations for aging effects of clean sands: time-dependent recovery increases in horizontal stresses; and a dispersive particle reorientation with time resulting in a purely frictional gain in modulus and strength with time.

Dowding and Hryciw (1986) conducted a laboratory study on blast densification of saturated sand. Blasting densification was simulated in laboratory and cone penetration and settlement were measured. The results showed that point resistance increased gradually with time after each blast. They suggested that the increase in penetration resistance may be resulted from gradual improvement of intergranular bonds and dissipation of explosion produced gases.

Mesri et al. (1990) studied previous laboratory measurements of dynamic shear modulus after primary consolidation and field measurements of penetration resistance after ground densification. They were concerned only with time-dependent behavior of clean sand under drained aging condition after densification. Although no direct evidence was presented to reject the cementing-bond hypothesis, Mesri et al. (1990) stated that time-dependant strength gains of clean sands result from increased micro-interlocking of particles that result from rearrangement of sand grains during secondary compression.

Schmertmann (1991) critically reviewed previous cases of aging improvement in soil engineering behavior, both from the lab and the field, for short and long aging times, and for clays, silts, sands, and even gravel. He studied whether the improvements in engineering properties of soil result from an increase in the cohesive component of mobilized strength as a result of some form of cementation or internal bonding, or from an increase in frictional or mechanical component of strength by conducting a special type of triaxial test, denoted as IDS test (Independent and Dependent components of Strength). Samples of Boston blue clay aged for 5 days, and samples of extruded kaolinite aging from 1.5 hr to 5 weeks were tested. The results indicated that the increased stiffness and strength from aging resulted entirely from an increased friction capability that developed within the samples during the aging periods. Based on these results and all previous investigations and evidence, Schmertmann (1991) suggested that aging effects over engineering times (a few days to 100 years) occur mostly, and perhaps sometimes entirely, because of increases in the soil friction strength mobilization capability of the sands, silts, and clays involved. He concluded that mechanical mechanisms like dispersive particle movements, internal stress arching, and increased interlocking are responsible for aging effects during engineering time. Considering the locked-sand studies by Dusseault and Mogenstern (1979), Schmertmann (1991) explained that chemical action that changes the surface of soil particles during aging may produce mechanical-frictional strength-increase effects.

Joshi et al. (1995) investigated the influence of aging on the penetration resistance of freshly deposited sands by conducting laboratory tests. Two types of sands were aged for up to two years under a constant stress of 100 kPa in three environmental conditions: dry state, submerged in distilled water and in simulated sea water. Penetration resistance of sand beds was measured by pushing a 4-probe penetrometer into the sand beds. The results showed that penetration resistance of sands significantly increased by age. Also, the rate of increase in penetration resistance was higher for the submerged sand as compared with the dry sand. Based on mineralogical and morphological studies of freshly deposited and aged sand samples, Joshi et al. (1995) reported the presence of weak cementation bonds at grain contacts and in interspaces of sands aged in submerged water. The cementation bonds were composed of calcium and other acid-soluble material (salts), but they couldn't be clearly attributed to silica with any degree of confidence. They concluded that the increase in penetration resistance of the sand in the dry state was resulted from rearrangement of sand grains, while in the submerged states, besides the rearrangement of sand particles, partial cementation caused by dissolution and precipitation of salts and probably also silica on the sand grains and in the pores resulted in the larger increase in the penetration resistance.

Baxter and Mitchell (2004) conducted a laboratory program under controlled conditions to study different possible mechanism responsible for aging effects after densification. The testing program included measurements of the small-strain shear modulus, electrical conductivity, pore fluid chemistry, and mini-cone penetration

resistance. Two different sands were tested in cylindrical rigid wall cells with 14.5 cm inside diameter and 16.5 cm high. Aging effects were evaluated for different combinations of relative density (40 or 80%), temperature (25 or 40º C), and pore fluid composition (distilled water, ethylene glycol CO_2 saturated water, air (dry)). A total of 22 tests in rigid wall cells were performed after different periods of aging (up to 118 days) under a constant vertical effective stress of 100 kPa. The test results indicated that although the small-strain shear modulus increased with time throughout most of the tests, there was no increase in the mini-cone penetration resistance with time in any of the tests. Electrical conductivity measurements showed that, in most of the tests, there was continual dissolution of minerals with time. But in two tests the electrical conductivities decreased with time. Mineralogical studies and chemical analyses showed that in at least two of the tests, some precipitation of carbonates and silica occurred. This was consistent with the electrical conductivity measurements results. Scanning electron micrograph showed no visible evidence of precipitation. Based on the test results, Baxter and Mitchell (2004) concluded that precipitation of carbonate or silica was not responsible for aging effects in sands and other possible mechanisms included arching due to dissipation of blast gases and redistribution of stresses through the soil skeleton. Also, they mentioned that the boundary conditions imposed by the laboratory tests may obscure changes in penetration resistance that would be measured if the volume of sand tested had been much larger.

Based on the above review, the following have been suggested as possible mechanisms: cementation/participation, crystal overgrowth, increases in effective stress with time, dispersive particle reorientation/movement, dissipation of gases, micro-interlocking during secondary compression, and internal stress arching. To assess the possibility of cementation in aged deposits in the Greater Charleston area, samples were collected from near-surface deposits using a hand auger at twenty-six sites.

7.3 Database

Locations of the twenty-six auger sample site are shown in Figure 7.1. The site numbers correspond to the SCPTu site numbers used in previous chapters. The two criteria used for selecting the hand auger sites were as follows: samples were collected from near the SCPTu sites considered in previous chapters, and samples were taken from just below the groundwater table. Shown in Figure 7.2 is a photograph of hand auger sampling in the Charleston area. Presented in Table 7.1 are depth of the groundwater table, depth of the collected sample, soil index properties, grain size data, Munsell color code, inferred geology of the collected samples, MEVR, and calcite equivalent.

In addition, considered in this study are samples collected at three sites developed as part of a three-year National Science Foundation research project on characterization of the liquefaction resistance of aged soils (Boller 2008; Boller et al. 2008; Hayati 2009; Geiger 2010; Geiger et al. 2010;). The three sites are the Clemson University Coastal Research and Education Center (CREC) near Charleston; the Hobcaw Borrow Pit site

located near Georgetown, SC; and the Rest Area Ponds site near Walterboro, SC. The Hobcaw Borrow Pit site and the Rest Area Ponds site are located outside the study area shown in Figure 7.1.

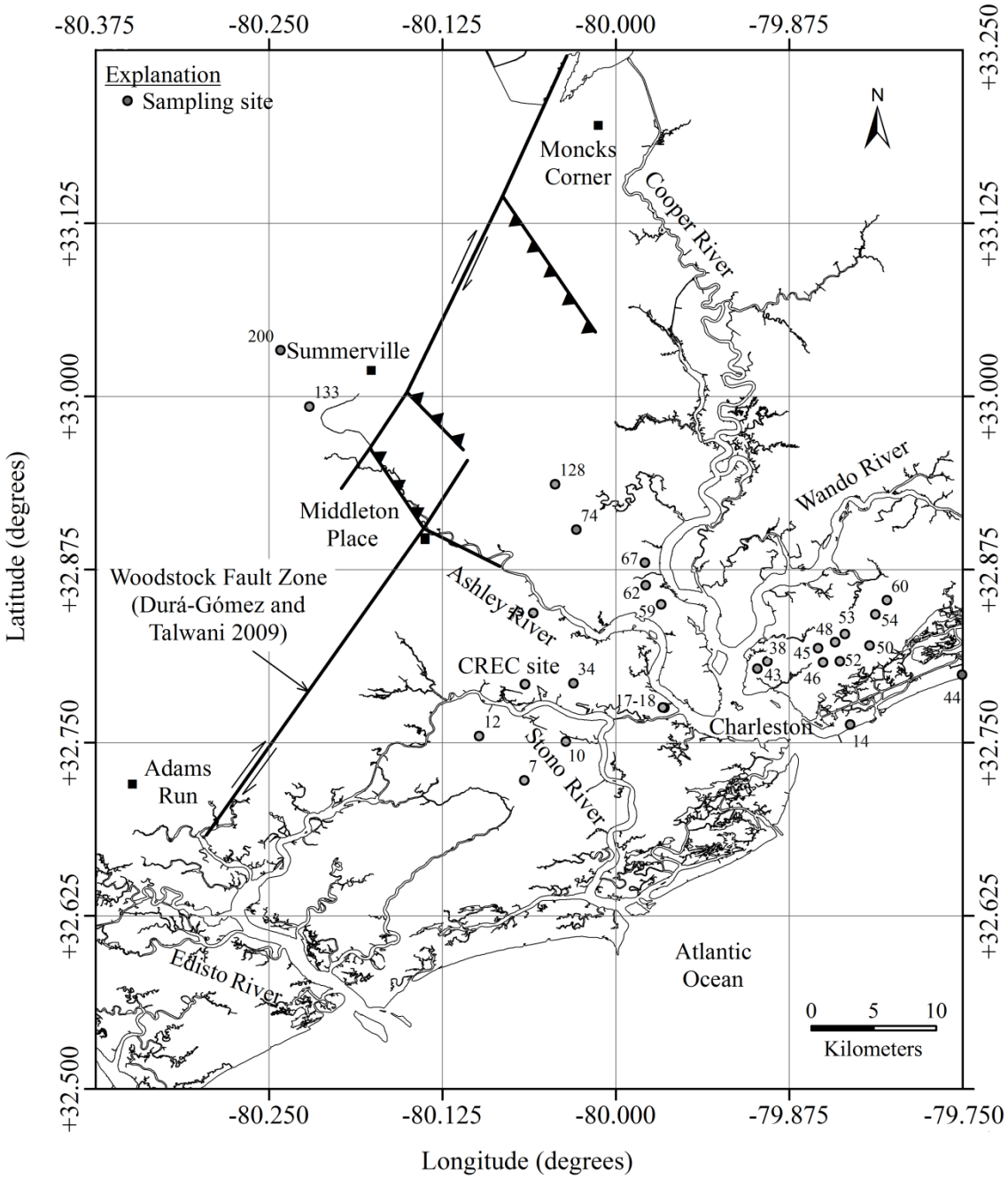

Figure 7.1 Map of the Greater Charleston area showing the Woodstock fault as presented in Durá-Gómez and Talwani (2009) and the locations of auger samples for carbonate testing.

Figure 7.2 The author and Shimelies Aboye collecting near-surface samples using a hand auger.

Table 7.1 Soil index properties and calcite equivalent for the samples collected from near-surface layers below the groundwater table using a hand auger.

Site No.	W.T. (m)	Depth (m)	C_u[a]	C_c[b]	D_{50}[c]	Grain Size Data - Percent Retained on Sieve								Fines %	Munsell Color[d]	Soil Type[e]	Inferred Geology	MEVR	Calcite Equivalent (%)
						Gravel	Sand												
						#4	#10	#20	#40	#60	#80	#100	#200						
7	1.42	1.65-1.72	1.69	1.15	0.18	0	0	0.19	0.16	8.71	39.83	34.34	14.84	1.93	10YR 2/1	SP	Qws	1.31	0.00
10	1.60	1.60-1.70	1.63	1.06	0.20	0	0	0	0.08	11.56	50.06	24.91	12.14	1.25	10Y 5/4	SP	Qws	1.51	0.00
12	0.64	0.64-0.91	1.98	1.02	0.15	0	0	0	0.05	1.39	18.95	29.03	43.95	6.63	10YR 7/2	SP	Qws	-	1.23
14	0.64	0.74-0.81	1.83	1.01	0.15	0.05	0.1	0.24	0.13	2.25	22.81	26.72	46.73	0.97	5Y 4/2	SP	Qhs	1.52	0.62
17	0.38	0.38-0.46	2.10	1.48	0.17	0	0.09	0.09	0.04	4.58	36.41	32.27	19.61	6.91	5Y 5/3	SP	Qws	-	0.00
18	1.68	1.70-2.00	1.53	1.02	0.21	0	0	0.03	0.1	16.82	52.58	19.54	10.07	0.85	5Y 7/2	SP	Qws	2.17	0.00
34	1.68	1.68-1.75	1.96	1.51	0.16	0	0	0	0	0.16	15.09	53.36	24.59	6.79	2.5Y 6/4	SP	Qws	-	0.00
38	1.30	1.30-1.42	2.71	1.49	0.22	0	0.08	2.48	12.1	19.66	34.37	12.73	10.36	8.22	5Y 5/3	SP	Qhes	-	0.00
43	1.40	1.40-1.50	1.77	1.14	0.19	0	0	0	0	10.36	47.16	25.6	15.44	1.44	2.5Y 4/3	SP	Qws	-	0.00
44	0.66	0.66-0.74	1.83	1.16	0.16	0	0	0	0	1.47	31.16	31.9	34.61	0.86	2.5Y 3/2	SP	Qhs	-	0.62
45	1.42	1.42-1.52	1.72	1.08	0.21	0	0	0.40	3.93	17.15	45.34	19.84	11.67	1.66	2.5Y 3/2	SP	Qws	1.79	0.00
46	1.45	1.45-1.52	2.94	1.57	0.21	0	0.02	1.35	12.19	15.4	36.54	10.42	14.62	9.46	10YR 2/2	SP	Qws	1.37	0.00
48	1.22	1.22-1.30	1.87	1.17	0.20	0	0.27	1.85	3.86	12.84	46.08	19.55	12.48	3.07	2.5Y 3/3	SP	Qws	-	0.00
50	1.04	1.04-1.14	1.69	1.03	0.21	0	0.05	0.79	6.84	19.31	41.89	18.75	11.73	0.65	5Y 5/2	SP	Qws	1.23	0.00
52	1.93	1.93-1.98	2.27	1.43	0.20	0	0	0	0.75	17.79	47.93	16.32	10.07	7.14	2.5Y 5/4	SP	Qws	-	0.00
53	1.96	1.96-2.11	2.44	1.49	0.20	0	0	0.07	0.62	15.11	45.73	18.56	11.86	8.05	2.5Y 5/6	SP	Qws	2.71	0.00
54	0.86	0.86-1.09	1.49	0.98	0.21	0	0	0.20	3.90	64.00	159.8	61.80	29.50	2.30	10YR 3/4	SP	Qws	-	0.00
55	0.51	0.72-0.81	2.20	1.02	0.15	0	0.06	0.12	0.06	6.89	22.4	20.02	40.34	10.1	2.5Y 6/3	SP	Qws	-	0.00
59	1.63	1.63-1.70	1.70	1.05	0.21	0	0.12	0.46	0.88	22.82	43.92	18.80	12.89	0.12	2.5Y 5/2	SP	Qws	-	0.00
60	1.22	1.35-1.42	1.76	1.28	0.17	0	0	0	0.23	3.61	34.14	34.55	26.88	0.59	5Y 4/3	SP	Qws	-	0.00
62	-	-	1.71	0.96	0.14	0	0	0	0	2.4	15.09	21.12	60.91	0.47	2.5Y 5/3	SP	Qwls	-	1.85
67	1.63	1.63-1.73	1.87	1.21	0.19	0	0.04	0.16	0.25	7.7	45.62	27.07	16.30	2.87	10YR 2/1	SP	Qwls	1.97	0.00

Table 7.1. Soil index properties and calcite equivalent for the samples collected from near-surface layers below the groundwater table using a hand auger (Continued).

Site No.	W.T. (m)	Depth (m)	C_u[a]	C_c[b]	D_{50}[c]	Grain Size Data - Percent Retained on Sieve								Fines %	Munsell Color[d]	Soil Type[e]	Inferred Geology	MEVR	Calcite Equivalent (%)
						Gravel	Sand												
						#4	#10	#20	#40	#60	#80	#100	#200						
74	2.00	2.09-2.16	1.95	0.98	0.13	0	0	0	0	0.47	12.2	26.01	51.98	9.35	2.5Y 6/6	SP	Qts	1.97	1.23
128	2.44	2.44-2.51	2.08	0.99	0.13	0	0	0	0.04	1.75	13.84	21.27	49.79	13.31	5Y 7/3	SP	Qtc	1.21	3.08
133	1.57	1.73-1.85	6.17	4.61	0.17	0.00	0.00	0.05	0.05	4.85	33.77	36.96	8.87	15.44	5Y 7/1	SP	Qpc?	-	0.00
200f	0.81	0.81-0.97	1.80	1.42	0.17	0	0	0.08	0.24	2.56	26.36	46.33	20.03	4.39	2.5Y 6/4	SP	Qts	-	0.00

[a] *C_u=Coefficient of uniformity.*
[b] *C_c=Coefficient of curvature.*
[c] *D_{50}=Median grain size.*
[d] *Munsell color of wet fines (hue value/chroma).*
[e] *Soil type based on unified soil classification system ASTM D-2487.*
[f] *Not a SCPTu site, located near the Charleston Airport.*

Geotechnical investigations at the CREC site were presented by Boller (2008), Boller et al. (2008) and Hayati (2009). As described by Boller et al. (2008), below the land surface is the younger beach sand facie of the 100,000-year-old Wando Formation (Qws) with thickness of 3.5 to 3.9 m. Underlying the Wando Formation is the 30 million-year-old Cooper Marl. The split-spoon samples from boring B-3 down to the depth of 11 m were tested for carbonate content.

Geotechnical investigations at the Hobcaw Borrow site were presented by Geiger (2010) and Geiger et al. (2010). As described by Geiger et al. (2010), the Hobcaw site is located on a 200,000-year-old beach to barrier-island sand deposit ranging in thickness from 9 to 15 m. The split spoon samples from boring B-1 down to the depth of 11.5 m were tested for carbonate content.

Geotechnical investigations at the Rest Area Ponds site were presented by Geiger (2010). As described by Geiger (2010), the Rest Area Ponds is located on a beach sand deposit that is at least 1,000,000 year old. The split spoon samples from boring B-3 down to the depth of 10.8 m were tested for carbonate content.

7.4 Methodology

The carbonate analyzer, “carbonate-bombe”, introduced by Müller and Gastner (1971) is commonly used by geologists and engineers for rapid determination of carbonate content of soils. The test is based on a gasometric method that utilizes a simple

portable apparatus. Shown in Figure 7.3 is a photograph of the rapid carbonate analyzer manufactured by Humboldt used in this study. The basic components of this apparatus include: 1) 0.374 L reaction cylinder with threaded cap and O-ring seal to enclose the cylinder, 2) pressure gauge with a readability of 0.5 kPa (0.1 psi), 3) an acid container, and 4) pressure relief valve. Reagents are calcium carbonate ($CaCO_3$) for analyzer calibration and hydrochloric acid (HCL) in 1 N solution.

The procedure described by ASTM D 4373-02 is followed in this study. Carbonate content or calcite equivalent of soil is determined by treating a 1 g dried soil specimen with hydraulic chloric acid (HCL) in an enclosed reaction cylinder (reactor). Carbone dioxide (CO_2) gas is produced during the reaction between the acid and carbonate fraction of specimen as indicated as follows:

$$2\ HCl + CaCO_3 + \text{soil (inert)} \longrightarrow CaCl_2 + H_2O + CO_2 \uparrow + \text{soil (inert)}$$

The resulting pressure generated in the closed reactor is proportional to the calcite equivalent of the specimens. This pressure is measured with a suitable pressure gauge that is pre-calibrated with reagent grade calcium carbonate. Results are stated as the calcite equivalents. This method does not distinguish between different carbonate minerals (e.g., magnesite, dolomite, calcite, aragonite, rhodocrosite, siderite, smithsonite, witherite, and cerrusite). However, calcite and aragonite (polymorphs of calcium

carbonate) reactions typically complete very fast, while dolomite reaction sets in very slowly (Müller and Gastner, 1971).

Figure 7.3 Rapid carbonate analyzer manufactured by Humboldt.

According to ASTM D 4373-02, after 10 min. reaction time, the pressure value indicates the carbonate content. To evaluate whether other carbonate minerals are present, additional readings need to be taken until the reaction is complete using the following criteria: (a) the change in calcite equivalent is less than 0.3% over a ten-minute time period for testing time up to 120 minute; (b) the change in calcite equivalent is less than 0.3% over 30-minute time period for testing time greater than 120 minute.

One of the limitation of this method is if low carbonate contents are measured, the user does not know whether the soil is low in carbonate content or contains cerrusite, witherite, etc., which are carbonate minerals whose reactions with hydrochloric acid are either very slow or limited. Also, testing times may be extensive (longer than 1 hour) for some carbonate minerals (such as dolomite) if calcite equivalents within about 1% are required. The effects of specimen grain size, duration of testing, PH and specimen mass are discussed by Demars et al. (1983). The accuracy of this method is within ±5% calcite equivalent.

7.5 Calibration of the Carbonate Analyzer

Calibration of the analyzer for this study was accomplished by conducting a series of tests using reagent-grade $CaCO_3$ to obtain the relationship between the mass of $CaCO_3$ and the pressure generated in the constant volume reactor. The reagent-grade $CaCO_3$ specimens with the mass of 0.0, 0.2, 0.4, 0.6, 0.8, and 1.0 g were treated by 20 mL of acid

solution in the enclosed reactor. ASTM D 4373-02 states that even calcite powder may not completely react in less than 10 minutes. The pressure was monitor to verify that the reaction was complete (pressure stabilized) and to confirm that reactor was properly sealed. The pressure gage was individually calibrated.

Presented in Figure 7.4(a) are variations of the cylinder pressure with time for calibration tests with 0.0, 0.2, 0.4, 0.6, 0.8, and 1.0 g $CaCO_3$. The pressure in all specimens continued to increase even after 24 hours. These results were unexpected, particularly the blank test without any $CaCO_3$ added. The increase of pressure with time for the blank test (0.0 g $CaCO_3$) may be due to the evaporation of the acid solution or reaction of the acid with impurities in the metal disc at the bottom of the reactor. It should be noted that all tests were conducted in an approximately constant temperature of 70˚ F.

Subtracting the blank test's curve from each curve provides the family of curves shown in Figure 7.4(b). All five curves indicate that the pressures are almost constant with time for the period of 10 to 120 min for each test. Therefore, to develop a calibration curve, the cylinder pressure at 2 hours was considered and the pressure of blank test was subtracted from the calibration test results. Presented in Figure 7.5 are the calibration results for determining calcite equivalent, and the least squares regression fit. Considering the fluctuations exhibited in Figures 7.4 and 7.5, the accuracy of the calibration curve is within about ±4%.

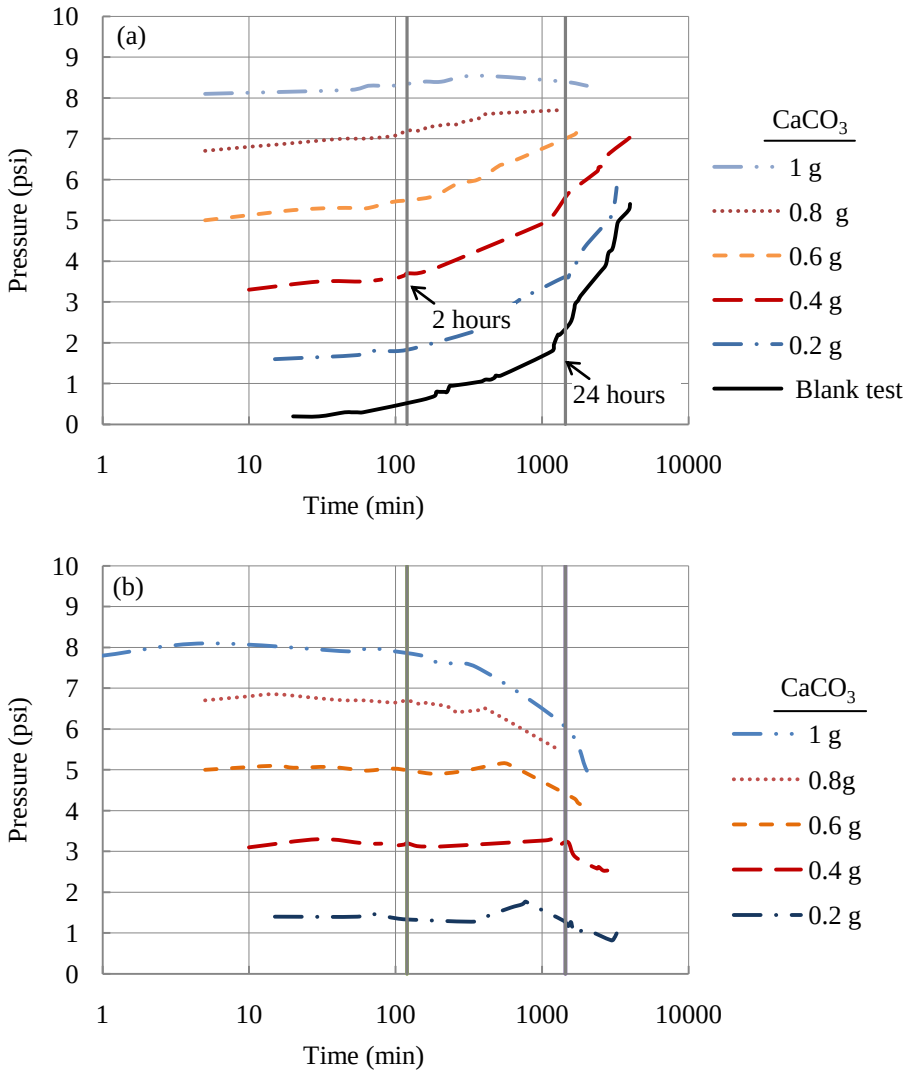

Figure 7.4 Results of calibration tests showing (a) variations of the cylinder gas pressure with time for various amounts of calcium carbonate (b) after correcting for the blank test.

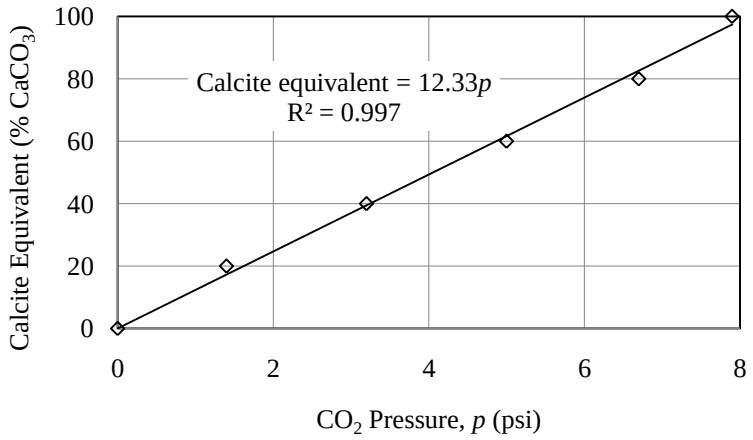

Figure 7.5 Calibration curve for the carbonate analyzer at 2 hours.

7.6 Results

To determine the calcite equivalent of samples from the South Carolina Costal Plain, the cylinder gas pressure was monitored for 2 hours and the 2-hour pressure reading was corrected based on the blank test. The blank test was repeated after every four soil tests. Presented in the last column of Table 7.1, 7.2, 7.3, and 7.4 are the calcite equivalents for soil samples collected from the sub-surface at the twenty-six hand-auger sites in the Charleston area, at the CREC site, at the Hobcaw Borrow site, and at the Rest Area Ponds site, respectively. For almost all of the sandy samples, the calcite equivalent is < 3% which is less than the accuracy of the method indicating little if any carbonate in the sand deposits.

Presented in Figure 7.6 are cone profiles, geologic profile, and the variation of calcite equivalent with depth for boring B-3 at CREC. The results indicated that the calcite equivalent is practically zero in layers A and B. In layer C, the calcite equivalent is about 7% due to shell fragments (Boller 2008). In layer D (Cooper Marl), the calcite equivalent is about 80%. This finding is consistent with the characteristic of Cooper Marl presented by Camp (2004) who reported that the Cooper Marl consists of about 60–80% calcium carbonate and much of the calcium carbonate is in the form of skeletal remains of microscopic marine organisms.

Because calcite equivalent values for samples from the Hobcaw Borrow site and the Rest Area Ponds site are nearly all zero, profiles of these sites are not shown. Only

one sample from boring B-1 at the Hobcaw Borrow Pit site has a calcite equivalent of 14%. This sample contained shell fragment.

Table 7.2 Soil index properties and calcite equivalent for the samples collected from boring B-3 at CREC (modified from Boller 2008).

Depth (m)	C_u [a]	C_c [b]	D_{50} [c]	Fines %	Munsell Color[d]	Soil Type[e]	Inferred Geology	MEVR	Calcite Equivalent (%)
0-0.46	2.00	0.99	0.300	1	10YR 5/4	SP	Qws?	-	0.00
0.91-1.37	2.40	1.42	0.190	7	10YR 6/6	SP-SM	Qws	1.68[f]	0.00
1.83-2.29	2.00	1.24	0.190	3	10YR 6/6	SP	Qws		1.23
2.74-3.20	2.20	1.30	0.190	4	10YR 7/3	SP	Qws		0.00
3.66-4.11	1.90	1.20	0.200	3	10YR 7/3	SP	Qws		2.47
4.57-5.03	10.1	0.66	0.480	13	5Y 3/1	SP-SC	Qwc	-	6.78
6.40-6.86	21.1	5.49	0.094	43	2.5Y 5/2	SM	Marl	-	77.69
7.62-8.08	18.3	3.23	0.059	42	2.5Y 4/3	SM	Marl	-	80.16
9.14-9.60	6.67	1.78	0.121	31	2.5Y 4/3	SM	Marl	-	76.46
10.67-11.13	5.70	2.10	0.110	28	2.5Y 4/3	SM	Marl	-	73.38

[a] *C_u=Coefficient of uniformity.*
[b] *C_c=Coefficient of curvature.*
[c] *D_{50}=Median grain size.*
[d] *Munsell color of wet fines (hue value/chroma).*
[e] *Soil type based on unified soil classification system ASTM D-2487.*
[f] *Hayati (2009, p. 169).*

Table 7.3 Soil index properties and calcite equivalent for the samples collected from boring B-1 at the Hobcaw Borrow Pit site (modified from Geiger 2010).

Depth (m)	C_u [a]	C_c [b]	D_{50} [c]	Fines %	Munsell Color[d]	Soil Type[e]	Inferred Geology	MEVR	Calcite Equivalent (%)
0.0-0.46	1.83	1.37	0.21	5.43	10YR 4/4	SP-SM	Q3b[f]	-	0.00
	2.30	1.57	0.21	6.99	10YR 4/4	SP-SM	Q3b	-	0.00
1.07-1.52	1.77	1.23	0.22	4.92	10YR 4/4 7.5YR 6/6	SP	Q3b	-	0.00
1.83-2.29	2.10	1.38	0.19	7.44	10YR 4/4	SP-SM	Q3b	-	0.00
2.59-3.05	1.67	1.20	0.19	5.02	10YR 7/4 7.5YR 6/6	SP-SM	Q3b	1.30[h]	0.00
3.35-3.81	2.63	1.72	0.19	8.76	7.5YR 5/6	SP-SM	Q3b		0.00
4.11-4.57	2.29	0.73	0.31	5.27	-	SP-SM	Q3b		0.00
4.88-5.33	1.88	0.89	0.28	3.30	7.5YR 5/6	SP	Q3b		0.00
5.64-6.10	107.5	23.3	0.32	15.42	7.5YR 6/8 7.5YR 3/4	SM	Q3b		0.00
6.40-6.86	1.4	0.92	0.20	3.87	10YR 7/6	SP	Q3b		0.00
7.16-7.62	1.75	0.98	0.24	3.73	10YR 7/3	SP	Q3b		0.00
7.92-8.38	1.81	1.04	0.25	2.45	2.5YR 5/3	SP	Q3b		13.57[g]
8.67-9.14	133.3	0.36	0.083	46.54	10YR 5/1	SC	NA	-	0.00
	63.3	29.65	0.17	17.38	10YR 5/1	SM	NA	-	0.00
	2.5	1.98	0.16	10.18	10YR 5/1	SP-SM	NA	-	0.00
9.45-9.91	2.5	1.51	0.16	11.18	7.5Y 5/1	SP-SM	NA	-	0.00
10.21-10.67	2.18	1.75	0.18	7.13	2.5Y 5/0	SP-SM	NA	-	0.00
10.97-11.43	2.15	1.74	0.19	6.11	2.5Y 4/0	SP-SM	NA	-	0.00

[a] *C_u=Coefficient of uniformity.*
[b] *C_c=Coefficient of curvature.*
[c] *D_{50}=Median grain size.*
[d] *Munsell color of wet fines (hue value/chroma).*
[e] *Soil type based on unified soil classification system ASTM D-2487.*
[f] *Beach sand; inferred from McCartan et al (1984). Their age would be equivalent to the beach to barrier island deposits designated as Qts in the Charleston area by Weems and Lemon (1993).*
[g] *sample contains shell fragment.*
[h] *Geiger (2010, p. 59)*

Table 7.4 Soil index properties and calcite equivalent for the samples collected from boring B-1 at the Rest Area Ponds site (modified from Geiger 2010).

Depth (m)	C_u[a]	C_c[b]	D_{50}[c]	Fines %	Munsell Color[d]	Soil Type[e]	Inferred Geology	MEVR	Calcite Equivalent (%)
0-0.61	2.50	1.41	0.18	9.02	7.5YR 3/2	SP-SM	af	-	0.00
0.61-1.07	2.71	1.69	0.17	10.91	10YR 5/6	SP-SM	af	-	0.00
1.22-1.68	2.50	1.60	0.19	9.22	10YR 5/4	SP-SM	af	-	0.00
1.83-2.29	3.00	1.74	0.19	11.34	10YR 2/1 10YR 2/2	SP-SM	Q6b[f]	1.15[g]	0.00
2.44-2.90	2.63	1.52	0.19	8.59	7.5YR 3/4	SP-SM	Q6b		0.00
3.05-3.51	2.20	1.31	0.2	4.95	-	SP	Q6b		0.00
3.66-4.11	2.71	1.27	0.17	12.05	10YR 6/4	SM	Q6b		0.00
4.27-4.72	2.07	1.29	0.17	2.89	10YR 7/4	SP	Q6b		0.00
4.88-5.33	2.13	1.06	0.16	8.02	10YR 8/3	SP-SM	Q6b		0.00
5.49-5.94	2.83	1.19	0.15	15.15	10YR 8/1	SM	Q6b		0.00
6.10-6.55	-	-	0.09	46.33	10YR 8/2	SC or CH	NA	-	0.00
6.71-7.16	2.71	1.27	0.17	12.08	10YR 8/2	SM	NA	-	0.00
7.62-8.08	2.86	1.03	0.17	11.9	10YR 7/2 7.5YR 6/8	SP-SM	NA	-	0.00
9.14-9.60	-	-	0.13	22.02	10YR 6/1	SM	NA	-	0.00
10.36-10.82	2.74	0.83	0.15	10.88	2.5Y 5/0	SP-SM	NA	-	0.62

[a] *C_u=Coefficient of uniformity.*
[b] *C_c=Coefficient of curvature.*
[c] *D_{50}=Median grain size.*
[d] *Munsell color of wet fines (hue value/chroma).*
[e] *Soil type based on unified soil classification system ASTM D-2487.*
[f] *Q6b= >1,000,000 year-old beach sand deposit; inferred from McCartan et al (1984).*
[g] *Geigor (2010, p. 85).*

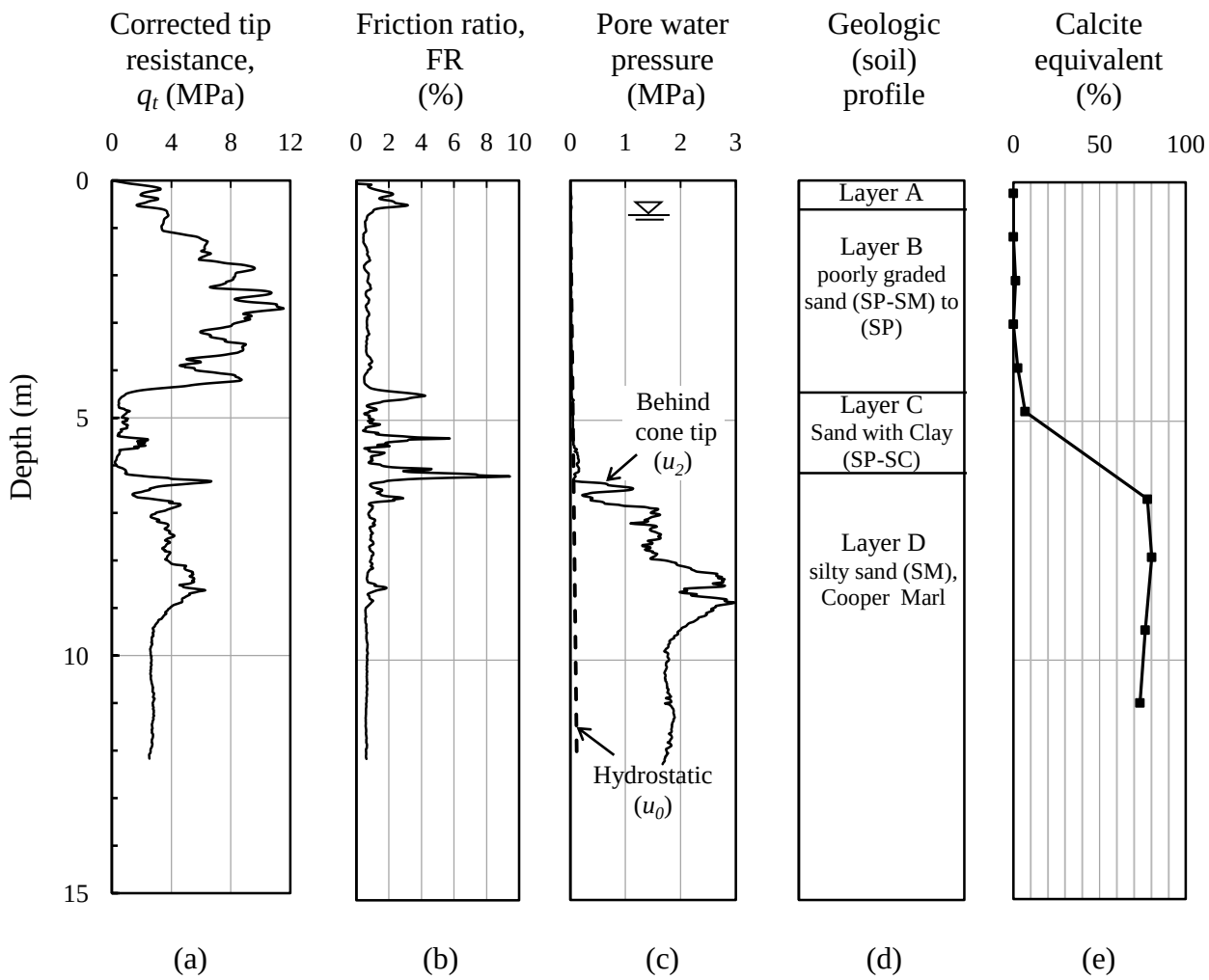

Figure 7.6 Profiles of cone, geology and calcite equivalent for the boring B-3 at CREC (modified from Boller et al. 2008).

Presented in Figures 7.7 and 7.8 are the variation of calcite equivalent in various sandy deposits with fines content and median grain size, and MEVR, respectively. Plotted values from the CREC, Hobcaw and Rest Area sites are averages for the sand deposit. In Figure 7.7(a), no trend can be seen between fines content and calcite equivalent. Although there is a slight trend between D_{50} and calcite equivalent in Figure 7.7(b) and between MEVR and calcite equivalent in the Figure 7.8, the calcite equivalents are less than the accuracy range (±4%) of the method. The averages of calcite equivalent for sand deposits with different geologic age are almost the same (~1%), indicating that carbonate content does not explain difference in MEVR and liquefaction resistance between deposits.

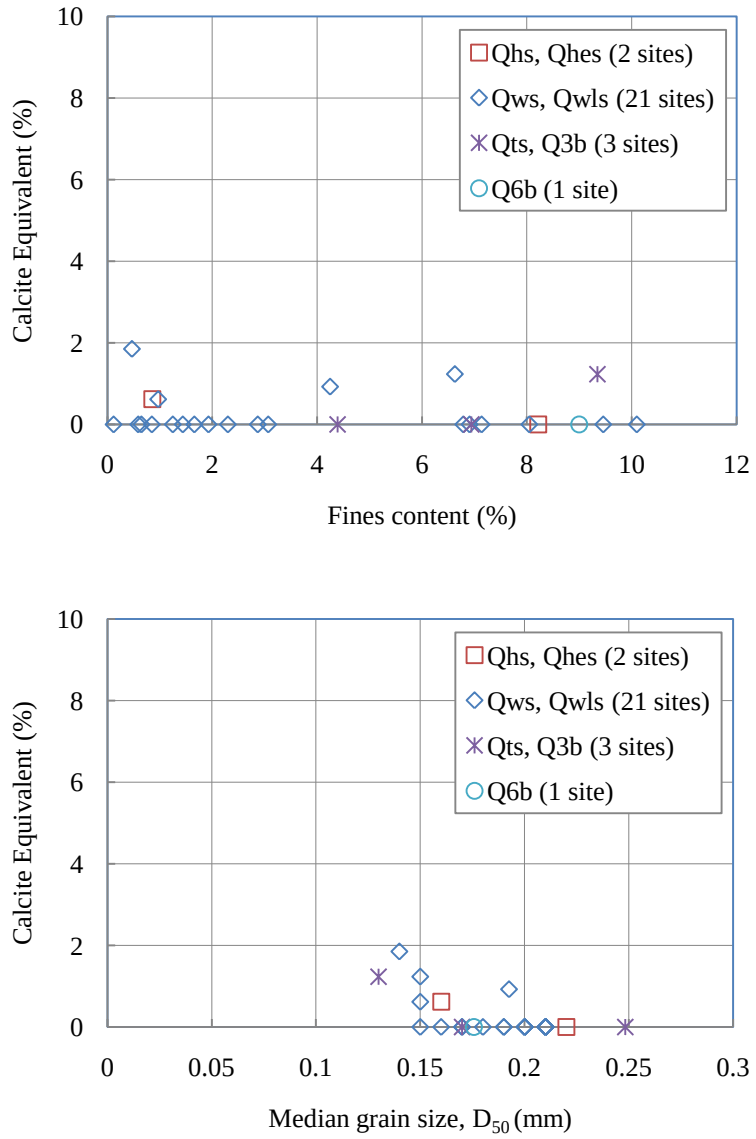

Figure 7.7 Variations of calcite equivalent with fines content and D_{50} for sand samples.

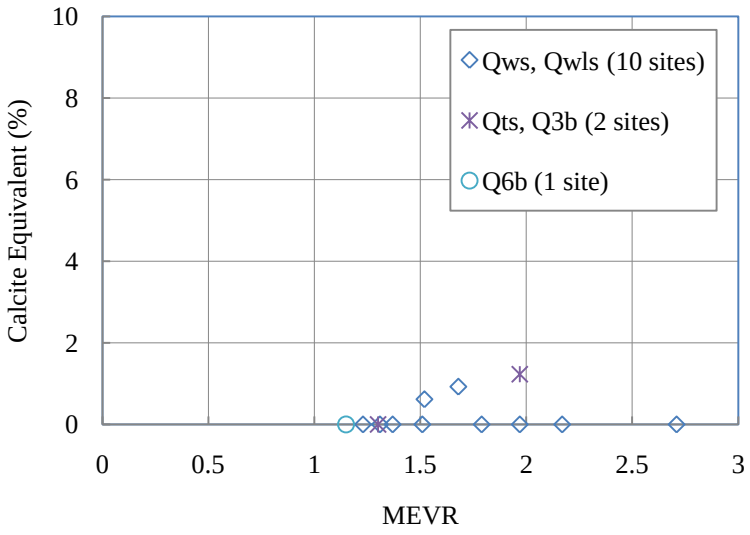

Figure 7.8 Variations of calcite equivalent with MEVR for sand samples.

7.7 Conclusion

Several previous studies were reviewed to identify possible mechanisms for the often observed increase in MEVR and liquefaction resistance of soils with time. These mechanisms include: cementation/participation, crystal overgrowth, increases in effective stress with time, dispersive particle reorientation/movement, dissipation of gases, micro-interlocking during secondary compression, and internal stress arching. This chapter investigated the likelihood that carbonate cementations contributed to high MEVR in some Pleistocene sand deposit in the South Carolina Coastal Plain.

The carbonate contents of soil samples from the Greater Charleston area were determined using a rapid carbonate analyzer. The samples included 26 auger samples collected from the sub-surface at sites in the Charleston area, 10 borehole samples from the CREC, 18 borehole samples from the Hobcaw Borrow site, and 15 borehole samples from the Rest Area Ponds. The procedure described by ASTM D 4373-02 was modified to account for pressure increases observed in blank tests. The cylinder gas pressure was monitored for 2 hours, and the pressure was corrected based on the blank test.

For all the samples except the Cooper Marl and clayey layers with shell fragments, no pressure or a minor effervescent reaction was observed. The averages of calcite equivalent for sand deposits with different geologic age were practically the same <3% calcite equivalent. The results indicated that carbonate cementation is not the cause for the aging effects observed in sands in the Greater Charleston area.

CHAPTER EIGHT

SUMMARY, CONCLUSIONS, AND RECOMMENDATIONS

8.1 Summary and Conclusions

This dissertation addressed the need for characterizing liquefaction potential of aged soil deposits in the Charleston area, South Carolina. The 1886 liquefaction and ground deformation behavior of deposits during the 1886 earthquake were studied and age-corrected LPI values were used to develop liquefaction potential curves. The study initially focused on the Mount Pleasant area, and then expanded to include the Greater Charleston area.

In this dissertation, liquefaction potential were expressed as a probability of LPI $\geq$ 5. It is important to note that LPI is an index, and not an absolute value. Computed probabilities of LPI $\geq$ 5 are not as important as a comparison between probabilities. For example, if one area has a computed 60% probability of LPI $\geq$ 5 and another area has a computed 30% probability of LPI $\geq$ 5, the fact that liquefaction is twice as likely to occur in the area with higher probability is more important than the values of probability.

8.1.1 Mount Pleasant

Liquefaction potential of soil deposits in Mount Pleasant was characterized in Chapter 2 through careful review of early Mount Pleasant history, comparison of 1886 ground behavior with geology, and analysis of available CPTu and V_S measurements. Based on the review of early Mount Pleasant history, four areas of af not previously mapped were identified and added to the geologic map by Weems and Lemon (1993). It was also noted that much of the Qht deposit along Mount Pleasant water front south of Shem Creek is thin and underlain by beach sand.

Ten cases of 1886 surface effects of liquefaction and ground deformation, and four cases of no surface effects of liquefaction were located. Eight of the ten cases of surface effects of liquefaction plotted in Qhes and younger sandy soil deposits. The four cases of no surface effects of liquefaction plotted in Qws deposits.

The finding that Qws had significantly less potential for liquefaction than Qhes and younger sands was supported by measured-to-estimated shear wave velocity ratios. The ratios indicated that Qhes/younger sands and Qws have velocities 9% and 38%, respectively, greater than typical shear wave velocities in uncemented 6-year-old quartz sands with the same cone tip resistances.

LPI values were computed from 31 CPTu profiles, after first screening out layers not susceptible to liquefaction. The middle range M_w of 6.9 and a_{max} of 0.25 g were used for calculation of CSR. Assuming K_{DR} = 1.0 for all geology units, median LPI values for

five site categories or subcategories ranged from 7 to 15, suggesting moderate to high liquefaction potential for the entire Mount Pleasant area. Because a median LPI of 11 computed for Category E (Qws) sites did not agree with observed field behavior, the LPI calculations were repeated using K_{DR} correction factors estimated from the age/MEVR relationships proposed by Hayati and Andrus (2009). The adjusted LPI analysis resulted in median LPI values of 4 for Category E (Qws) sites and 7 for Category $D_{1\&2}$ (Qhes and younger sand deposits along streams) sites. These LPI values agree with observed field behave.

A liquefaction map of Mount Pleasant was created by dividing the area into three liquefaction zones characterized with 65%, 30% and 15% probability of LPI $\geq$ 5. The zone of 65% probability of exceeding LPI of 5 includes all areas covered by af, Qhes, Qhec, Qht and Qal, except an area in the south-western part of USS Yorktown State Park. The zone of 30% probability corresponds to areas where Qws is exposed at the ground surface. The zone of 15% probability includes part of the area covered by af in the USS Yorktown State Park, where thick clayey sediment deposits are present. The map (Figure 2.6) provides useful information needed for mitigating liquefaction damage in future earthquakes, but should not replace site-specific evaluations for final project design. Additional CPTu data are needed to refine the liquefaction potential map.

8.1.2 Pleistocene Sand Deposits

Liquefaction potential of Pleistocene sand deposits in the Greater Charleston area was characterized in Chapter 3 and 4 through reviewing mapped cases of 1886 ground failure, and analyzing eighty-two SCPTu profiles. Grouping cases of ground failure by surficial sand deposits, it was found that 45% of the ground failure cases were associated with the 200,000-year-old Ten Mile Hill beds (Qts) located within 13 km of the Woodstock fault. About 25% of the cases were associated with the 100,000-year-old Wando Formation (Qws, Qwls) located within 17 km of the fault. About 25% cases were associated with the Holocene to late Pleistocene deposits (Qhs/Qhes) that lie adjacent to the harbor, rivers, and creeks located within 31 km of the fault. The remaining cases were associated with the 400,000-year-old Ladson Formation (Qls) located within 3 km of the fault.

Ratios of measured-to-estimated shear wave velocity were calculated using the SCPTu profiles. Mean MEVRs computed for Qhs/Qhes and Qts were found to be 1.11 and 1.15, respectively, which are consistent with severe liquefaction observed in these deposits. Mean MEVRs for the Qws and Qwls deposits located > 12 km from the inferred fault were 1.38 and 1.49, respectively, which agree with the observation of little or no liquefaction in these areas.

Variation of MEVRs with distance to the Woodstock fault for Qts indicated a slight increase with increasing distance, suggesting that the degree of liquefaction in Qts

deposits decreased away from the fault. No significant correlations between MEVR and distance to the fault were observed for the three younger sands groups.

LPI values were computed for the SCPTu profiles, after screening out layers not susceptible to liquefaction and correcting CRR for the influence of digenetic processes using MEVR. Considering a constant level of shaking (a_{max}= 0.25g) for all the sites regardless of distance to the fault, variation of LPIs with distance to the fault were examined. Only the LPIs for Qts sites exhibited a decrease with increasing distance to the fault, which is consistent with the variation of MEVR values.

Liquefaction probability curves were developed for four major sand groups considering the effect of distance to the fault. The probability curves for Qhs/Qhes and Qts located 16-38 km and 6-9 km from the fault, respectively, predict significantly higher potentials than the probability curves for Qwls and Qws deposits located over 12 km from the fault. Additional SCPTu data are needed to decrease the large uncertainties associated with liquefaction probability curves for Qhs/Qhes, Qwls and Qts. The results of this study can be used in probabilistic liquefaction hazard mapping of the Charleston area.

The influence of distance to the Woodstock fault, depth to top of the Cooper Marl, and depth to the groundwater table on LPI for the areas covered by Qws was further investigated. It was found that LPI values computed assuming a scenario shaking are independent of the distance to the Woodstock fault. The LPI values indicate a slight

increase with increasing depth to top of the Cooper Marl, and a slight decrease with increasing depth to the groundwater table. Liquefaction probability curves were developed for the areas covered by Qws considering the influence of depth to the groundwater table and depth to the non-liquefiable Cooper Marl. These curves can be used for mapping liquefaction potential of Qws near Charleston.

8.1.3 Artificial Fill Areas

The liquefaction potential of areas covered by af in the Charleston area was characterized in Chapter 5. The characterization involved reviewing 1886 liquefaction and ground failure cases that plot in areas now covered by af and analyzing twenty-three seismic cone soundings. All the cases of 1886 ground failure that plot in af areas on Charleston Peninsula and around Mount Pleasant appeared to be located where Qhes or younger sand deposits are believed to be in the subsurface.

Liquefaction probability curves were developed for three categories. The probability curves for category af III, where Qhes or younger sand deposits is present within the top 10 m, predict significantly higher potentials than the probability curve for category af I, where Qht extends to depths > 10 m. It is recommended that the probability curves for af III (Figure 5.9) be used in areas of af where Qhes and younger sands are likely present in the subsurface. In area where Qhes and younger sands are less likely, the probability curves for all af (Figure 5.8) are suggested.

8.1.4 Surficial Clayey Deposits

The liquefaction potential of areas covered by surficial clayey deposits in the Charleston area was characterized in Chapter 6. The characterization involved reviewing 1886 liquefaction and ground failure cases that plot in surficial clayey deposits and analyzing thirty-two seismic cone soundings. Somewhat surprising was that more than sixty percent of the total reported cases of 1886 horizontal ground displacement and conspicuous craterlets were found to plot in the surficial clayey deposits. This finding agreed with the previous study by Balon and Andrus (2006) who found the surficial clayey deposits to have just as high liquefaction potential as surficial sand deposits based on cone penetration test data without the MEVR correction.

Liquefaction probability curves developed for Qhec and Qtc were not consistent with the numbers of 1886 liquefaction cases that plot in the surficial clayey deposits. Therefore, it was recommended that the liquefaction probability curves for Qhs/Qhes (Figure 3.9a, Figure 6.7) and Qts (Figure 3.9d, Figure 6.8) be used for estimating the liquefaction potential of Qht/Qhec and Qtc. The liquefaction probability curves for Qhs/Qhes (Figure 3.9a, Figure 6.7) were also recommended for Qhm surficial deposits because no SCPTu data were available and there were several cases of 1886 ground failure that plotted in these areas. Because no SCPTu data were available for Qwc surficial deposits, the liquefaction probability curve for Qws (Figure 3.9b, Figure 6.8)

was recommended. For Qlc and Qpc, the liquefaction probability curves presented in Figure 6.6 are tentatively suggested. These recommendations are believed to be conservative. Additional SCPTu data are needed for all surficial clayey deposits to further establish the recommended curves.

8.1.5 Carbonate Content of Surface Sand Deposits

The carbonate contents of soil samples from the Greater Charleston area were determined in Chapter 7. The samples include: 26 auger samples collected from the subsurface at sites in the Charleston area, 10 borehole samples from the CREC, 18 borehole samples from the Hobcaw Borrow site, and 15 borehole samples from the Rest Area Ponds. The procedure described by ASTM D 4373-02 was modified to consider gas pressure due to impurities in the base of the cylinder analyzer. The cylinder gas pressure was monitored for 2 hours, and the pressure was corrected based on the blank test (0.0 g $CaCO_3$).

For all the sand samples, no pressure or a minor effervescent reaction was observed. The averages of calcite equivalent determined for deposits with different geologic age are all practically zero. The results indicated that carbonate cementation does not explain the aging effects of sands in the Greater Charleston area.

8.2 Recommendations for Future Work

Based on the results of this research, the following are tasks recommended for future work:

1. More SCPTu data are needed to decrease the uncertainties associated with liquefaction probability curves.
2. The calibration of LPI value with severity of liquefaction proposed by Toprak and Holzer (2003) were used in this study to develop the liquefaction probability curves. The calibration is based on the observation of liquefaction and no liquefaction observed during the 1989 Loma Prieta. Additional calibration is needed to verify and refine the calibration of LPI = 5 for sand boil generation.
3. The procedure to correct the liquefaction resistance of the soil deposit for the influence of digenetic process using MEVR needs to be further validated.
4. The results of this study indicated that carbonate content cannot be the mechanism responsible for aging effect in sand deposits in the Charleston area. More study is needed to identify the actual mechanisms causing high MEVR values and liquefaction resistance in Qws.

APPENDIX A

LOCATIONS OF 1886 HORIZONTAL GROUND DISPLACEMENT AND CONSPICUOUS CRATERLETS MAPPED BY EARLE SLOAN

Table A.1 Location of 1886 conspicuous craterlet areas mapped by Earle Sloan (Dutton 1889, PL. XXVIII).

Area No.	Latitude (degrees)	Longitude (degrees)	Surface Geology[a]	Distance to Woodstock fault (km)	Area No.	Latitude (degrees)	Longitude (degrees)	Surface Geology[a]	Distance to Woodstock fault (km)
1	32.5283	-80.2794	Qws?	17.3	28	32.9096	-80.0239	Qts	9.2
2	32.6780	-80.2286	Qht	5.7	29	32.9100	-80.0004	Qts	11.1
3	32.7042	-80.1209	Qht	12.8	30	32.9223	-79.9807	Qts	12.3
4	32.6353	-80.1556	Qhes	14.0	31	32.9131	-79.9794	Qts	12.8
5	32.6800	-80.0962	Qws?	16.2	32	32.8858	-80.1257	Qts	2.1
6	32.7464	-79.9814	Qhec	21.6	33	32.8954	-80.1477	Qtc	0.2
7	32.7566	-79.9666	Qhes	22.3	34	32.9195	-80.0811	Qts	3.9
8	32.7138	-80.2215	Qhec	4.2	35	32.9203	-80.0990	Qtc	2.4
9	32.7316	-80.1896	Qhec	5.7	36	32.9196	-80.1307	Qtc	0.2
10	32.7382	-80.2187	Qwls	3.0	37	32.9311	-80.1175	Qtc	0.3
11	32.7489	-80.2013	Qwls	3.8	38	32.9388	-80.1083	Qtc	0.9
12	32.7610	-80.2469	Qts	0.5	39	32.9477	-80.0943	Qhm	1.4
13	32.7539	-80.1849	Qwls	4.9	40	32.9661	-80.0665	Qlc	4.0
14	32.7685	-80.1868	Qht	3.9	41	32.9332	-80.1325	Qhm	1.0
15	32.7655	-80.1627	Qht	6.0	42	32.9400	-80.1212	Qhm	0.4
16	32.7537	-80.1611	Qwls	6.8	43	32.9589	-80.1040	Qhm	0.6
17	32.7819	-80.1859	Qhec	3.2	44	32.9728	-80.1490	Qtc	1.8
18	32.7803	-80.2294	Qts	0.2	45	33.0055	-80.1817	Qal	2.7
19	32.8017	-80.1864	Qhec	2.0	46	32.9608	-79.9899	Qtc	11.0
20	32.8061	-80.2025	Qhm	0.5	47	32.9700	-79.9739	Qts	12.6
21	32.8186	-80.1769	Qhec	1.8	48	32.9467	-79.9120	Qht	18.3
22	32.8357	-80.1842	Qhm	0.3	49	32.9586	-79.9130	Qht	18.2
23	32.7686	-80.3006	Qts	4.9	50	32.8458	-79.9142	Qhec	21.6
24	32.8987	-80.0684	Qts	6.1	51	32.8597	-79.9185	Qhec/Qws	20.5
25	32.9059	-80.0624	Qts	6.2	52	32.7996	-79.8968	Qhes	25.5
26	32.9164	-80.0556	Qts	6.2	53	32.8025	-79.8985	Qhes	25.2
27	32.9109	-80.0347	Qts	8.2	54	32.8085	-79.9010	Qhes	24.6
					55	32.8406	-79.9511	af	11.7

[a]Based on various 1:24,000 geologic maps by Weems and Lemon (e.g., 1988, 1993, 1996) and Weems et al. (e.g., 1997).

Table A.2 Location of 1886 ground displacement mapped by Earle Sloan (Dutton 1889, PL. XXVII).

Area No.	Latitude (degrees)	Longitude (degrees)	Surface Geology[a]	Distance to Woodstock fault (km)	Area No.	Latitude (degrees)	Longitude (degrees)	Surface Geology[a]	Distance to Woodstock fault (km)
1	32.5362	-80.2693	Qws?	16.5	33	32.8500	-80.1795	Qhm	0.2
2	32.5995	-80.2893	Qhec	9.3	34	32.8443	-80.1830	Qhm	0.1
3	32.5952	-80.2648	Qhes	10.2	35	32.8281	-80.1617	Qht	2.5
4	32.5792	-80.2304	Qhes	13.1	36	32.8325	-80.1379	qhec	4.2
5	32.5794	-80.1824	Qht	15.6	37	32.7805	-79.9325	af	23.6
6	32.5977	-80.2002	Qhes	13.0	38	32.8082	-79.9008	Qhes	24.7
7	32.7555	-80.3469	Qtc	8.3	39	32.7924	-79.8758	Qhes	27.6
8	32.7538	-80.3054	Qts	4.8	40	32.7577	-79.8569	Qhs	31.0
9	32.6759	-80.2289	Qhec	5.7	41	32.9446	-80.2137	Qhm	1.9
10	32.6479	-80.1753	Qhec	11.7	42	32.9082	-80.1902	Qhm	2.9
11	32.6444	-80.1510	Qht	13.8	43	32.8699	-80.1705	Qhm	0.6
12	32.6948	-80.2027	Qht	6.8	44	32.8619	-80.1296	Qwls	3.2
13	32.7044	-80.1874	Qht	7.5	45	32.8584	-80.1142	Ps	4.6
14	32.6780	-80.1581	Qhm	11.3	46	32.8465	-79.9912	Qwls	15.2
15	32.6873	-80.0821	Qht	16.9	47	32.8313	-79.9624	af/Qhec	18.4
16	32.6929	-80.0130	Qhec	22.1	48	32.8212	-79.9404	af/Qht	20.7
17	32.7046	-79.8944	Qht	31.0	49	32.8753	-79.9732	af	15.2
18	32.7447	-79.9006	Qht	28.2	50	32.8783	-80.0347	Ps	9.9
19	32.7741	-79.9631	Qhes	21.5	51	32.8739	-80.0828	Qws	6.2
20	32.7614	-80.2479	Qts	0.6	52	32.8826	-80.0717	Ps	6.7
21	32.7475	-80.2088	Qwls	3.3	53	32.8801	-80.0981	Qws	4.7
22	32.7352	-80.1758	Qht	6.6	54	32.8967	-80.0884	Qtc	4.6
23	32.7504	-80.1413	Qht	8.6	55	32.8975	-80.1028	Ps	3.3
24	32.7692	-80.1974	Qts	3.0	56	32.8836	-80.1148	Qts	3.1
25	32.7763	-80.1679	af/Qhec	4.9	57	32.9001	-80.1375	Qtc	0.4
26	32.7819	-80.1479	Qwls	6.2	58	32.9116	-80.1405	Qht	0.5
27	32.7833	-80.1423	Qwc	6.6	59	32.9138	-80.1425	Qht	0.8
28	32.7862	-80.1351	Qhec	7.0	60	32.9189	-80.1399	Qht	0.9
29	32.8117	-80.1726	Qhec	2.5	61	32.9482	-80.1695	Qtc	1.4
30	32.8207	-80.2197	Qts	1.8	62	32.9509	-80.1706	Qhec	1.2
31	32.8479	-80.2112	Qhec	2.6	63	32.9586	-80.1936	Qhec	1.1
32	32.8489	-80.1864	Qhm	0.7	64	32.9425	-80.1119	Qlc	0.2

Table A.2 Location of 1886 ground displacement mapped by Earle Sloan (Dutton 1889, PL. XXVII) (Continued).

Area No.	Latitude (degrees)	Longitude (degrees)	Surface Geology[a]	Distance to Woodstock fault (km)	Area No.	Latitude (degrees)	Longitude (degrees)	Surface Geology[a]	Distance to Woodstock fault (km)
65	32.9432	-80.1016	Qtc	1.0	90	33.0856	-79.9274	Qht	15.8
66	32.9472	-80.0707	Qtc	3.5	91	33.0829	-79.9288	Qht	15.8
67	32.9135	-80.0426	Qts	7.4	92	33.1038	-79.9451	Qht	13.5
68	32.9456	-80.0593	Qtc	4.6	93	33.0835	-79.9513	Qht	13.8
69	32.9357	-80.0314	Qtc	7.3	94	33.0361	-79.9644	Qhec	14.7
70	32.9418	-80.0357	Qtc	6.8	95	33.0867	-79.9704	Qhec	12.0
71	32.9510	-80.0351	Qtc	6.7	96	33.1109	-79.9632	Qht	11.7
72	32.9576	-80.0428	Qts	6.0	97	32.9655	-80.0894	Qtc	2.1
73	32.9535	-80.0501	Qts	5.3	98	32.9868	-80.0899	Qlc	4.0
74	32.9626	-80.0605	Qlc	4.5	99	32.9773	-80.1016	Qlc	2.7
75	32.9708	-80.0382	Qhm	6.7	100	32.9849	-80.1094	Qlc	3.5
76	32.9894	-80.0328	Qlc	8.0	101	32.9724	-80.1302	Qtc	3.0
77	32.9266	-79.9808	Qts	12.2	102	32.9914	-80.1218	Qls	3.0
78	32.9179	-79.9439	af	15.8	103	32.9950	-80.1451	Qls	0.9
79	32.9725	-79.9338	Qht	16.3	104	33.0175	-80.1783	Qpc	3.0
80	32.9676	-79.9503	Qhec	14.7	105	33.0645	-80.2665	Qpc	12.6
81	32.9735	-79.9654	Qtc	13.4	106	33.0771	-80.2342	Qlc	10.3
82	32.9731	-79.9965	Qhec	10.6	107	33.1292	-80.1812	Qpc	8.0
83	33.0115	-79.9748	Qtc	14.0	108	33.1380	-80.1698	Qpc	7.3
84	33.0233	-80.0079	Qhec	11.5	109	33.0581	-80.0892	Qlc	3.0
85	33.0252	-80.0294	Qlc	9.5	110	32.7889	-80.1080	Ps	9.0
86	33.0849	-79.8348	Qhec	23.9	111	32.8331	-80.1536	Qht	2.9
87	33.0973	-79.8362	Qht	23.3	112	32.9050	-80.1170	Ps	1.8
88	33.0854	-79.8551	Qht	22.1	113	32.6124	-80.1552	Qhes	15.3
89	33.0698	-79.8951	Qht	19.3					

[a]Based on various 1:24,000 geologic maps by Weems and Lemon (e.g., 1988, 1993, 1996) and Weems et al. (e.g., 1997).

REFERENCE

American Society for Testing and Materials (2006), D2487-02, "Standard Practice for Classification of Soils for Engineering Purposes." Annual *Book of ASTM Standards*, 04.08. ASTM International, West Conshohocken, PA.

American Society for Testing and Materials (2002), D4373-02, "Standard Test Method for Rapid Determination of Carbonate Content of Soils." *Annual Book of ASTM Standards*, 04.08, 610-614. ASTM International, West Conshohocken, PA.

Anderson, L. R., Keaton, J. R., Aubrey, K., and Ellis, S. (1982). "Liquefaction potential map for Davis County, Utah." Technical Report No. 94-7, Utah Geological Survey, Salt Lake City, Utah.

Andrus, R. D., Piratheepan, P., Ellis, B. S., Zhang, J., and Juang, C. H. (2004a). "Comparing liquefaction evaluation methods using penetration-V_S relationships." *Soil Dyn. Earthquake Eng.*, 24(9-10), 713-721.

Andrus, R. D., Stokoe, K. H., II, and Juang, C. H. (2004b). "Guide for shear-wave-based liquefaction potential evaluation." *Earthquake Spectra*, 20 (2), 285-308.

Andrus, R. D., Hayati, H., and Mohanan, N. P. (2009). "Correcting liquefaction resistance for aged sands using measured to estimated velocity ratio." *J. Geotech. Geoenviron. Eng.*, 135(6), 735-744.

Arango, I., Lewis, M. R., and Kramer, C. (2000). "Updated liquefaction potential analysis eliminates foundation retrofitting of two critical structures." *Soil Dyn. Earthquake Eng.*, 20(1-4), 17-25.

Bakun, W. H., and Hopper, M. G. (2004). "Magnitudes and locations of the 1811-1812 New Madrid, Missouri, and the 1886 Charleston, South Carolina, earthquakes." *Bull. Seismol. Soc. Am.*, 94(1), 64-75.

Balon, D. R., and Andrus, R. D. (2006). "Liquefaction potential index of soils in Charleston, South Carolina based on the 1886 earthquake." *Proc., 8th U.S. National Conference on Earthquake Engineering*, San Francisco, CA, Mira Digital Publishing, St. Louis, MO.

Baxter, C. D. P., and Mitchell, J. K. (2004). "Experimental study on the aging of sands." *J. Geotech. Geoenviron. Eng.* 130 (10), 1051-1062.

Berkeley Gazette (1886a). "A terrible night." *The Berkeley Gazette*, Sept. 4, 1.

Berkeley Gazette (1886b). "After the quake." *The Berkeley Gazette*, Sept. 11, 1.

Boller Jr., R. C. (2008). "Geotechnical investigations at three sites in the South Carolina Coastal Plain that did not liquefy during the 1886 Charleston earthquake." M.S. Thesis, Clemson Univ., SC.

Boller Jr., R. C., Andrus, R. D., Hayati, H., Camp, W. M., Gassman, S. L., and Talwani, P. (2008). "Liquefaction evaluation of the Coastal Research and Education Center geotechnical experimentation site near Charleston, South Carolina based on cone tests." *Proc. 6th National Seismic Conference on Bridge and Highways, Seismic Technologies for Extreme Loads*, MCEER-08-SP04, held July 28-30 in Charleston, SC, MCEER, Buffalo, NY, Poster No. P23.

Bollinger, G. A. (1977). "Reinterpretation of the intensity data for the 1886 Charleston, South Carolina, earthquake." *Studies Related to the Charleston, South Carolina, Earthquake of 1886: A Preliminary Rep.*, D. W. Rankin, ed., USGS Professional Paper, 1028, 17–32.

Bollinger, G. A. (1986). "Historical seismicity of South Carolina." 81st SSA Annual Meeting (Abstract), Earthquakes Notes 57, 15-16.

Boulanger, R.W., and Idriss, I.M. (2006). "Liquefaction susceptibility criteria for silts and clays." *J. Geotech. Geoenviron. Eng.* 132 (11), 1413-1426.

Bray, J. D., and Sancio, R. B. (2006). "Assessment of the liquefaction susceptibility of fine-grained soils." *J. Geotech. Geoenviron. Eng.*, 132(9), 1165-1177.

Camp, W. M., III (2004). "Site characterization and subsurface conditions of the Cooper River Bridge." *Geotechnical Engineering for Transportation Projects, Geotechnical Special Publication No. 26*, M. K. Yegian, and E. Kavazanjian, eds., ASCE, Reston, VA., 347–360.

CDMG, (1996). “Seismic hazard zones, South half of San Francisco North and north part of the Oakland West Quadrangles.” *California Division of Mines and Geology Seismic Hazard Zone Map, 1:24,000*, Sacramento, CA.

Cetin, K. O., et al. (2004). “Standard penetration test-based probabilistic and deterministic assessment of seismic soil liquefaction potential.” *J. Geotech. Geoenviron. Eng.,* 130(12), 1314-1340.

City of Charleston (1885). *Year book of the city of Charleston*, Charleston, SC.

City of Charleston (1886). *Year book of the city of Charleston*, Charleston, SC.

Chang, W. J., Rathje E. M., Stokoe, K. H., II, and Hazirbaba K. (2007). “In situ pore-pressure generation behavior of liquefiable sand.” *J. Geotech. Geoenviron. Eng.,* 133(8), 921-931.

Chapman, M. C., and Beale, J. N. (2010). “On the geologic structure at the epicenter of the 1886 Charleston, South Carolina, earthquake.” *Bull. Seismol. Soc. Am.,* 100(3), 1010-1030.

Chapman, M. C., Martin, J. R., Olgun, C. G., and Beale, J. N. (2006). “Site-response models for Charleston, South Carolina and vicinity developed from shallow geotechnical investigations.” *Bull. Seismol. Soc. Am.,* 96 (2), 467-489.

Côté, R. N. (2006). “City of Heroes: The Great Charleston Earthquake of 1886”. *Corinthian Books*, Mount Pleasant, SC.

Cramer, C. H., Rix, G. J., and Tucker K. (2008). “Probabilistic liquefaction hazard maps for Memphis, Tennessee.” *Seismol. Res. Lett.,* 79(3), 416-423.

Demars, K. R., Chaney, R. C., and Richter, J. A. (1983). “The rapid carbonate analyzer.” *Geotechnical Testing Journal*, 6(1), 30-34.

Dobry, R., Ladd, R. S., Yokel, F. Y., Chung, R. M., and Powell, D. (1982). “Prediction of pore water pressure buildup and liquefaction of sands during earthquake by the cyclic strain method.” *NBS building science series 138,* National Bureau of Standards, Gaithersburg, MD.

Dowding, C. H., and Hryciw, R. D. (1986). “A laboratory study of blast densification of saturated sand.” *J. Geotech. Eng.,* 112(2), 187–199.

Drnevich, V. P., and Richart Jr., F. E. (1970). “Dynamic prestraining of dry sand.” *J. Soil Mech. and Found. Div.,* 96(2), 453-469.

Dupré, W. R., and Tinsley, J. C., III (1980). “Maps showing geology and liquefaction potential of northern Monterey and southern Santa Cruz Counties, California.” *U.S. Geological Survey Miscellaneous Field Studies Map MF-1199, 2 sheets, 1:62:500,* Menlo Park, CA.

Durá-Gómez, I., and Talwani, P. (2009). “Finding faults in the Charleston area, South Carolina: 1. Seismological data.” *Seismol. Res. Lett.,* 80(5), 883-900.

Dusseault, M. B., and Mogenstern, N. R. (1979). “Locked sands.” *Q, J. Engrg. Geol.,* 12, 117-131.

Dutton, C. E. (1889). “The Charleston earthquake of August 31, 1886.” *USGS Ninth Annual Rep. 1887-1888*, U.S. Geological Survey, Washington, D.C., 203-528.

Elton, D. J., and Hadj-Hamou, T. (1990). “Liquefaction potential map for Charleston, South Carolina.” *J. Geotech. Engrg*., 116 (2), 244-265.

Fairbanks, C. D., Andrus, R. D., Zhang, J., Camp, W. M., Casey, T. J., and Clearly, T. J. (2004). “Electronic files of shear-wave velocity and cone penetration test measurements from the Charleston quadrangle, South Carolina.” *Data Rep. to the U. S. Geological Survey, Award No. 03HQGR0046*, Civil Engineering Dept., Clemson Univ., Clemson, S.C.

Frankel, A. D., Petersen, M. D., Mueller, C. S., Haller, K. M., Wheeler, R. L., Leyendecker, E. V., Wesson, R. L., Harmsen, S. C., Cramer, C. H., Perkins, D. M., and Rukstales, K. S. (2002). “Documentation for the 2002 update of national seismic hazards maps.” *USGS Open-File Report No. 02-420*, U.S. Geological Survey, Denver.

Friedman, G. M., and Sandres, J. E. (1978). *Principles of Sedimentology*. John Wiley&Sons, New York, NY.

Geiger, A. J. (2010). “Liquefaction analysis of three Pleistocene sand deposits that did not liquefy during the 1886 Charleston, South Carolina earthquake based on shear wave velocity and penetration resistance.” M.S. Thesis, Clemson Univ., SC.

Geiger, A.J., Boller, R.C., Andrus, R.D., Heidari, T., Hayati, H., and Camp, W.M., III. (2010). “Estimating liquefaction potential of a 200,000 year-old sand deposit near Georgetown, SC.” *5th International Conf. on Recent Advances in Geotechnical Earthquake Engr. and Soil Dynamics and Symposium in Honor of Professor I.M. Idriss,* San Diego, CA.

Hayati, H. (2009). “Characterizing liquefaction resistance of aged sand deposits.” Ph.D. Dissertation, Clemson University, Clemson, SC.

Hayati, H., and Andrus, R. D. (2008a). “Liquefaction potential map of Charleston, South Carolina based on the 1886 earthquake.” *J. Geotech. Geoenviron. Eng.,* 134(6), 815-828.

Hayati, H., and Andrus, R. D. (2008b). “Liquefaction susceptibility of fine-grained soils in Charleston, South Carolina based on CPT.” Proc., *GeoCongress 2008, Geosustainability and Geohazard Mitigation, Geotechnical Special Publication No. 178*, K. R. Reddy, M. V. Khire and A. N. Alshawabkeh, ASCE, Reston, VA, 327-334.

Hayati, H., and Andrus, R. D. (2009). “Updated liquefaction resistance correction factors for aged sands.” *J. Geotech. Geoenviron. Eng.,* 135(11), 1683-1692.

Heidari, T., and Andrus, R. D. (2010). “Mapping liquefaction potential of aged soil deposits in Mount Pleasant, South Carolina.” *Eng. Geol.,* 112(1-4), 1-12.

Heidari, T., and Andrus, R. D. (2011). “Liquefaction potential of Pleistocene sands in the Charleston area, South Carolina.” Submitted to *J. Geotech. Geoenviron. Eng.*

Heidari, T., Andrus, R. D., Moysey, S. M. J. (2011). “Characterizing the liquefaction potential of the Pleistocene-age Wando Formation in the Charleston area, South Carolina.” Submitted to *Risk Assessment and Management in Geoengineering, GeoRisk,* Atlanta, GA.

Holzer, T. L. (2008). "Probabilistic liquefaction hazard mapping." Proc., *Geotechnical Earthquake Engineering and Soil Dynamics IV, Geotechnical Special Publication No. 181,* D. Zheng, M. Manzari, and D. Hiltunen, ASCE, Reston, VA, 1-32.

Holzer, T. L., Bennett, M. J., Noce, T. E., Padovani, A. C., and Tinsley III, J. C. (2006). "Liquefaction hazard mapping with LPI in the Greater Oakland, California, area." *Earthquake Spectra,* 22(3), 693-708.

Holzer, T. L., Noce, T. E., and Bennett, M. J. (2009). "Scenario liquefaction hazard maps of Santa Clara Valley, Northern California." *Bull. Seismol. Soc. Am.,* 99(1), 367-381.

Holzer, T. L., Noce, T. E., and Bennett, M. J. (2010). "Liquefaction probability curves for surficial geologic deposits." *Environ. Eng. Geosci.,* Vol. XVII, No. 1.

Hu, K., Gassman, S. L., and Talwani, P. (2002). "In-situ properties of soils at paleoliquefaction sites in the South Carolina Coastal Plain." *Seismol. Res. Lett.,* 73(6), 964-978.

Idriss, I. M., and Boulanger, R. W. (2008). "Soil liquefaction during earthquakes." EERI Publication MNO-12.

Iwasaki, T., Tatsuoka, F., Tokida, K.-I., and Yasuda, S. (1978). "A practical method for assessing soil liquefaction potential based on case studies at various sites in Japan." *Proc., 2nd Int. Conf. on Microzonation,* San Francisco, National Science Foundation, Washington, D.C., 885-896.

Iwasaki, T., Tokida, K., Tatsuoka, F., Watanabe, S., Yasuda, S., and Sato, H. (1982). "Microzonation for soil liquefaction potential using simplified methods." *Proc., 3rd Int. Earthquake Microzonation Conf.,* Seattle, 1319-1330.

Johnston, A. C. (1996). "Seismic moment assessment of earthquakes in stable continental regions, III. New Madrid 1811-1812, Charleston 1886 and Lisbon 1755." *Geophy. J. Int.,* 126(2), 314-344.

Joshi, R. C., Achari, G., Kaniraj, R., and Wijeweera, H. (1995). "Effect of aging on the penetration resistance of sands." *Can. Geotech. J.,* 32, 767–782.

Juang, C. H., Jiang, T., and Andrus, R. D. (2002). "Assessing probability-based methods for liquefaction potential evaluation." *J. Geotech. Geoenviron. Eng.*, 128(7), 580-589.

Juang, C. H., and Li, D. K. (2007). "Assessment of liquefaction hazards in Charleston quadrangle, South Carolina." *Engineering Geology*, 92(1-2), 59–72.

Juang, C. H., Liu, C. N., Chen, C. H., Hwang J. H., and Lu, C. C. (2008). "Calibration of liquefaction potential index: A re-visit focusing on a new CPTU model." *Engineering Geology*, 102(1-2), 19–30.

Juang, C. H., Lu, C. C., Hwang, J. H. (2009). "Assessing probability of surface manifestation of liquefaction at a given exposure time using CPTU." *Engineering Geology*, 104(3-4), 223–231.

Knudsen, K. L., Noller, J. S., Sowers, J. M., and Lettis, W. R. (1996). "Maps showing Quaternary geology and liquefaction susceptibility in San Francisco, California, 1:100,000 Quadrangle: A digital database." *U.S. Geological Survey Open-File Report 97-715*, U.S. Geological Survey, Menlo Park, CA.

Lenz, J. A., and Baise, L. G. (2007). "Spatial variability of liquefaction potential in regional mapping using CPT and SPT data." *Soil Dyn. Earthquake Eng.*, 27(7), 690-702.

Leon, E., Gassman, S. L., and Talwani, P. (2006). "Accounting for soil aging when assessing liquefaction potential." *J. Geotech. Geoenviron. Eng.*, 132(3), 363-377.

Lewis M. R., Arango, I., Kimball, J. K., and Ross, T. E. (1999). "Liquefaction resistance of old sand deposits." *Proc., 11th Panamerican Conference on Soil Mechanics and Geotechnical Engineering*, ABMS, San Paulo, Brazil, 821-829.

Li, D. K., Juang, C. H., Andrus, R. D., and Camp, W. M. (2007). "Index properties-based criteria for liquefaction susceptibility of clayey soils: a critical assessment." *J. Geotech. Geoenviron. Eng.*, 133(1), 110-115.

Lilliefors, H. W. (1967). "On the Kolmogorov-Smirnov test for normality with mean and variance unknown." *J. Amer. Statist. Assoc.*, 62, 399–402.

Lunne, T., Robertson, P. K., and Powell, J. J. M. (1997). "Cone penetration testing in geotechnical practice." Blackie Academic and Professional, London.

Mabey, M. A., Madin, I. P., Youd, T. L., and Jones, C. F. (1993). "Earthquake hazard maps of the Portland Quadrangle, Multnomah County, Oregon and Clark Count County, Washington." *Oregon Department of Geology and Mineral Industries Geological Map Series, GMS-79,* Oregon Department of Geology and Mineral Industries, Portland, OR.

Marple, R. T., and Talwani, P. (2000). "Evidence for a buried fault system in the Coastal Plain of South Carolina of the Carolinas and Virginia: Implications for neotectonics in the southeastern United States." *Bull. Seismol. Soc. Am.,* 112 (2), 200-220.

Martin, J. R., II, and Clough, G. W. (1990). "Implication from a geotechnical investigation of liquefaction phenomena associated with seismic events in the Charleston, SC area." *Rep. to the U.S. Geological Survey,* Virginia Polytechnic Institute and State University, Blacksburg, VA.

Martin, J. R., II, and Clough, G. W. (1994). "Seismic parameters from liquefaction evidence." *J. Geotech. Eng.,* 120(8), 1345-1361.

McCartan, L., Lemon, E.M., Jr., and Weems, R.E. (1984). "Geologic map of the area between Charleston and Orangeburg." *Misc. Investigations Series Map I-1472,* scale 1:250,000, U.S. Geological Survey, Reston, VA.

McIver, P. R. (1994). "History of Mount Pleasant, South Carolina." Christ Church Parish Preservation Society, Mount Pleasant, SC, Second edition.

Mesri, G., Feng, T. W., and Benak, J. M. (1990). "Postdensification penetration resistance of clean sands." *J. Geotech. Engrg.,* ASCE, 116(7), 1095-1115.

Mitchell, J. K., and Solymar, Z. V. (1984). "Time-dependent strength gain in freshly deposited or densified sand." *J. Geotech. Eng.,* 110 (11), 1559-1576.

Mohanan, N. P., Fairbanks, C. D., Andrus, R. D., Camp, W. M., Clearly, T. J., Casey, T. J., and Wright, W. B. (2006). "Electronic files of shear wave velocity and cone penetration test measurements from the Greater Charleston area, South Carolina." *Data Rep. to the U.S. Geological Survey, Award No. 05HQGR0037,* Civil Engineering Dept., Clemson Univ., Clemson, SC.

Monaco, P., Marchetti, S., Totani, G., and Calabrese, M. (2005). "Sand liquefiability assessment by flat dilatometer test (DMT)." *Proc., XVI ICSMGE*, Osaka, 4, 2693-2697.

Moss, R. E. S., Seed, R. B., Kayen, R. E., Stewart, J. P., Kiureghian, A. D., and Cetin, K. O. (2006). "CPT-based probabilistic and deterministic assessment of in situ seismic soil liquefaction potential." *J. Geotech. Geoenviron. Eng.,* 132(8), 1032-1051.

Moss, R. E. S., Thornhill, D. M., Nelson, A. I., and Levulett, D. A. (2008). "Influence of aging on liquefaction potential: preliminary results." *Proc., Geotechnical Earthquake Engineering and Soil Dynamics IV, Geotechnical Special Publication No. 181* (CD-ROM), D. Zeng, M. Manzari, and D. Hiltunen, eds., ASCE, Reston, VA.

Müller, G., and Gastner, M. (1971). "The "Karbonate-bombe", a simple device for the determination of carbonate content in sediments, soil and other material." *N. Jb. Miner. Mh.*, 10, 466–469.

News & Courier (1886a). "The shake at Mount Pleasant." *The News & Courier*, Sept. 3, 2.

News & Courier (1886b). "Damage at Mount Pleasant." *The News & Courier*, Sept. 4, 3.

Ohta, Y., and Goto, N. (1978). "Empirical shear wave velocity equations in terms of characteristic soil indexes." *Earthquake Eng. Struct. Dyn.,* 6(2), 167-187.

Park, T. K., and Silver, M. L. (1975). "Dynamic triaxial and simple shear behavior of sand." *J. Geotech. Engrg. Div.,* 101(6), 513-529.

Power, M. S., and Holzer, T. L. (1996). "Liquefaction maps." *ATC Tech-Brief 1*, Applied Technology Council, Redwood City, CA.

Rix, G. J., and Romero-Hudock, S. (2007). "Liquefaction potential mapping in Memphis and Shelby County, Tennessee." *Rep. to the U. S. Geological Survey*, Denver, Colorado, 27 pp: available at http://earthquake.usgs.gov/regional/ceus/products/download/Memphis_LPI.pdf.

Robertson, P. K., Woeller, D. J., and Fin, W. D. L. (1992). "Seismic CPT for evaluating liquefaction potential." *Can. Geotech. J.*, 29, 686-695.

Robertson, P. K., and Wride, C. E. (1998). "Evaluating cyclic liquefaction potential using the cone penetration test." *Can. Geotech. J.*, 35(3), 442-459.

Rollins, K. M., Evans, M. D., Diehl, N. B., and Daily III., W. D. (1998). ''Shear modulus and damping relationships for gravels.'' *J. Geotech. Geoenviron. Eng.*, ASCE, 124(5), 396–405.

Roy, D. (2008). "Coupled use of cone tip resistance and small strain shear modulus to assess liquefaction potential." *J. Geotech. Geoenviron. Eng.*, ASCE, 134(4), 519–530.

Schiff, D., and D'Agostino, R. B. (1996). "Practical engineering statistics." *John Wiley & Sons, Inc.*, New York.

Schmertmann, J. H. (1987). Discussion of "Time-dependent strength gain in freshly deposited or densified sand," by J. Mitchell and Z. V. Solymar, *J. Geotech. Engrg.*, ASCE, 113(2), 173-175.

Schmertmann, J. H. (1991). "The mechanical aging of soils." *J. Geotech. Eng.*, (9), 1288-1330.

Seed, H. B. (1979). "Soil liquefaction and cyclic mobility evaluation for level ground during earthquakes." *J. Geotech. Eng. Div.*, 105(GT2), 201-255.

Seed, H. B., and Idriss, I. M. (1971). "Simplified procedure for evaluating soil liquefaction potential." *J. Soil Mech. and Found. Div.*, 97(9), 1249-1273.

Seed, H. B., and Idriss, I. M. (1982). "Ground motions and soil liquefaction during earthquakes." Earthquake Engineering Research Institute Monograph, Oakland, CA.

Seed, H. B., Idriss, I. M., and Arango, I. (1983). "Evaluation of liquefaction potential using field performance data." *J. Geotech. Eng.*, 109(3), 458-482.

Seed, H. B., Tokimatsu, K., Harder, L. F., and Chung, R. M. (1985). "The influence of SPT procedures in soil liquefaction resistance evaluations." *J. Geotech. Eng.*, 111(12), 1425-1445.

Shibata, T., and Teparaksa, W. (1988). "Evaluation of liquefaction potentials of soils using cone penetration tests." *Soils Found.*, 28(2), 49-60.

Sowers, J. M., Noller, J. S., and Lettis, W. R. (1994). "Maps showing Quaternary geology and liquefaction susceptibility in Napa, California," 1:100,000 sheet, *U.S. Geological Survey Open-File Report 95-205*, Menlo Park, CA.

Talwani, P., and Gassman, S. L. (2008). "The use of paleoliuefaction features in seismic hazard assessment- the Charleston experience." *Proc. 6th National Seismic Conference on Bridge and Highways, Seismic Technologies for Extreme Loads*, MCEER-08-SP04, held July 28-30 in Charleston, SC, MCEER, Buffalo, NY, Poster No. P30.

Talwani, P., and Schaeffer, W. T. (2001). "Recurrence rates of large earthquakes in the South Carolina Coastal Plain based on paleoliquefaction data." *J. Geophys. Res.*, 106, 6621–6642.

Tinsley, J. C., Youd, T. L., Perkins, D. M., and Chen, A. T. F. (1985). "Evaluating liquefaction potential." in J. I. Ziony, ed., Evaluating earthquake hazards in the Los Angeles Region: An earth science prespective., *U.S. Geological Survey Prof. Paper 1360*, 263-316.

Tokimatsu, K., and Uchida, A. (1990). "Correlation between liquefaction resistance and shear wave velocity." *Soils Found.*, 30(2), 33-42.

Toprak, S., and Holzer, T. L. (2003). "Liquefaction potential index: Field assessment." *J. Geotech. Geoenviron. Eng.,* 129(4), 315-322.

Troncoso, J. H., Ishihara, K., and Verdugo, R. (1988). "Ageing effects on cyclic shear strength of tailings materials." *Proc., 9th World Conf. on Earthquake Engineering,* Vol. III, 121-126.

Weems, R. E., and Lemon, E. M., Jr. (1988). "Geologic map of the Ladson quadrangle, Berkeley, Charleston, and Dorchester counties, South Carolina." *U.S. Geological Survey Geologic Quadrangle Map GQ-1630, Scale 1:24,000.*

Weems, R. E., and Lemon Jr., E. M. (1989). "Geology of the Bethera, Cordesville, Huger, and Kittredge quadrangles, Berkeley county, South Carolina." *U.S. Geological Survey Miscellaneous Investigations Map I-1854, Scale 1:24,000.*

Weems, R. E., and Lemon, E. M., Jr. (1993). "Geology of the Cainhoy, Charleston, Fort Moultrie, and North Charleston quadrangles, Charleston and Berkeley counties, South Carolina." *U.S. Geological Survey Miscellaneous Investigation Map I-1935, Scale 1:24,000,* U.S. Geological Survey, Reston, VA.

Weems, R. E., and Lemon, E. M., Jr. (1996). "Geology of the Clubhouse, Crossroads and Osborn quadrangles, Charleston, and Dorchester counties, South Carolina." *U.S. Geological Survey Miscellaneous Investigations Map 2491, Scale 1:24,000.*

Weems, R. E., Lemon, E. M., Jr., and Nelson, M. S. (1997). "Geology of the Pringletown, Ridgeville, Summerville, and Summerville Northwest 7.5-minute quadrangles, Berkeley, Charleston, and Dorchester counties, South Carolina." *U.S. Geological Survey Miscellaneous Investigations Map 2502, Scale 1:24,000.*

Weems, R. E., and Lewis, W. C. (2002). "Structural and tectonic setting of the Charleston, South Carolina, region: Evidence from the Tertiary stratigraphic record." *GSA Bull.,* 114(1), 24-42.

Youd, T. L. (1972). "Compaction of sands by repeated shear straining." *J. Soil Mech. and Found. Div.,* 98(7), 709-725.

Youd, T. L., and Hoose, S. N. (1977). “Liquefaction susceptibility and geologic setting.” Proc., *6th World Conference on Earthquake Engineering*, 2189-2194.

Youd, T. L., and Perkins, D. M. (1978). “Mapping liquefaction-induced ground failure potential.” *J. Geotech. Engrg. Div.*, 104(4), 433-446.

Youd, T. L., and Perkins, D. M. (1987). “Map showing liquefaction susceptibility of San Mateo County, California.” *U.S. Geological Survey Miscellaneous Investigations Map I-1257-G, 1:62,500*, U.S. Geological Survey, Denver, CO.

Youd, T. L., Tinsley, J. C., Perkins, D. M., King, E. J., and Preston, R. F. (1978). “Liquefaction potential map of San Fernando, California.” Proc. *2nd International Conference on Microzonation*, San Francisco, CA, 267-278.

Youd, T. L., et al. (2001). “Liquefaction resistance of soils: Summary report from the 1996 NCEER and 1998 NCEER/ NSF workshops on evaluation of liquefaction resistance of soils.” *J. Geotech. Geoenviron. Eng.*, 127(10), 817-833.